BMC Neuroscience

Research article

Open Access

Slow $GABA_A$ mediated synaptic transmission in rat visual cortex

Michael P Sceniak*[1,2] and M Bruce MacIver[2]

Address: [1]Department of Pharmacology, Case Western Reserve University, Cleveland, OH 44106, USA and [2]Department of Anesthesia, Stanford University School of Medicine, Stanford, CA 94305, USA

Email: Michael P Sceniak* - michael.sceniak@case.edu; M Bruce MacIver - maciver@stanford.edu

* Corresponding author

Published: 16 January 2008

BMC Neuroscience 2008, **9**:8 doi:10.1186/1471-2202-9-8

Received: 19 July 2007
Accepted: 16 January 2008

This article is available from: http://www.biomedcentral.com/1471-2202/9/8

© 2008 Sceniak and MacIver; licensee BioMed Central Ltd.
This is an Open Access article distributed under the terms of the Creative Commons Attribution License (http://creativecommons.org/licenses/by/2.0), which permits unrestricted use, distribution, and reproduction in any medium, provided the original work is properly cited.

Abstract

Background: Previous reports of inhibition in the neocortex suggest that inhibition is mediated predominantly through $GABA_A$ receptors exhibiting fast kinetics. Within the hippocampus, it has been shown that $GABA_A$ responses can take the form of either fast or slow response kinetics. Our findings indicate, for the first time, that the neocortex displays synaptic responses with slow $GABA_A$ receptor mediated inhibitory postsynaptic currents (IPSCs). These IPSCs are kinetically and pharmacologically similar to responses found in the hippocampus, although the anatomical specificity of evoked responses is unique from hippocampus. Spontaneous slow $GABA_A$ IPSCs were recorded from both pyramidal and inhibitory neurons in rat visual cortex.

Results: $GABA_A$ slow IPSCs were significantly different from fast responses with respect to rise times and decay time constants, but not amplitudes. Spontaneously occurring $GABA_A$ slow IPSCs were nearly 100 times less frequent than fast sIPSCs and both were completely abolished by the chloride channel blocker, picrotoxin. The $GABA_A$ subunit-specific antagonist, furosemide, depressed spontaneous and evoked $GABA_A$ fast IPSCs, but not slow $GABA_A$-mediated IPSCs. Anatomical specificity was evident using minimal stimulation: IPSCs with slow kinetics were evoked predominantly through stimulation of layer 1/2 apical dendritic zones of layer 4 pyramidal neurons and across their basal dendrites, while $GABA_A$ fast IPSCs were evoked through stimulation throughout the dendritic arborization. Many evoked IPSCs were also composed of a combination of fast and slow IPSC components.

Conclusion: $GABA_A$ slow IPSCs displayed durations that were approximately 4 fold longer than typical $GABA_A$ fast IPSCs, but shorter than $GABA_B$-mediated inhibition. The anatomical and pharmacological specificity of evoked slow IPSCs suggests a unique origin of synaptic input. Incorporating $GABA_A$ slow IPSCs into computational models of cortical function will help improve our understanding of cortical information processing.

Background

Inhibition plays an important role in visual cortical processing for receptive field formation and stimulus specificity at the local [1-3] and global network level [4-6]. *In vivo* pharmacological manipulation of inhibitory neurons alters visual cortical receptive field properties [7-9]. Understanding the kinetics of synaptic currents that give rise to inhibitory responses will be necessary to describe cortical network function and dynamics [10-13].

Within the neocortex γ-aminobutyric acid ($GABA_A$) is the primary inhibitory neurotransmitter [14-21]. $GABA_A$ kinetics are known to be faster than $GABA_B$ by roughly 10-fold [14,22]. There is variability in $GABA_A$ subunit composition across different interneuron subtypes but the functional consequences of this subunit variability are not well known [23,24]. Different combinations of $GABA_A$ receptor subunits have been shown to contribute to unique inhibitory phasic and tonic response kinetics [23,25-27].

The present study of inhibition in neocortex was motivated by reports of two forms of $GABA_A$-mediated inhibition in the hippocampus [28]. $GABA_A$ receptor mediated IPSCs in the hippocampus have fast (3–8 ms) and slow (30–70 ms) kinetic forms [28-33]. In the hippocampus, it has been shown that slow TTX insensitive spontaneous IPSCs exist, albeit infrequently, and that they can be evoked by focal electrical stimulation in the CA1 apical and basal dendritic zones, but not in the cell body layer. In contrast, fast IPSCs occur spontaneously at a high rate, but can only be evoked by micro-stimulation in the cell body layer [28,30]. Fast IPSCs are depressed by the subtype-specific $GABA_A$ antagonist, furosemide [34-37], while slow IPSCs are insensitive to furosemide [28,31,38]. The anatomical and pharmacological specificity argues for functionally distinct forms of $GABA_A$ receptor subunit combinations mediating fast and slow IPSCs.

We demonstrate here, for the first time, that $GABA_A$ slow currents occur both spontaneously and as evoked responses in the neocortex. Cortical $GABA_A$ slow responses are both quantitatively and pharmacologically distinct from $GABA_A$ fast responses and are evoked from anatomically distinct regions in the cortical columns.

Results

In order to study a homogeneous population of neurons, our study focused primarily on excitatory layer 4 pyramidal neurons of visual cortex. Slow $GABA_A$ spontaneous synaptic currents were observed in most pyramidal neurons (35 out of 47) as well as a subset of histologically identified inteneurons (3 out of 5). Fast IPSCs were observed in all pyramidal neurons and inhibitory interneurons.

Spontaneous IPSCs were recorded in rat visual cortical neurons perfused with room temperature ACSF containing 2 mM Ca^{2+} and Mg^{2+} (see Methods) to limit the occurrence of IPSC bursts, allowing the distinction of isolated events (Salin, 1996; Bacci, 2004). IPSCs were isolated from EPSCs through bath application of CNQX/APV (see Methods) to block glutamate-mediated events. The chloride channel blocker, picrotoxin (150 μM) completely abolished both slow and fast $GABA_A$ IPSCs. Across the entire population and within any single recording, sIPSCs were observed with a wide range of kinetics and amplitudes (Figure 1).

Spontaneous IPSC parametric analysis

In order to quantify the amplitude and temporal characteristics of the spontaneously occurring IPSCs in our population of cells, single isolated IPSCs were sorted from our recordings (see Methods). All sorted IPSCs (slow and fast) were then individually analyzed to determine their amplitude from baseline and rise time (10 to 90% of peak amplitude from baseline). The decaying slope of each

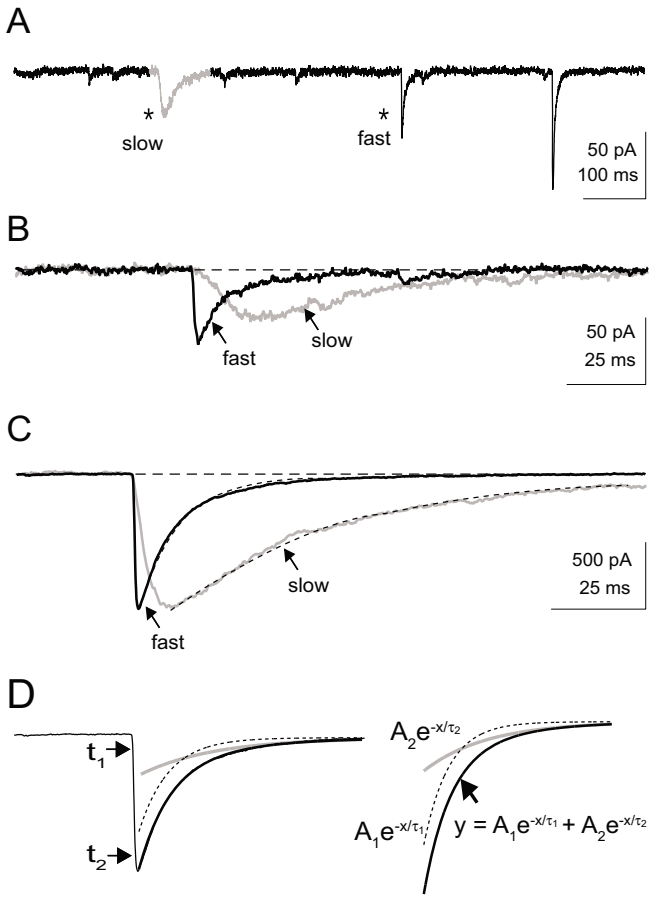

Figure 1

Representative whole-cell voltage-clamp recording of spontaneous activity of a neocortical pyramidal cell. A) Current recording of spontaneous IPSCs from a single cell with asterisks indicating a representative slow and fast isolated IPSC and the slow IPSC highlighted in gray. B) Overlay view of the isolated IPSCs indicated by asterisks in A. The horizontal dashed line represents the baseline current. C) Representative large amplitude spontaneous currents, showing both slow and fast events with matched amplitudes from the same cell. Dashed horizontal line represents the baseline current. The dashed line along the decaying slope represents empirical fits to the data. D) IPSC isolated events were quantified by estimating the peak amplitude from baseline, as well as the rise time and decay time constant (τ_1). Rise times were estimated as the time between 10 and 90% of the peak amplitude (t_1 and t_2 respectively). Decay time constants were estimated from empirical fits with a double exponential equation. The exponential time constants (τ_1 and τ_2) were used as estimates of the decay time ($\tau_2 > \tau_1$).

IPSC was fitted with a double exponential equation to determine the temporal properties of the decay to baseline (see Methods section and Figure 1D).

Across the population of sorted isolated IPSCs (n = 954), a parametric comparison of kinetic properties revealed two distinct populations. Rise time (> 3 ms) and decay time (τ_1 > 20 ms) limits were used to segment the population into fast (n = 714) and slow (n = 240,) events (Figure 2A, gray and black points respectively). IPSCs with slow kinetics occurred far less frequently than fast events (0.01 Hz vs. 2.2 Hz, respectively). For events that displayed an observable second component to their decaying slope (n = 319), there was also clustering into two groups (see Methods, $|A_2|$ > 10 pA, Figure 2B). IPSC kinetics were not correlated with amplitude for either rise time or decay time (Figure 2C–D).

For a representative neuron, all IPSC events (n = 574) were sorted and analyzed to determine the quantitative kinetics and amplitudes of all events for a given cell (see Additional file 1). The mean (geometric) amplitude (53 ± 45 pA) rise time (1.1 ± 0.9 ms) and decay time constant (7.3 ± 3.1 ms) for the representative neuron was not statistically different (p > 0.05, Wilcoxon signed-rank test) from the estimates for our randomly sampled fast population (n = 714, see Table 1).

In order to test for possible space clamp artifacts, spontaneous IPSCs were recorded using a CsCl-based internal electrode solution (see methods), to block potassium leak currents. On average, both rise times and decay times forslow spontaneous IPSCs recorded using a CsCl-based internal solution remained within the ranges of recordings made using a KCl-based internal solution: 12.5 ± 6 ms for average slow event (n = 8) rise times and 44 ± 22 ms for slow event (n = 10) decay time constants. A random sample (n = 100) of spontaneous events recorded using CsCl-based internal solution also revealed kinetics that were similar to those recorded with KCl-based internal solution for fast spontaneous IPSCs: 1.8 ± 0.8 ms rise time and 10.4 ± 5 ms decay time constant.

To compare spontaneous IPSC events statistically, slow and fast events were quantitatively analyzed as separate populations (open and gray bars respectively, Figure 3). Fast and slow IPSC events (see Figure 3A) were separated based on rise time and decay time constant clustering as in Figure 2. Decay time constants (τ_1) for both fast and slow IPSCs were skewed on a linear scale and were well fitted by a Gaussian distribution on a logarithmic scale (solid and dashed lines respectively, Figure 3B). There was significant separation of the population mean (μ indicates geometric mean, Figure 3) for the decay time constants of fast and slow events, τ_1 (Table 1). Rise time estimates for fast and slow events also showed significant separation between the two populations (Table 1, Figure 3C). Similar separation was observed for IPSC duration (defined as rise time + decay time constant) (Figure 3D). However, amplitude estimates for fast and slow events were not significantly different across the population (Table 1, Figure 3E).

For events with an observable second component to the decaying slope of the IPSC (n = 319, $|A_2|$ > 10 pA), the second time constants (τ_2) were log Gaussian distributed for fast (n = 277) and slow (n = 42) events (Figure 3F). There was significant separation between the mean population τ_2 for fast and slow events (Table 1).

Anatomical specificity of evoked $GABA_A$ IPSCs

Extracellularly evoked IPSCs were characterized based on the anatomical locus of stimulation in a sample of pyramidal cells (Figure 4A). Bipolar stimulating electrodes were positioned close to the dendrites of the recorded pyramidal neurons near (100–300 μm) the distal apical (Figure 4A, n = 18 cells), proximal apical (n = 21 cells) and basal (n = 22 cells) regions. Distal apical stimulating electrodes were placed in layer I/II directly above the dendritic axis of the cell. Basal stimulating electrodes were placed below (> 150 μm, toward the white matter) the cell body (± 100 μm from the dendritic axis). Proximal apical dendrite stimulating electrodes were placed roughly half-way between the soma and the pia off axis (100–300 μm).

Evoked IPSCs were recorded in the presence of CNQX/APV (see Methods) and the holding potential was set at rest (mean = -62 ± 4 mV). Averaged IPSCs (up to 10 repeats per cell with failures removed) were characterized for rise time, decay time and duration (Figure 4 and Table 2). Evoked responses were recorded from two locations per cell (two fixed stimulating electrodes positioned in either the proximal, distal or basal regions) in 60% of the cells and a single anatomical per cell in the remaining 40%. Slow evoked ISPCs (rise time > 3 ms and decay time, τ_1 > 20 ms) were found predominantly in responses evoked from stimulation near the basal (9 out of 18) and distal apical dendrites (16 out of 21). Evoked IPSCs resulting from stimulation near the proximal apical dendrites (n = 22) were all fast IPSCs (rise time < 3 ms and decay time, τ_1 < 20 ms).

IPSC rise times (10 to 90% of peak amplitude) estimates were smallest for evoked responses elicited from stimulation near the proximal dendrites (median = 2.6 ms, Figure 4B). Responses evoked through stimulation in the region near the distal apical dendrites displayed rise times (median = 4.6 ms) that were significantly greater than those near the proximal dendritic region (p = 0.009, Tukey-Kramer test, ANOVA, Table 2). Evoked responses from stimulation near the basal dendrites displayed a

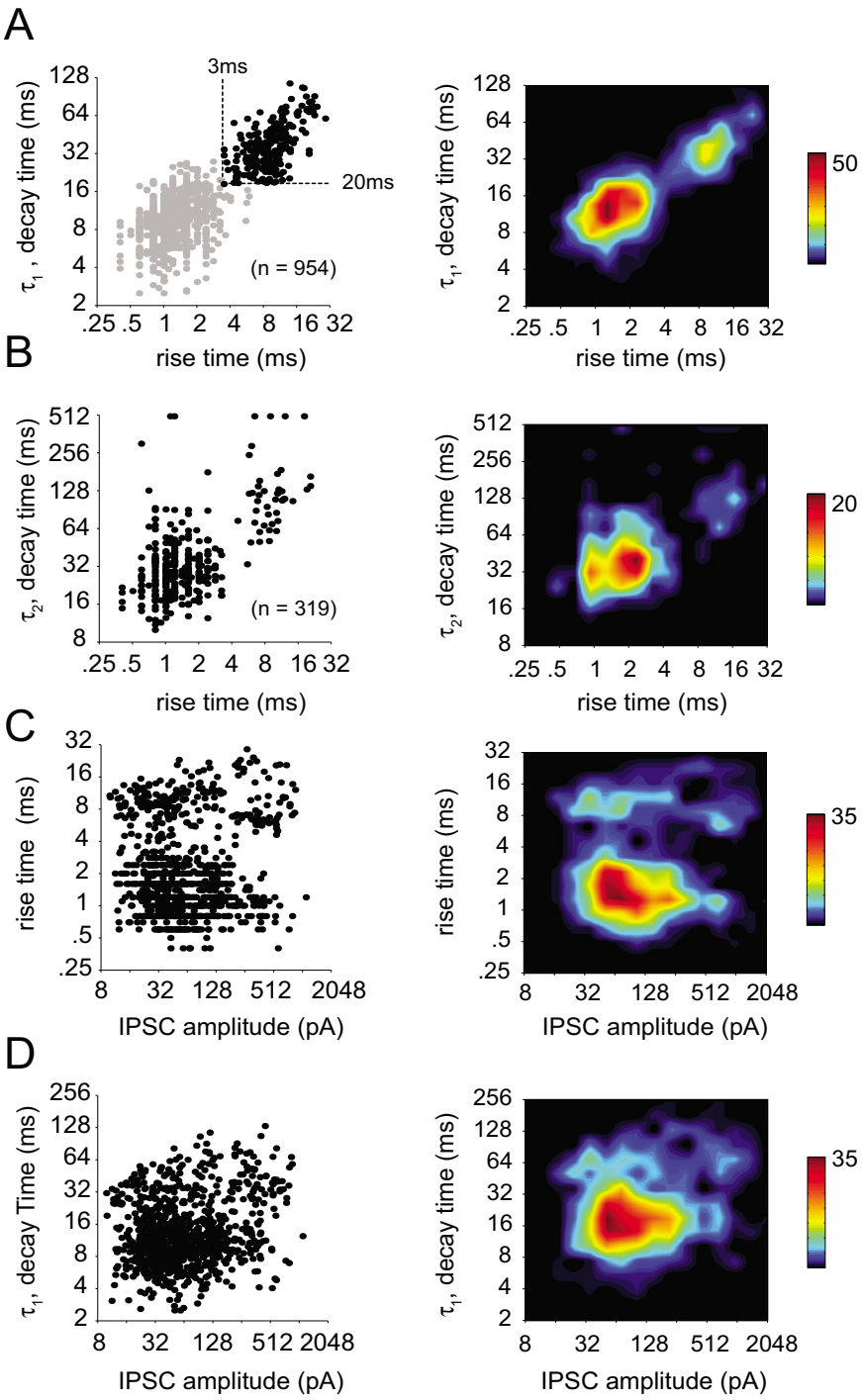

Figure 2

Quantitative population analysis of spontaneous isolated IPSCs. Trends in the properties of isolated IPSC amplitudes and kinetics (rise and decay time) were determined by comparing these parameters across the entire population of measured isolated IPSCs (n = 954). A) Isolated IPSC decay time constants are shown plotted vs. rise times. Two distinct populations are revealed by a correlation between rise time and decay time constants (τ_1, first component of the double exponential). Fast IPSCs are shown in gray and slow IPSCs are shown in black. Dashed lines represent the estimated demarcation between populations, based on a slow rise time > 3 ms and decay time > 20 ms. Smoothed density plots are shown to the right. The color-coded density plots indicate that the population is bimodal with separate fast and slow sub-populations that are correlated along rise and decay (τ_1) times. B) For those events with a significant second exponential component ($|A_2|$ > 10 pA, n = 319), τ_2 (second decay time constant) are shown vs. rise time. Smoothed density profile to the right reveals that these parameters are correlated and cluster into two groups (fast and slow). C-D) Rise time and decay time are shown plotted against event amplitude with smoothed density profile to the right. Neither rise time nor decay time (τ_1) was correlated with amplitude. The density profiles indicate bimodality along rise time that is uncorrelated with amplitude.

Table 1: Statistical summary of spontaneous IPSC kinetics and amplitudes.

	fast ‡	slow‡	p-value*
rise time	1.3 ± 0.7 ms	9.0 ± 2.5 ms	$p < 0.001$
decay time†			
τ_1	10 ± 4.4 ms	36 ± 19 ms	$p < 0.001$
τ_2	30 ± 42 ms	120 ± 58 ms	$p < 0.001$
amplitude	57 ± 100 pA	79 ± 194 pA	$p > 0.05$
duration	11 ± 5 ms	43 ± 22 ms	$p < 0.001$

†decay time constants from double exponential fit
‡standard deviation of the mean
*Student's t-test
Decay time constants τ_1 and τ_2 are shown for double exponential fits to the data. τ_1 is shown for all IPSCs in the sample population (n = 954) and τ_2 for responses with a significant second exponential (n = 319).

range of rise times (median = 3.8 ms) that overlapped those from stimulation near the proximal dendritic region.

The decay time constant (τ_1) was also characterized according to the anatomical origins of evoked stimulation (Figure 4C). Stimulation sites near the distal apical dendritic region and the basal region evoked IPSCs with decay time constants (median = 22 ms and 32 ms respectively) that were significantly slower than those evoked in the proximal apical dendritic region (median = 14 ms, p = 0.0045, Tukey-Kramer test, ANOVA, Table 2). Variability was greatest for stimulation near the distal apical and basal dendritic regions (first and third quartiles = 20 ms, 27 ms and 14 ms, 37 ms respectively) and lowest in the proximal dendritic region (first and third quartile = 12 ms and 18 ms).

Estimates of the IPSC total duration (rise time + decay time constant) were dominated by the decay time constant (τ_1) and followed similar trends (Figure 4D). Both the distal apical and basal dendritic region stimulation estimates of duration (median = 27 ms and 24 ms respectively) were significantly longer than estimates from proximal apical dendritic region stimulation (median = 18 ms, p = 0.005, Tukey-Kramer test, ANOVA, Table 2). The distal apical and basal dendritic region stimulation estimates displayed greater range and variability (first and third quartiles = 23 ms, 35 ms and 17 ms, 41 ms respectively). Proximal apical dendritic stimulation sites produced IPSCs with the least variability (first and third quartile = 13, 22 ms).

Slow evoked IPSCs were observed concurrently with fast and slow sIPSCs (n = 5 cells). During periods of evoked stimulation with pulses delivered near the distal dendrites, fast and slow sIPSCs were observed (Figure 5). Evoked IPSCs and sIPSCs did not appear to interact during distal dendritic region stimulation. Fast and slow sIPSCs were observed within the period immediately preceding and following evoked stimulation, as well as overlapping evoked IPSCs (Figure 5). Neocortical evoked slow IPSCs do not appear to suppress sIPSCs with either slow or fast kinetics.

Furosemide action on $GABA_A$-mediated IPSCs

Furosemide, the subunit selective $GABA_A$ receptor blocker, selectively depresses $GABA_A$ fast IPSCs in the hippocampus, while leaving $GABA_A$ slow responses unaffected [28,31,32,38]. The effects of furosemide were tested on spontaneous currents from layer 4 cortical pyramidal neurons (Figure 6A). Furosemide (1 mM) had no significant effect on the amplitude of slow IPSCs compared to control (mean = 42 ± 12 pA, mean = 40 ± 9 pA, control and treated conditions respectively) observed in our sample population ($p > 0.05$, Wilcoxon test, n = 5, Figure 6B). In contrast, the amplitude of fast IPSCs was significantly reduced (65%) in the presence of furosemide (mean = 45 ± 1.9 pA, mean = 16 ± 0.7 pA, control and treated respectively) compared to control ($p < 0.01$, Wilcoxon signed-rank test, Figure 6B). IPSC frequency was not significantly reduced in the presence of furosemide for either fast (mean = 2.2 ± 3.7 Hz, mean = 1.4 ± 2.6 Hz control and treated respectively) or slow events (mean = 0.012 ± 0.004 Hz, mean = 0.019 ± 0.0034 Hz control and treated respectively, see Figure 6D&E).

Evoked responses were recorded from extracellular stimulation of the distal and proximal apical as well as the basal dendritic region of pyramidal cells in control and furosemide (1 mM) treated conditions (n = 29, Table 3, Figure 7). Furosemide significantly depressed ($p < 0.01$, MANOVA, Table 4) evoked fast IPSC responses from stimulation sites originating in the proximal apical dendritic region (median = 114 pA and 28 pA for control and furosemide condition respectively; Table 3, Figure 7A). Responses evoked from stimulation near the basal dendritic region showed a trend toward depression from application of furosemide (median = 95 pA and 39 pA, control and furosemide respectively). Furosemide did not significantly alter evoked response amplitudes (median = 68 pA and 113 pA, control and furosemide respectively) originating in the distal apical dendrites ($p = 0.05$, Table 4, Figure 7A).

Treatment with furosemide resulted in prolonged rise times for evoked IPSCs for responses evoked from stimulation of the basal (median = 2.8 ms and 10.2 ms, control and furosemide respectively, Table 3) and proximal apical (median = 3.3 ms and 5.3 ms, control and furosemide respectively) dendritic regions (Table 3, Figure 7B). The rise times were not significantly ($p > 0.05$, ANOVA factorial) altered for responses evoked through stimulation of

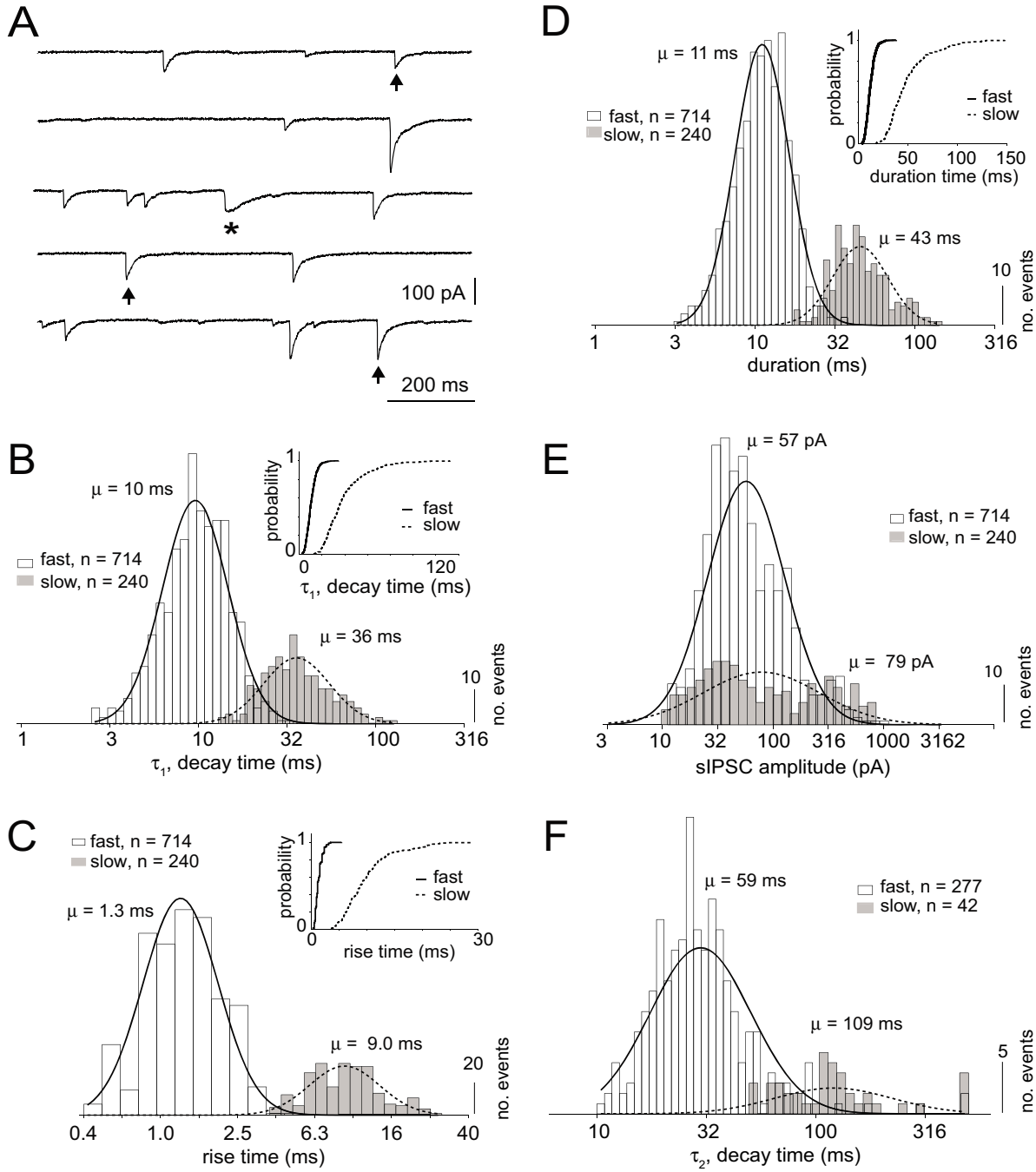

Figure 3

Population analysis (μ indicates geometric mean) of spontaneous isolated IPSC kinetics. The population of spontaneous isolated IPSCs was divided into two sub-populations based on the bimodal clustering in the correlation scatter plot of rise and decay time (τ_1) (see Figure 2A). A) Representative current recording of a pyramidal neuron. Asterisk indicates the identified slow IPSC event and the vertical arrows indicate the randomly selected events. B) Population histograms and Gaussian fits of the decay time constant (τ_1) estimates for fast (open, solid, μ = 10 ms) and slow (gray, dashed, μ = 36 ms) event sub-populations are shown plotted on the same axis. Inset plot shows cumulative distribution for the fast and slow populations (solid and dashed lines respectively). C) Population histograms of rise times for both fast (open, n = 714) and slow (gray, n = 240) events. Solid and dashed curves (fast and slow respectively) represent Gaussian fits to the distributions on a log scale (μ = 1.3 ms and 9.0 ms respectively, $p < 0.01$). D) Duration estimates (rise time + decay time (τ_1) or rise time + decay time (τ_2) for cases where $|A_2| > 10$pA) are shown for fast (open, μ = 11 ms) and slow (gray, μ = 45 ms) populations. Population distributions and the cumulative distributions (inset) show minimal overlap. E) IPSC amplitudes are shown for fast (open, n = 714) and slow (gray, n = 240) events. Amplitudes for the fast and slow event groups show considerable overlap (μ = 57 pA, 79 pA respectively). F) For events with significant second decay components ($|A_2| > 10$ pA), the second decay time distributions are shown for the fast (open, n = 277) and slow (gray, n = 42) events. Smooth curves are Gaussian fits to the fast (solid, μ = 30 ms) and slow (dashed, μ = 120 ms) population distributions.

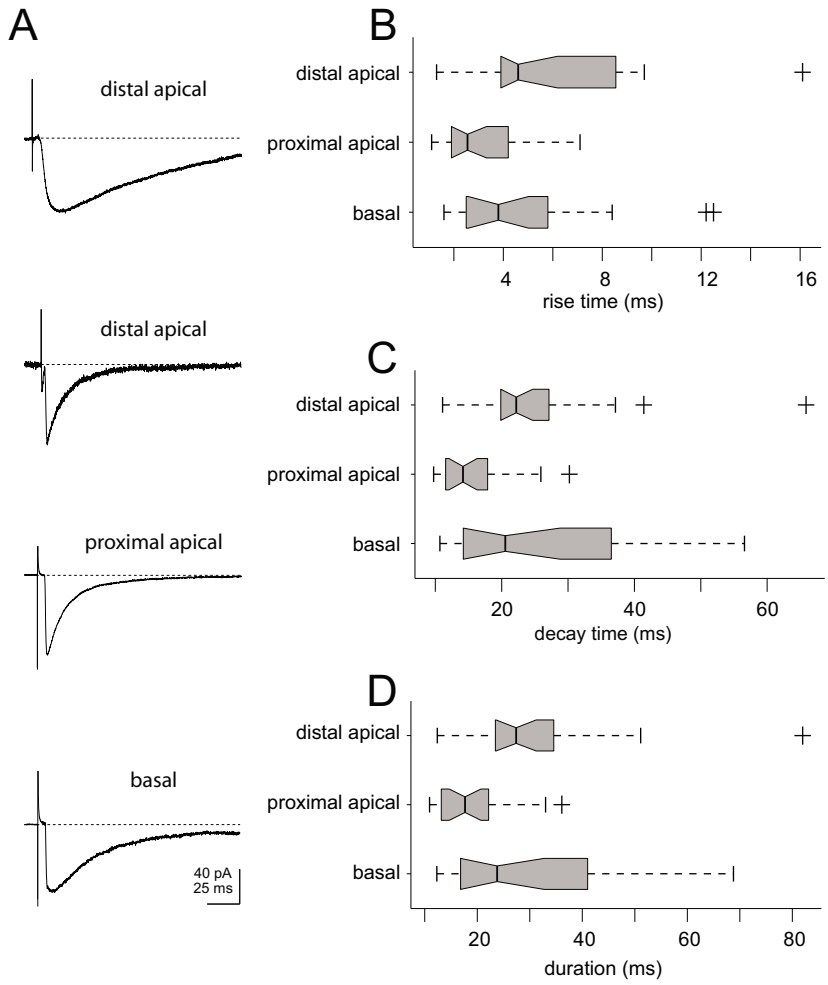

Figure 4

Statistical summary of anatomically classified evoked synaptic responses. A) Representative IPSC trace averages (n = 10 repeats) are shown based on the location of stimulating electrode placement: distal apical (top and second from top), proximal apical (third from top) and basal (bottom). B) Box plots show the first and third quartiles around the median with the notch signifying 95% of the median for each sample population (distal apical, n = 18; proximal apical, n = 21; basal, n = 22) and dashed lines indicate the whiskers (1.5× inter-quartile range) and crosses indicate outliers. Rise time estimates are shown summarized by the box plot for distal (median = 4.6 ms), proximal (median = 2.6 ms) and basal (median = 3.8 ms) responses. C) Decay time (τ_1) estimates from the double-exponential fits to the IPSCs evoked from stimulation distally (median = 22 ms), proximally (median = 14 ms) or basally (median = 21 ms). D) Population summary of the total duration (rise time + decay time (τ_1)) estimates are shown for responses evoked distally (median = 27 ms), proximally (median = 17.7 ms) and basally (median = 24 ms). Proximal stimulation produced short duration IPSCs, while distal and basal IPSCs contained a mixture of slow and fast IPSCs with greater range and variability (quartile difference (third-first) = 12 ms, 9 ms and 24 ms for distal, proximal and basal respectively).

the distal apical dendritic regions (median = 6.6 ms and 6.0 ms, control and furosemide respectively, Table 3).

Evoked IPSCs displayed increased decay time constants in the presence of furosemide for stimulation sites originating near the basal and proximal apical dendritic regions (Figure 7C, Table 3). Decay time constants were significantly longer ($p < 0.01$, ANOVA factorial) in the presence furosemide (median = 47.2 ms) versus control (median = 18.5 ms) for stimulation sites located near the basal dendrites (Figure 7C, Table 3). Evoked IPSC responses showed a trend toward increased decay time constant duration in the presence of furosemide (median = 31.1 ms) compared to control (median = 13.8 ms) for stimulation sites near the proximal apical dendrites (Figure 7C, Table 3). Stimulation sites located near the distal apical dendrites produced IPSCs with no significant difference ($p > 0.05$, ANOVA factorial, MANOVA, Table 4) in the median decay time constants in control or furosemide treated condtions (median = 28.1 ms and 39.3 ms, control and furosemide respectively).

Furosemide only partially depressed many of the evoked responses and the residual components often displayed slower kinetics than the control condition. In other cases furosemide completely suppressed the evoked response.

Table 2: Statistical summary of evoked IPSC kinetics across anatomical origin of stimulation.

	rise time (ms)†	decay time, τ_1 (ms)†	duration (ms)†
distal apical	5.8 ± 0.6	25.2 ± 2.5	31.0 ± 3.1
proximal apical	3.0 ± 0.6	15.5 ± 2.4	18.6 ± 3.0
basal	5.0 ± 0.7	26.9 ± 2.7	32.0 ± 3.3

†mean ± standard error

ANOVA Table†	SS	df (error)	df	MS	F	Prob>F
rise time	85.5	58	2	42.7	5.12	0.0089
decay time, τ_1	1574	58	2	787	5.95	0.0045
duration	2327	58	2	1163	5.85	0.0049

†each parameter compared across 3 groups (distal apical, proximal apical, basal)
‡ Tukey-Kramer post hoc test
Evoked IPSC were collected for stimulating electrodes placed in either the distal apical (n = 22), proximal apical (n = 18) or basal (n = 21) dendritic regions of excitatory pyramidal cells.

Increasing the stimulus intensity in the presence of furosemide revealed an evoked IPSC with slow kinetics even in cases (n = 8) where the responses were completely suppressed (prior to stimulus intensity increase). Picrotoxin (150 μM) completely suppressed all evoked responses. Furosemide appeared to selectively depress the fast component of responses, revealing a slow IPSC that contributed to most evoked responses. This occurred for responses evoked through distal and proximal apical dendritic and basal dendritic region stimulation.

Discussion

Our study shows that both evoked and spontaneous $GABA_A$-mediated slow IPSCs occur in neocortex. Slow $GABA_A$-mediated IPSCs display quantitatively similar kinetics properties for rise time and decay time (τ_1) as those observed in the hippocampus [28,29,31,32,38-40].

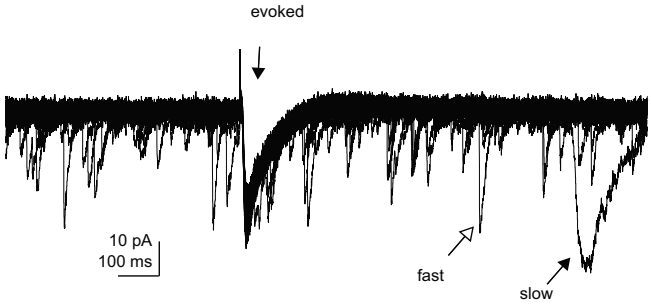

Figure 5
Evoked IPSCs do not inhibit the occurrence of spontaneous IPSCs Representative IPSC recording of a pyramidal cell evoked through stimulation of the input fibers within the distal apical dendrites. Slow IPSCs were evoked with 1 s separation (30 consecutive repeats). Fast spontaneous IPSCs occurred immediately before, during or following evoked ISPC stimulation. Arrows indicate specific spontaneous fast and slow events. The kinetics of the slow spontaneous events was consistent with the evoked responses. Vertical arrow marks the electrically evoked response.

Spontaneous $GABA_A$ slow IPSCs in the neocortex occurred infrequently compared to $GABA_A$ fast events. The low frequency of occurrence of spontaneous slow $GABA_A$-mediated IPSCs could explain the lack of previous reports of this slow synaptic inhibition in neocortex.

Inhibitory interneurons within the neocortex form a highly interconnected and heterogeneous population of cells that appear to segregate into unique groups both morphologically and functionally [1,20,23,24,41-43]. Two well described neocortical interneuron subtypes, fast-spiking (FS) and low-threshold-spiking (LTS) cells, can be distinguished by their unique synaptic kinetics [25,27,41,42,44,45]. The IPSCs from FS and LTS cells have fast synaptic current rise times, but LTS cells have slower decay time constants. The slow $GABA_A$-mediated currents presented here display even slower rise times and decay time constants than the IPSCs reported for FS and LTS cells. Perhaps $GABA_A$ slow IPSCs also arise from of a unique subtype of interneuron.

It is unlikely that slow $GABA_A$ IPSCs are merely a result of filtering from the cable properties of dendrites. We have shown here that pure fast as well as slow $GABA_A$-mediated IPSCs were preferentially evoked through electrical stimulation of the distal apical dendritic zones (superficial layer 1/2) of layer 4 pyramidal neurons. Previous reports have shown that, unlike EPSCs, IPSCs evoked in distal apical dendrites of pyramidal neurons show little effects of kinetic slowing from dendritic cable properties [28,40,46-50]. Also we have observed similar time constants of IPSCs recorded with either CsCl or KCl internal solutions. CsCl is known to block K+ channels and increase the signal to noise ratio for distal IPSCs. In addition, furosemide failed to block distally evoked evens, suggesting a distinct

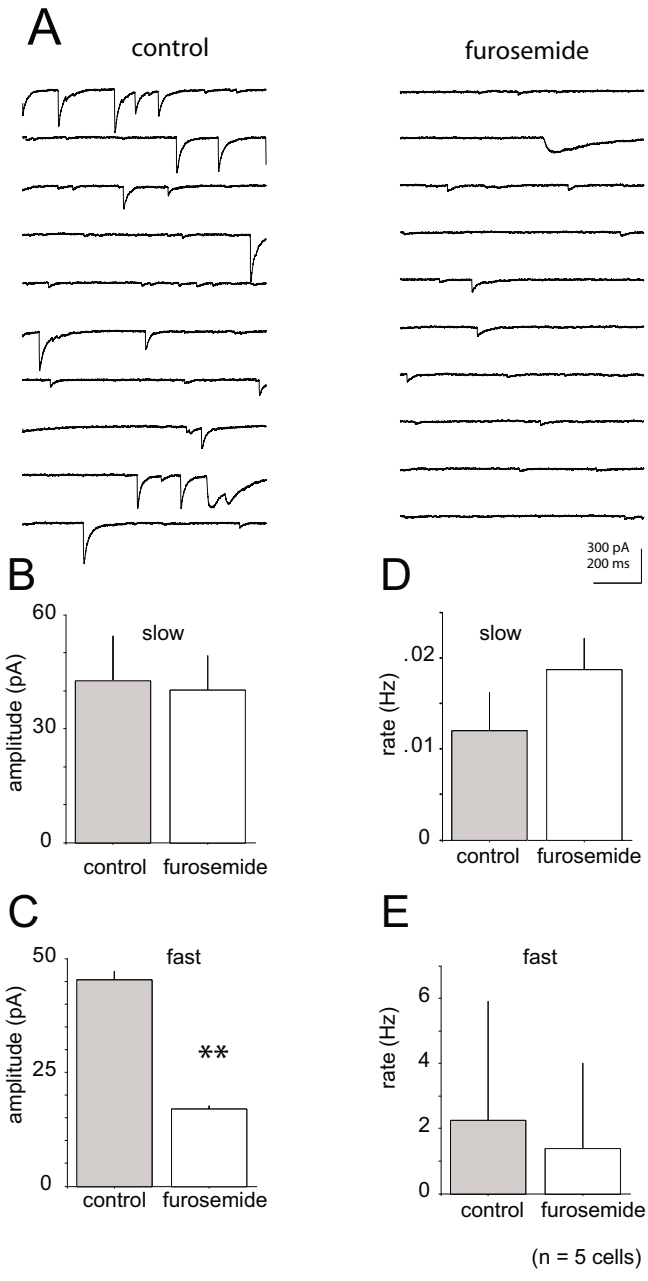

Figure 6

Furosemide selectively depressed $GABA_A$ fast spontaneous events. Population (n = 5 cells) summary for spontaneous IPSCs in control and furosemide treated conditions. A) Representative recording or spontaneous events in control and furosemide treated conditions. B) The average amplitude of slow sIPSCs was not significantly different between control and furosemide treated conditions (mean = 43 ± 12 pA and mean = 40 ± 9 pA respectively). C) The amplitude of sIPSCs was significantly reduced (mean control = 45 pA, mean treated = 16 pA) with treatment of furosemide (** indicates $p < 0.001$, Wilcoxon signed-rank test). D-E) The frequency of spontaneous IPSCs in the presence of furosemide was not significantly reduced for fast (mean = 2.2 ± 3.7 Hz, mean = 1.4 ± 2.6 Hz, control and treated respectively) or slow events (mean = 0.012 ± 0.004 Hz, mean = 0.019 ± 0.0034 Hz, control and treated respectively).

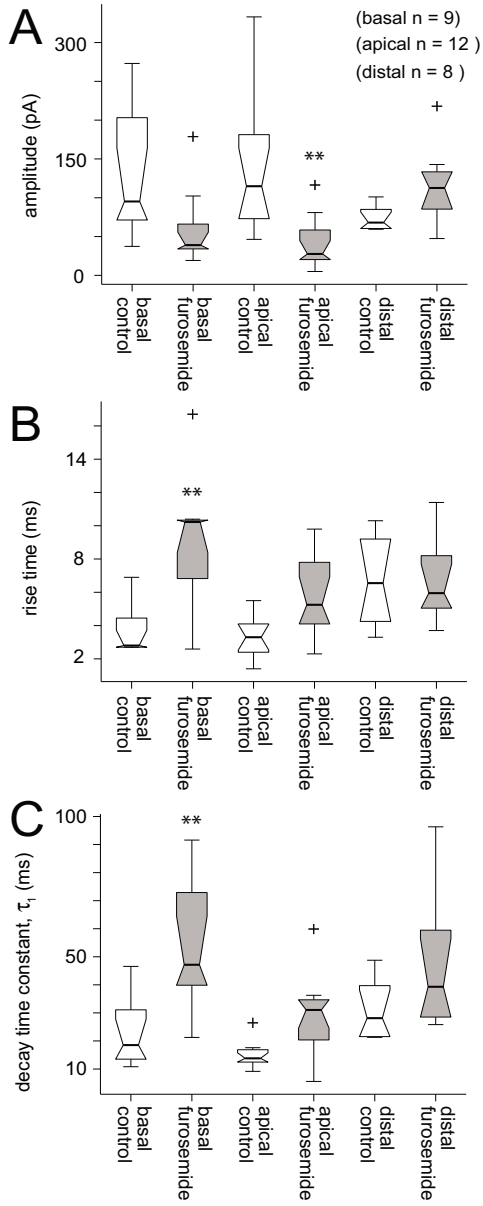

Figure 7

Effects of furosemide on evoked IPSCs based on anatomical origins of stimulation. Controls vs. furosemide treated (1 mM) conditions are shown in box plot form. Furosemide responses are shown in gray and control groups as open boxes. Evoked IPSC response amplitude, rise time and decay time constants are shown for stimulation of the basal (basal, n = 9), proximal apical (apical, n = 12) and distal apical (distal, n = 8) dendritic regions. Significance ($p < 0.01$) is indicated by ** (MANOVA and ANOVA factorial, see Table 4). Boxes span the first and third quartiles with medians indicated by thick center line and notch. A) Evoked IPSC amplitudes were reduced in the presence of furosemide compared to control for the stimulation sites in the region of the basal and proximal apical dendrites, but not the distal apical dendrites (see Table 3 for quantification). B) Rise time estimates were greater in the presence of furosemide for stimulation sites near the basal and proximal apical dendrites but not the distal apical dendrites. C) On average, the decay time constants (τ_1) for evoked IPSCs were significantly greater with furosemide treatment than control conditions for stimulation sites near the basal dendrites. Decay time constants were not significantly different for responses evoked through stimulation of the distal apical dendrites in the presence of furosemide compared to control.

Table 3: Summary of furosemide effects on synaptic responses vs. anatomical location of stimulation site.

	control	furosemide	n
amplitude			
basal	95 (71, 203) pA	39 (34, 66) pA	9
apical	114 (73, 181) pA	28 (20, 58) pA	12
distal	68 (60, 85) pA	113 (85, 133) pA	8
rise time			
basal	2.8 (2.7, 4.5) ms	10.2 (6.9, 10.4) ms	9
apical	3.3 (2.4, 4.1) ms	5.3 (4.1, 7.8) ms	12
distal	6.6 (4.3, 9.2) ms	6.0 (5.1, 8.2) ms	8
decay time constant, τ_1			
basal	18.5 (13.5, 31.0) ms	47.2 (40.0, 73.0) ms	9
apical	13.8 (12.5, 17.0) ms	31.1 (20.4, 34.7) ms	12
distal	28.1 (21.6, 39.7) ms	39.3 (28.5, 59.5) ms	8

Median values for control and furosemide groups are shown with the first and third quartiles indicated in parentheses. Stimulation sites were grouped according to their proximity to the basal (basal), proximal apical (apical), or the distal apical (distal) dendritic region of each pyramidal neuron. The decay time constants were estimated from the double exponential fits to the IPSC decaying response phase.

pharmacological action based on the anatomical origin of stimulation.

Slow $GABA_A$-mediated IPSCs observed in the neocortex are pharmacologically distinct from fast $GABA_A$ IPSCs. A $GABA_A$ subtype-specific antagonist, furosemide [34-37], did not alter $GABA_A$ slow IPSCs, while it markedly attenuated spontaneous $GABA_A$ fast responses amplitudes (~90%). $GABA_A$-mediated IPSCs observed within the hippocampus show similar furosemide selectivity [28]. The differential sensitivity of fast and slow components to furosemide suggests that slow and fast responses in neocortex have unique $GABA_A$ receptor subunit compositions. GABA receptors containing either α1 or α4 subunits display the fastest decay time constants [51,52]. GABA receptors containing either α2 [51], α3 [53], or α5 [52] have slower decay kinetics than either α1 or α4. Furthermore, furosemide has a 50-fold greater selectivity at α4βγ2 $GABA_A$ receptors, which have fast kinetics, compared to other isoforms [54]. Blocking these fast-decaying receptors would yield a pool of slower (α2, α3, α5) or similarly slow decaying (α1) receptors.

Table 4: MANOVA: Furosemide effects vs. stimulation site.

	dfW	dfB	dfT	Λ	p
basal	16	1	17	0.46	0.009**
proximal apical	22	1	23	0.45	0.001**
distal	14	1	15	0.52	0.05

One-way multivariate analysis of variance (MANOVA) table for the effects of furosemide on evoked synaptic responses resulting from stimulation at sites near the basal, proximal apical, and distal apical dendritic regions. Degrees of freedom are shown for each stimulation category for within-group sum of squares and cross-products (dfW), between-group sum of squares and cross-products (dfB) and the total sum of squares and cross-products (dfT). Wilk's Λ test statistics are shown for each stimulation category along with the resulting p-value (** indicates significance < 0.01).

It has been shown previously that furosemide nonspecifically blocks the K^+/Cl^- cotransporters NKCC1 and KCC2 [55-57]. Blocking Cl^- cotransporters would increase internal Cl^- concentrations and likely decrease the time constants of IPSCs by increasing membrane resistance. However, we observed a time constant increase in the presence of furosemide. Nonspecific effects on Cl^- cotransporters are also unlikely to affect synaptic responses in our preparation, because the chloride gradient was already reversed with a KCl-based internal solution (see Methods).

Some evoked and spontaneous responses were composed of a combination of slow and fast components. Similar combined fast and slow components of $GABA_A$-mediated IPSCs have also been observed in piriform cortex [58]. The slower second components of evoked IPSCs were proposed to result from activation of GABAa slow receptors. However, spontaneously occurring slow IPSCs have not been shown in piriform cortex.

At least one-third of spontaneous events in our study contained a significant slow second component decay time constant as revealed with double-exponential fits. Application of furosemide revealed a residual response component with slow kinetics in evoked IPSCs for many cells. The decay time constants (τ_1) of the residual currents were consistent with $GABA_A$ slow currents.

Anatomical comparison revealed that IPSC responses with purely slow components were evoked in layer 4 pyramidal neurons through microstimulation of either the distal apical (layers 1/2) or basal (layers 5 or 6) dendrites but not the proximal apical dendrites. In contrast, fast IPSC responses were evoked with near-threshold stimulation throughout the dendritic arbor. In the presence of furosemide, slow IPSCs were revealed in otherwise fast IPSC evoked responses at all locations of dendritic stimulation (distal, proximal and basal). IPSCs evoked through stimulation of distal apical dendrites were also not depressed by furosemide. The presence of slow IPSC components in the evoked responses at proximal apical dendrites with application of furosemide suggests that $GABA_A$ slow responses occur throughout the dendritic length but are masked by stronger fast responses. This might result from a higher density of $GABA_A$ receptor subtypes responsible for fast responses at these locations. The exact location of synapses evoked through our stimulation might not correspond to our stimulation sites. Because the syn-

apses of any particular stimulation site might terminate some distance from the origin of stimulation, our anatomical classification cannot distinguish between the location of cell bodies versus synaptic inputs.

Slow spontaneous IPSCs might result from a unique population of inhibitory synapses containing $GABA_A$ receptors composed of subunits with only slow kinetics [26,28,39]. Another possibility is that perisynaptic tonic receptors are activated by spillover of GABA from nearby fast phasic synapses without activating $GABA_A$ receptors that contribute to fast responses [29,33,39,59]. The low frequency of occurrence of these slow spontaneous events might result from the unique anatomical arrangement required for such an event to occur. Both mechanisms have been suggested previously to explain $GABA_A$ slow responses observed in the hippocampus [28,31,32,59]. At this time, it is not possible to distinguish between activation of synapses with purely slow $GABA_A$ receptors versus spillover. Selective agonists and antagonists for both types of receptors or specific knockout/knockin genetic models will be needed for future studies [26].

The results presented here focused primarily on inhibitory synaptic inputs to excitatory pyramidal neurons. However, we observed spontaneous slow $GABA_A$ IPSCs in neocortical interneurons as well. Because of the diversity of subtypes of inhibitory neurons, a systematic analysis of each subtype will be required to make meaningful statistical arguments for each subtype and is beyond the scope of this study [23,24]. $GABA_A$ slow IPSC responses evoked in inhibitory neurons may provide a fruitful direction for future investigations.

Conclusion

Inhibitory synaptic inputs of neocortical neurons are an important component of feedforward and feedback processing [1-3,9,60]. It has been shown that visual evoked field potentials display differential sensitivity to $GABA_A$ and $GABA_B$ blockade for afferent feedforward components versus long-range feedback interactions [6]. It will be important to determine what role slow GABA responses have in specific aspects of visual feedforward or feedback processing. New genetic and molecular tools will be necessary to study these mechanisms *in vivo*.

Intrinsic network oscillations also appear to be controlled by inhibitory inputs [38,61]. $GABA_A$ slow IPSCs displayed durations ranging from 30 to 125 ms; therefore, slow $GABA_A$-mediated IPSCs might play a role in controlling alpha or beta rhythm (8 to 30 Hz) activity [25,62-65]. Incorporating $GABA_A$ slow IPSCs into computational models of cortical function will help improve our understanding of cortical information processing.

Methods

Electrophysiology

All procedures and protocols were approved by the Institutional Animal Care Committee at Stanford University and adhered to guidelines published by the National Institutes of Health. All experiments were performed on rat brain slices dissected from the visual cortex of young (P16-P28) male Long-Evans rats (Charles River Laboratories, Wilmington, MA). The preparation of rat neocortical brain slices was identical to that described in Sceniak and MacIver [66].

Briefly, parasagittal brain slices were cut in cold (4°C) oxygenated (95% O_2, 5% CO_2) artificial cerebral spinal fluid (ACSF) into 350 μm thick sections. The brain slices were then placed in room temperature ACSF containing the following: NaCl, KCl, $MgSO_4$, NaH_2PO_4 $NaCHO_3$, dextrose and $CaCl_2$ in the following mM concentrations: 124, 3.5, 2, 1.25, 26, 10 and 2 [25,66,67]. All recordings were conducted at room temperature with the same ACSF. Slices were visualized with an upright microscope (Zeiss Axioskop, Germany), using a water immersion objective (40×, Zeiss) with near infrared illumination and a CCD camera (COHU, San Diego, CA).

Whole-cell patch clamp recordings were amplified with a Multiclamp 700A patch clamp amplifier (Axon Instruments, Foster City, CA). Voltage and current traces were sampled at 10 kHz. Data acquisition was controlled using the commercially available software package, pCLAMP 9.0 (Axon Instruments, Foster City, CA). Recording electrodes were filled with a KCl-based internal solution containing, in mM 100 KCl, 10 EGTA, 40 HEPES, 5 $MgCl_2$, 2 Na_2ATP and 1.5 Na_2GTP (pH 7.3 and osmolarity 290–295 mOsm).

In a subset of cells (n = 4), artifacts from space clamp were tested by recording spontaneous IPSCs with a CsCl-based internal electrode solution. Internal patch pipette solution contained, in mM, 140 CsCl, 2 $MgCl_2$, 40 HEPES, 10 EGTA, 2 Na_2ATP, 1.5 Na_2GTP (pH 7.3 with CsOH and 290–295 mOsM).

Synaptically evoked responses were elicited using bipolar stimulating electrodes fabricated with either theta-glass pipettes or pairs of epoxy-coated tungsten microelectrodes encased in a single barrel glass pipette (Harvard Apparatus, Holliston, MA). Stimulating electrodes of either theta-glass or tungsten (10–30 μm or 5 MΩ tips respectively) were positioned near the dendritic field of targeted pyramidal cells (100–300 μm from the dendritic axis). Stimulus intensity was optimized for each cell to produce monosynaptic near-threshold amplitude IPSCs (0.005 mA to 1.0 mA, 0.1 ms pulse). Minimal responses were determined to be near-threshold level when decreasing the stimulus

intensity resulted in failures < 50% of the time and the response no longer decreased in amplitude. Minimally evoked responses also displayed amplitudes that were similar to spontaneously occurring events. Synaptically evoked IPSC responses were recorded with the cell clamped at its resting membrane potential (-65 ± 5 mV) to avoid imposing additional leak currents within the cell.

All EPSCs were blocked by bath application of (±)-2-amino-5-phosphonopentanoic acid (APV) (100 μM) and 6-cyano-7-nitro-quinoxaline-2, 3-dione (CNQX) (17.2 μM) to block NMDA and AMPA receptor-mediated synaptic currents respectively. Spontaneous IPSCs were recorded with each cell voltage-clamped at its resting membrane potential using KCl-based internal solution that reversed the driving force of the chloride currents and increased the amplitude of small IPSCs.

Drug treatment with furosemide (1 mM) and picrotoxin (150 μM) were always preceded by data collection of at least five runs with 10 repeats over a 20 m period to determine baseline response. Drugs were allowed to perfuse into the tissue for at least 15 m with responses monitored during this period, in order to determine response stability. Next, drug responses were collected with a minimum of 5 runs with 10 repeats over 15 m for each condition. Responses were analyzed for the last 3 runs (10 repeats each) of each condition during the most stable periods of drug perfusion and control conditions.

Data collection and analysis

Average electrode series resistance ranged from 10–20 MΩ after break in. Whole-cell recording seal impedance ranged from 1–3 GΩ. Average resting membrane potentials were -65 ± 5 mV. Recordings with seals less than 1 GΩ or resting membrane potentials greater than -55 mV were not included in the analysis. In voltage-clamp experiments, access resistance was monitored using a 20 ms voltage step deviation from the holding potential and repeated throughout the duration of the recording.

Spontaneous current recordings were collected and digitally stored (30 s long continuous current recording, 10 repeats or more, 10 kHz sampling). IPSC events were automatically detected through a computer algorithm (custom routines written in MATLAB) that identified peaks that were negatively shifted at least 2 standard deviations from the baseline. Mean baseline noise floor was 12 ± 5 pA. Slow events were selected initially based on visual inspection. A control group of IPSCs was randomly selected from all recordings to compare to the sampled slow IPSC population. The control IPSC events were randomly selected from the recordings that contained the visually identified slow IPSCs as well as from randomly selected recordings that lacked slow IPSCs.

For a representative neuron all events (greater than 2 SD above baseline) were analyzed and the kinetics compared with our random sample of events from all cells. The kinetic and amplitude properties were quantitatively similar for the single cell estimates with all events included and the random sample population across all cells (see Results).

Isolated spontaneous and evoked IPSCs were fitted with a double exponential equation to determine the decay time constant after the IPSC peak. The double exponential empirical function was of the following form:

$$y = A_1 e^{-x/t_1} + A_2 e^{-x/t_2}.$$

The parameters A_1 and A_2 represent the amplitude of the two components. The equation was fitted to the data using a constrained nonlinear least squares optimization routine (fmincon, Matlab). Nonlinear constraints were used such that τ_2 was greater than τ_1. Rise times were estimated as the time from 10 to 90% of the peak amplitude (t_1 and t_2 respectively) from baseline (see Figure 1). For fast events the rise times show binning at the sampling rate (see Figure 2A), because the estimates were not fitted or interpolated.

IPSC events were classified as slow or fast based on the rise time and decay time kinetics [47]. Correlations of rise time and decay time revealed a clustering into two unique populations. The demarcation between the fast and slow population was determined from the local minimum in the intensity plot of the correlation between rise time and decay time. Slow events were defined as IPSCs with rise times greater than 3 ms and decay time constants greater than 20 ms. Events that were beyond the constraints of the slow classification were considered fast events (see Figure 2A).

All data analysis and statistical tests were performed using MATLAB Release 12 (Mathworks, Natick, MA). All statistics are expressed as the mean ± standard deviation unless otherwise stated. Statistical significance of data from control and drug treated groups was determined using the Student's *t* test or Wilcoxon signed-rank test, for cases where the data was not normal on a linear scale. One-way multivariate analysis of variance (MANOVA) was used to compare differences across groups of multivariate data. Multi-way factorial ANOVA was used to compare differences from three or more independent groups. Time locked current and voltage traces were averaged in Matlab to produce mean evoked IPSCs.

Histology

Excitatory pyramidal neurons were targeted for all recordings. However, histological reconstructions revealed that a

subset of the cells (5 out of 52) were inhibitory aspiny interneurons. All electrically evoked synaptic responses were recorded from excitatory layer 4 pyramidal neurons. In some cases the histological analysis was not successful and therefore, it is possible that layer 4 and 5 neurons have been combined. Cell body morphology and spiking responses were consistent across all pyramidal cells.

In order to perform histological reconstructions the internal solution contained 0.5% to 1% neurobiotin (Vector Laboratories, Burlingame, CA). Slices were processed with the Elite VectaStain ABC kit (Vector Laboratories, Burlingame, CA) according to the protocol described by Hamam and Kennedy [68]. Stained slices were mounted wet with Vectashield mounting medium (Vector Laboratories, Burlingame, CA). Digital images were reconstructed using Adobe Photoshop (Adobe Systems Incorporated, San Jose, CA) to determine cell morphology and the presence of dendritic spines.

Animals/Chemicals

All rats were obtained from Charles Rivers Laboratories (Wilmington, MA). Chemicals for the ACSF were reagent grade or better and obtained from J. T. Baker (Philadelphia, PA) or Sigma-Aldrich (St. Louis, MO).

Additional material

Additional file 1

IPSC analysis of all events for a representative cell. For a representative neuron, all isolated IPSC events (n = 461) were sampled and fitted to determine the amplitude, rise time and decay time. The vertical arrows indicate the population geometric mean for the amplitude (52.6 ± 44.6 pA) rise time (1.1 ± 0.9 ms) and the decay time constant (7.3 ± 3.1 ms). The average rate was 1.9 Hz across all sampled events (30 s long data records, 8 repeats, 240 s total). These measures are quantitatively similar to our random sample of fast IPSC events.

Click here for file

[http://www.biomedcentral.com/content/supplementary/1471-2202-9-8-S1.eps]

Acknowledgements

We thank Dr. Bruce Winegar for comments on the manuscript. This research was supported by NIH grantsR01GM54767 and R01DA17884.

References

1. Borg-Graham LJ, Monier C, Fregnac Y: **Visual input evokes transient and strong shunting inhibition in visual cortical neurons.** *Nature* 1998, **393(6683):**369-373.
2. Anderson JS, Carandini M, Ferster D: **Orientation tuning of input conductance, excitation, and inhibition in cat primary visual cortex.** *J Neurophysiol* 2000, **84(2):**909-926.
3. Hirsch JA, Martinez LM, Pillai C, Alonso JM, Wang Q, Sommer FT: **Functionally distinct inhibitory neurons at the first stage of visual cortical processing.** *Nat Neurosci* 2003, **6(12):**1300-1308.
4. Sceniak MP, Hawken MJ, Shapley R: **Visual spatial characterization of macaque V1 neurons.** *J Neurophysiol* 2001, **85(5):**1873-1887.
5. Hupe JM, James AC, Girard P, Bullier J: **Response modulations by static texture surround in area V1 of the macaque monkey do not depend on feedback connections from V2.** *J Neurophysiol* 2001, **85(1):**146-163.
6. Kasamatsu T, Mizobe K, Sutter EE: **Muscimol and baclofen differentially suppress retinotopic and nonretinotopic responses in visual cortex.** *Vis Neurosci* 2005, **22(6):**839-858.
7. Ozeki H, Sadakane O, Akasaki T, Naito T, Shimegi S, Sato H: **Relationship between excitation and inhibition underlying size tuning and contextual response modulation in the cat primary visual cortex.** *J Neurosci* 2004, **24(6):**1428-1438.
8. Eysel UT, Shevelev IA, Lazareva NA, Sharaev GA: **Orientation tuning and receptive field structure in cat striate neurons during local blockade of intracortical inhibition.** *Neuroscience* 1998, **84(1):**25-36.
9. Sillito AM: **GABA mediated inhibitory processes in the function of the geniculo-striate system.** *Prog Brain Res* 1992, **90:**349-384.
10. Chance FS, Abbott LF, Reyes AD: **Gain modulation from background synaptic input.** *Neuron* 2002, **35(4):**773-782.
11. Gabernet L, Jadhav SP, Feldman DE, Carandini M, Scanziani M: **Somatosensory integration controlled by dynamic thalamocortical feed-forward inhibition.** *Neuron* 2005, **48(2):**315-327.
12. Gonchar Y, Burkhalter A: **Distinct GABAergic targets of feedforward and feedback connections between lower and higher areas of rat visual cortex.** *J Neurosci* 2003, **23(34):**10904-10912.
13. Cruikshank SJ, Lewis TJ, Connors BW: **Synaptic basis for intense thalamocortical activation of feedforward inhibitory cells in neocortex.** *Nat Neurosci* 2007, **10(4):**462-468.
14. Connors BW, Malenka RC, Silva LR: **Two inhibitory postsynaptic potentials, and GABAA and GABAB receptor-mediated responses in neocortex of rat and cat.** *J Physiol* 1988, **406:**443-468.
15. Farinas I, DeFelipe J: **Patterns of synaptic input on corticocortical and corticothalamic cells in the cat visual cortex. II. The axon initial segment.** *J Comp Neurol* 1991, **304(1):**70-77.
16. Farinas I, DeFelipe J: **Patterns of synaptic input on corticocortical and corticothalamic cells in the cat visual cortex. I. The cell body.** *J Comp Neurol* 1991, **304(1):**53-69.
17. Buhl EH, Han ZS, Lorinczi Z, Stezhka VV, Karnup SV, Somogyi P: **Physiological properties of anatomically identified axo-axonic cells in the rat hippocampus.** *J Neurophysiol* 1994, **71(4):**1289-1307.
18. Buhl EH, Szilagyi T, Halasy K, Somogyi P: **Physiological properties of anatomically identified basket and bistratified cells in the CA1 area of the rat hippocampus in vitro.** *Hippocampus* 1996, **6(3):**294-305.
19. Buhl EH, Tamas G, Szilagyi T, Stricker C, Paulsen O, Somogyi P: **Effect, number and location of synapses made by single pyramidal cells onto aspiny interneurones of cat visual cortex.** *J Physiol* 1997, **500 (Pt 3):**689-713.
20. Tamas G, Lorincz A, Simon A, Szabadics J: **Identified sources and targets of slow inhibition in the neocortex.** *Science* 2003, **299(5614):**1902-1905.
21. Mohler H: **GABA(A) receptor diversity and pharmacology.** *Cell Tissue Res* 2006, **326(2):**505-516.
22. Connors BW: **GABAA- and GABAB-mediated processes in visual cortex.** *Prog Brain Res* 1992, **90:**335-348.
23. Markram H, Toledo-Rodriguez M, Wang Y, Gupta A, Silberberg G, Wu C: **Interneurons of the neocortical inhibitory system.** *Nat Rev Neurosci* 2004, **5(10):**793-807.
24. Monyer H, Markram H: **Interneuron Diversity series: Molecular and genetic tools to study GABAergic interneuron diversity and function.** *Trends Neurosci* 2004, **27(2):**90-97.
25. Bacci A, Rudolph U, Huguenard JR, Prince DA: **Major differences in inhibitory synaptic transmission onto two neocortical interneuron subclasses.** *J Neurosci* 2003, **23(29):**9664-9674.
26. Prenosil GA, Schneider Gasser EM, Rudolph U, Keist R, Fritschy JM, Vogt KE: **Specific subtypes of GABAA receptors mediate phasic and tonic forms of inhibition in hippocampal pyramidal neurons.** *J Neurophysiol* 2006, **96(2):**846-857.
27. Galarreta M, Hestrin S: **Properties of GABAA receptors underlying inhibitory synaptic currents in neocortical pyramidal neurons.** *J Neurosci* 1997, **17(19):**7220-7227.

28. Pearce RA: **Physiological evidence for two distinct GABAA responses in rat hippocampus.** *Neuron* 1993, **10(2):**189-200.
29. Hajos N, Mody I: **Synaptic communication among hippocampal interneurons: properties of spontaneous IPSCs in morphologically identified cells.** *J Neurosci* 1997, **17(21):**8427-8442.
30. Lukatch HS, MacIver MB: **Voltage-clamp analysis of halothane effects on GABA(A fast) and GABA(A slow) inhibitory currents.** *Brain Res* 1997, **765(1):**108-112.
31. Banks MI, Li TB, Pearce RA: **The synaptic basis of GABAA,slow.** *J Neurosci* 1998, **18(4):**1305-1317.
32. Banks MI, Pearce RA: **Kinetic differences between synaptic and extrasynaptic GABA(A) receptors in CA1 pyramidal cells.** *J Neurosci* 2000, **20(3):**937-948.
33. Hardie JB, Pearce RA: **Active and passive membrane properties and intrinsic kinetics shape synaptic inhibition in hippocampal CA1 pyramidal neurons.** *J Neurosci* 2006, **26(33):**8559-8569.
34. Sigel E, Baur R: **Electrophysiological evidence for the coexistence of alpha1 and alpha6 subunits in a single functional GABA(A) receptor.** *J Neurochem* 2000, **74(6):**2590-2596.
35. Bosman LW, Rosahl TW, Brussaard AB: **Neonatal development of the rat visual cortex: synaptic function of GABAA receptor alpha subunits.** *J Physiol* 2002, **545(Pt 1):**169-181.
36. Minier F, Sigel E: **Positioning of the alpha-subunit isoforms confers a functional signature to gamma-aminobutyric acid type A receptors.** *Proc Natl Acad Sci U S A* 2004, **101(20):**7769-7774.
37. Burt DR: **Alpha subunit position and GABA receptor function.** *Sci STKE* 2005, **2005(270):**pe5.
38. Banks MI, White JA, Pearce RA: **Interactions between distinct GABA(A) circuits in hippocampus.** *Neuron* 2000, **25(2):**449-457.
39. Mody I, Pearce RA: **Diversity of inhibitory neurotransmission through GABA(A) receptors.** *Trends Neurosci* 2004, **27(9):**569-575.
40. Andrasfalvy BK, Mody I: **Differences between the scaling of miniature IPSCs and EPSCs recorded in the dendrites of CA1 mouse pyramidal neurons.** *J Physiol* 2006, **576(Pt 1):**191-196.
41. Salin PA, Prince DA: **Electrophysiological mapping of GABAA receptor-mediated inhibition in adult rat somatosensory cortex.** *J Neurophysiol* 1996, **75(4):**1589-1600.
42. Salin PA, Prince DA: **Spontaneous GABAA receptor-mediated inhibitory currents in adult rat somatosensory cortex.** *J Neurophysiol* 1996, **75(4):**1573-1588.
43. Szabadics J, Varga C, Molnar G, Olah S, Barzo P, Tamas G: **Excitatory effect of GABAergic axo-axonic cells in cortical microcircuits.** *Science* 2006, **311(5758):**233-235.
44. Xiang Z, Huguenard JR, Prince DA: **Synaptic inhibition of pyramidal cells evoked by different interneuronal subtypes in layer v of rat visual cortex.** *J Neurophysiol* 2002, **88(2):**740-750.
45. Thomson AM, West DC, Hahn J, Deuchars J: **Single axon IPSPs elicited in pyramidal cells by three classes of interneurones in slices of rat neocortex.** *J Physiol* 1996, **496 (Pt 1):**81-102.
46. Andreasen M, Lambert JD: **Factors determining the efficacy of distal excitatory synapses in rat hippocampal CA1 pyramidal neurones.** *J Physiol* 1998, **507 (Pt 2):**441-462.
47. Ling DS, Benardo LS: **Restrictions on inhibitory circuits contribute to limited recruitment of fast inhibition in rat neocortical pyramidal cells.** *J Neurophysiol* 1999, **82(4):**1793-1807.
48. Magee JC, Cook EP: **Somatic EPSP amplitude is independent of synapse location in hippocampal pyramidal neurons.** *Nat Neurosci* 2000, **3(9):**895-903.
49. Williams SR, Stuart GJ: **Dependence of EPSP efficacy on synapse location in neocortical pyramidal neurons.** *Science* 2002, **295(5561):**1907-1910.
50. Hefti BJ, Smith PH: **Distribution and kinetic properties of GABAergic inputs to layer V pyramidal cells in rat auditory cortex.** *J Assoc Res Otolaryngol* 2003, **4(1):**106-121.
51. Lavoie AM, Tingey JJ, Harrison NL, Pritchett DB, Twyman RE: **Activation and deactivation rates of recombinant GABA(A) receptor channels are dependent on alpha-subunit isoform.** *Biophys J* 1997, **73(5):**2518-2526.
52. Smith SS, Gong QH: **Neurosteroid administration and withdrawal alter GABAA receptor kinetics in CA1 hippocampus of female rats.** *J Physiol* 2005, **564(Pt 2):**421-436.
53. Gingrich KJ, Roberts WA, Kass RS: **Dependence of the GABAA receptor gating kinetics on the alpha-subunit isoform: implications for structure-function relations and synaptic transmission.** *J Physiol* 1995, **489 (Pt 2):**529-543.
54. Wafford KA, Thompson SA, Thomas D, Sikela J, Wilcox AS, Whiting PJ: **Functional characterization of human gamma-aminobutyric acidA receptors containing the alpha 4 subunit.** *Mol Pharmacol* 1996, **50(3):**670-678.
55. DeFazio RA, Keros S, Quick MW, Hablitz JJ: **Potassium-coupled chloride cotransport controls intracellular chloride in rat neocortical pyramidal neurons.** *J Neurosci* 2000, **20(21):**8069-8076.
56. Jarolimek W, Lewen A, Misgeld U: **A furosemide-sensitive K+-Cl- cotransporter counteracts intracellular Cl- accumulation and depletion in cultured rat midbrain neurons.** *J Neurosci* 1999, **19(12):**4695-4704.
57. Jin X, Huguenard JR, Prince DA: **Impaired Cl- extrusion in layer V pyramidal neurons of chronically injured epileptogenic neocortex.** *J Neurophysiol* 2005, **93(4):**2117-2126.
58. Kapur A, Pearce RA, Lytton WW, Haberly LB: **GABAA-mediated IPSCs in piriform cortex have fast and slow components with different properties and locations on pyramidal cells.** *J Neurophysiol* 1997, **78(5):**2531-2545.
59. Mody I: **Distinguishing between GABA(A) receptors responsible for tonic and phasic conductances.** *Neurochem Res* 2001, **26(8-9):**907-913.
60. Sceniak MP, Chatterjee S, Callaway EM: **Visual Spatial Summation in Macaque Geniculocortical Afferents.** *J Neurophysiol* 2006.
61. Lukatch HS, MacIver MB: **Physiology, pharmacology, and topography of cholinergic neocortical oscillations in vitro.** *J Neurophysiol* 1997, **77(5):**2427-2445.
62. Destexhe A: **Spike-and-wave oscillations based on the properties of GABAB receptors.** *J Neurosci* 1998, **18(21):**9099-9111.
63. Blumenfeld H, McCormick DA: **Corticothalamic inputs control the pattern of activity generated in thalamocortical networks.** *J Neurosci* 2000, **20(13):**5153-5162.
64. Jones EG: **Thalamic circuitry and thalamocortical synchrony.** *Philos Trans R Soc Lond B Biol Sci* 2002, **357(1428):**1659-1673.
65. Freund TF: **Interneuron Diversity series: Rhythm and mood in perisomatic inhibition.** *Trends Neurosci* 2003, **26(9):**489-495.
66. Sceniak MP, MacIver MB: **Cellular actions of urethane on rat visual cortical neurons in vitro.** *J Neurophysiol* 2006, **95(6):**3865-3874.
67. Bacci A, Huguenard JR, Prince DA: **Long-lasting self-inhibition of neocortical interneurons mediated by endocannabinoids.** *Nature* 2004, **431(7006):**312-316.
68. Hamam BN, Kennedy TE: **Visualization of the dendritic arbor of neurons in intact 500 microm thick brain slices.** *J Neurosci Methods* 2003, **123(1):**61-67.

Publish with **BioMed Central** and every scientist can read your work free of charge

"BioMed Central will be the most significant development for disseminating the results of biomedical research in our lifetime."

Sir Paul Nurse, Cancer Research UK

Your research papers will be:

- available free of charge to the entire biomedical community
- peer reviewed and published immediately upon acceptance
- cited in PubMed and archived on PubMed Central
- yours — you keep the copyright

Submit your manuscript here:
http://www.biomedcentral.com/info/publishing_adv.asp

BioMedcentral

Modulation of Firing Rate by Background Synaptic Noise Statistics in Rat Visual Cortical Neurons

Michael P. Sceniak and Shasta L. Sabo

J Neurophysiol 104:2792-2805, 2010. First published 25 August 2010; doi:10.1152/jn.00023.2010

You might find this additional info useful...

Supplemental material for this article can be found at:
http://jn.physiology.org/content/suppl/2010/12/06/jn.00023.2010.DC1.html

This article cites 57 articles, 28 of which can be accessed free at:
http://jn.physiology.org/content/104/5/2792.full.html#ref-list-1

This article has been cited by 1 other HighWire hosted articles
Using computer simulations to determine the limitations of dynamic clamp stimuli applied at the soma in mimicking distributed conductance sources
Risa J. Lin and Dieter Jaeger
J Neurophysiol, May , 2011; 105 (5): 2610-2624.
[Abstract] [Full Text] [PDF]

Updated information and services including high resolution figures, can be found at:
http://jn.physiology.org/content/104/5/2792.full.html

Additional material and information about ***Journal of Neurophysiology*** can be found at:
http://www.the-aps.org/publications/jn

This infomation is current as of December 22, 2011.

Journal of Neurophysiology publishes original articles on the function of the nervous system. It is published 12 times a year (monthly) by the American Physiological Society, 9650 Rockville Pike, Bethesda MD 20814-3991. Copyright © 2010 by the American Physiological Society. ISSN: 0022-3077, ESSN: 1522-1598. Visit our website at http://www.the-aps.org/.

Downloaded from jn.physiology.org on December 22, 2011

J Neurophysiol 104: 2792–2805, 2010.
First published August 25, 2010; doi:10.1152/jn.00023.2010.

Modulation of Firing Rate by Background Synaptic Noise Statistics in Rat Visual Cortical Neurons

Michael P. Sceniak and Shasta L. Sabo
Neuroscience and Pharmacology, Case Western Reserve University, Cleveland, Ohio

Submitted 11 January 2010; accepted in final form 21 August 2010

Sceniak MP, Sabo SL. Modulation of firing rate by background synaptic noise statistics in rat visual cortical neurons. *J Neurophysiol* 104: 2792–2805, 2010. First published August 25, 2010; doi:10.1152/jn.00023.2010. It has been shown previously that background synaptic noise modulates the response gain of neocortical neurons. However, the role of the statistical properties of the noise in modulating firing rate is not known. Here, the dependence of firing rate on the statistical properties of the excitatory to inhibitory balance (EI) in cortical pyramidal neurons was studied. Excitatory glutamatergic and inhibitory GABAergic synaptic conductances were simulated as two stochastic processes and injected into individual neurons in vitro through use of the dynamic-clamp system. Response gain was significantly modulated as a function of the statistical interactions between excitatory and inhibitory synaptic conductances. Firing rates were compared for noisy synaptic conductance steps by varying either the EI correlation or the relative delay between correlated E and I. When inhibitory synaptic conductances exhibited a short temporal delay (5 ms) relative to correlated excitatory synaptic conductances, the response gain was increased compared with noise with no temporal delay but with an equivalent degree of correlation. The dependence of neuronal firing rate on the EI delay of the noisy background synaptic conductance suggests that individual excitatory pyramidal neurons are sensitive to the EI balance of the synaptic conductance. Therefore the statistical EI interactions encoded within the synaptic subthreshold membrane fluctuations are able to modulate neuronal firing properties.

INTRODUCTION

Interactions of excitatory and inhibitory (EI) synaptic inputs are crucial for cortical circuit function. EI interactions have been shown to play a crucial role in regulating and establishing cortical receptive field properties (Borg-Graham et al. 1998; Connors et al. 1988; Douglas and Martin 2004; Douglas et al. 1991; Ferster and Jagadeesh 1992; Hirsch and Martinez 2006; Ozeki et al. 2009). Recent studies have suggested that EI balance, or the ratio of excitatory to inhibitory synaptic inputs, is one form of EI interaction that helps establish the intrinsic excitability of the cortex (Leger et al. 2005; Maffei et al. 2004; Trevelyan and Watkinson 2005; Xing and Gerstein 1996). It has been shown that correlated activity within the cortical network critically influences the response of individual neurons within the network (de la Rocha et al. 2007; Destexhe et al. 2001; Fellous et al. 2003; Nirenberg and Latham 2003; Pillow et al. 2008; Rauch et al. 2003). Besides the EI balance, other possible EI interactions exist within the cortical network that might regulate neuronal information processing such as the correlated firing and relative timing of excitation and inhibition. Such interactions have implications for neuronal processing where global network activity seems to modulate receptive field properties of individual neurons (Sceniak et al. 1999; Series et al. 2003).

Recent studies have shown that noisy background synaptic activity modulates the responsiveness of cortical neurons relative to a quiescent state (Chance et al. 2002; Fellous et al. 2003; Higgs et al. 2006; Mitchell and Silver 2003; Prescott and De Koninck 2003). Noisy background synaptic activity composed of excitatory and inhibitory synaptic conductances, simulated using the dynamic-clamp technique, have been shown to modulate response firing rate gain. Whether individual neurons are capable of detecting particular EI statistical interactions embedded within the noisy background signals has not been addressed previously.

A given excitatory pyramidal cortical neuron receives thousands of synaptic inputs from many neurons within the circuit (Douglas and Martin 1991, 2004; Thomson et al. 2002b). The pattern of activity converging on a given pyramidal neuron contains the sum of these synaptic inputs. Background synaptic activity can originate from either feed-forward or recurrent feedback drive from either excitatory or inhibitory neurons or a combination of these sources (Douglas and Martin 2004; Stepanyants et al. 2009). By simulating the pattern of activity converging on a given neuron, the interactions and statistics of excitatory and inhibitory synaptic conductance inputs can be controlled to determine their effects on firing rate. Such patterns of activity represent the relative correlation and synchrony of excitation and inhibition.

This study addresses to what extent the firing rate encoding of individual neurons is modulated by the EI interactions that define the background synaptic noise conductance. The EI interactions tested include the degree of correlation between excitation and inhibition and the relative temporal delay or phase between correlated excitation and inhibition. Using the dynamic-clamp system and a stochastic model to simulate in vivo–like synaptic conductances (Destexhe et al. 2001, 2003; Fellous et al. 2003), we were able to design particular synaptic conductance stimuli that isolated the effects of these particular EI interactions. Synaptic noise signals with identical mean, SD, and EI correlation were generated that differed in whether there was a relative delay between excitation and inhibition.

Understanding the effects of global network activity on the information processing of individual neurons is a necessary component to determining how network states contribute to perception and sensation (Fregnac 2003; de la Rocha et al. 2007; El Boustani et al. 2009). Classifying the population of synaptic inputs from the cortical network according to the statistical interactions between the excitatory and inhibitory synaptic inputs that make up the network allows us to deter-

Address for reprint requests and other correspondence: M. P. Sceniak, Case Western Reserve Univ., Dept. of Pharmacology, Wood Bldg. W343, 2109 Adelbert Rd., Cleveland, OH 44106 (E-mail: michael.sceniak@case.edu).

 0022-3077/10 Copyright © 2010 The American Physiological Society

Downloaded from jn.physiology.org on December 22, 2011

mine the response modulation from network activity in a reduced model system. Given the complexity of cortical networks, this allows one to reduce the problem to manageable comparisons and more straightforward interpretations. Our results indicate that neurons are sensitive to these subtle statistical interactions between excitation and inhibition and need to be considered in models of cortical function.

METHODS

All procedures and protocols used in this study adhere to published guidelines of the National Institutes of Health and were approved by the Institutional Animal Care and Use Committee at Case Western Reserve University. Rat brain slices were cut from dissected visual cortex of young adult (28–32 days postnatal) Long-Evans rats (Charles River Laboratories, Wilmington, MA). Animals used for the data in Figs. 6 and 7 were 14–21 days old. Initially, rats were anesthetized with isoflurane (4%). The brain was dissected and temporarily (<30 s) placed in ice-cold (1–4°C) oxygenated (95% O_2-5% CO_2) artificial cerebral spinal fluid (ACSF), composed of the following (in mM): 126 NaCl, 1 NaH_2PO_4, 25 $NaHCO_3$, 25 dextrose, 3 KCl, 2 $MgSO_4$, and 2 $CaCl_2$. Brain slices were cut in oxygenated ice-cold ACSF into 350-μm slices and placed in a holding chamber with 30–35°C ACSF that gradually (<30 min) equilibrated to room temperature (25°C).

Brain slices were transferred from the holding chamber after 1–2 h and placed in a submersion-recording chamber with a heated water jacket (Warner Instruments, Hamden, CT). Slices were perfused with oxygenated 30–35°C gravity-fed ACSF (2–4 ml/min). ASCF temperature was maintained with a ThermoClamp-1 (Automate Scientific, Berkeley, CA) inline heater and temperature controller. Neurons were visualized with an Olympus BX51WI microscope (Olympus America, Central Valley, PA) equipped with a water immersion objective (20×, with 2× after magnification) with near-infrared wavelength illumination, differential interference contrast optics (DIC), and a CCD camera (OLY-150, Olympus America) with contrast enhancement.

Electrophysiology

Membrane potentials and currents were collected using a Multi-clamp 700B patch clamp amplifier (Axon Instruments, Foster City, CA) and digitized with a Digidata 1440A analog to digital converter that was controlled by the pClamp 10.2 software package (Axon Instruments). Recording electrodes were filled with a K-gluconate–based internal solution composed of the following (in mM): 100 K-gluconate, 20 KCl, 10 phosphocreatine, 5 $MgCl_2$, 10 HEPES, 4 Na-ATP, and 0.3 Na-GTP (pH 7.3 and 290–300 mOsm). Some experiments (Figs. 6 and 7) were performed with the following internal electrode solution (in mM): 100 K-gluconate, 1 EGTA, 5 $MgCl_2$, 40 HEPES, 2 Na-ATP, and 0.3 Na-GTP (pH 7.3 and 290–300 mOsm). Electrode resistance ranged from 4 to 8 MΩ, and whole cell patch recordings were made with seal resistances of 1–3 GΩ. Successful whole cell recordings had resting membrane potentials of −57 mV or more negative. Average electrode series resistance ranged from 10 to 30 MΩ after whole cell patching. Recordings with seals <1 GΩ or resting potentials greater than −57 mV were not included in the analysis.

Excitatory pyramidal neurons were selected from within rat primary visual cortical layer 5. Pyramidal neurons were selected to establish the most homogeneous population possible. Pyramidal neurons were selected initially based on spiking and intrinsic electrical membrane properties and confirmed through histological reconstructions using biocytin fills (Sceniak and Maciver 2006, 2008).

Dynamic clamp

Conductance injection was accomplished through use of a computer-based dynamic-clamp system. The computer contained an Intel-based motherboard running the real-time Linux operating system (RTAI, www.rtai.org), with an open source data acquisition hardware driver (COMEDI, www.comedi.org) and open source dynamic-clamp software (RTXI; Dorval et al. 2001). Data acquisition and control was accomplished through a National Instruments data acquisition board (PCI-6251, Austin, TX) and interface breakout box (BNC-2090, National Instruments). The dynamic-clamp system sampled voltage measures at 15 kHz. The computer used for the dynamic-clamp system contained a dual microprocessor-based motherboard (Intel, Core 2 Duo, Santa Clara, CA) running at 2.53 GHz. Stimuli were constructed and delivered via custom written RTXI modules according to the equations described below.

Point conductance model

The synaptic conductance injected into the soma of each cell was generated from the point conductance model to simulate noisy background synaptic activity (Destexhe et al. 2001, 2003; Fellous et al. 2003). Excitatory and inhibitory synaptic conductances were combined by Ohm's law and Kirchhoff's current law to produce a total synaptic current to drive individual neurons to produce action potentials (Fig. 1). The total synaptic current, I_{syn}, was calculated in real time from the instantaneous membrane potential measure, V_m, and the time dependent excitatory, $g_e(t)$, and inhibitory, $g_i(t)$ synaptic conductances

$$I_{syn} = g_e(t)\left(V_m - E_e\right) + g_i(t)\left(V_m - E_i\right) \quad (1)$$

The reversal potential for glutamatergic excitation and GABAergic inhibition were $E_e = 0$ mV and $E_i = -75$ mV, respectively (Fig. 1), consistent with previous reports (Chance et al. 2002; Fellous et al. 2003).

The excitatory and inhibitory conductances used to simulate noisy background synaptic activity were defined by two stochastic processes based on the Ornstein-Uhlenbeck process originally introduced to describe Brownian motion (Destexhe et al. 2001). The time-dependent equations for these two processes for excitation, $g_e(t)$, and inhibition, $g_i(t)$, were as follows

$$\frac{dg_e(t)}{dt} = \frac{1}{\tau_e}\left[g_e(t) - g_{e0}\right] + \sqrt{D_e}\chi_1(t) \quad (2a)$$

$$\frac{dg_i(t)}{dt} = \frac{1}{\tau_i}\left[g_i(t) - g_{i0}\right] + \sqrt{D_i}\chi_2(t) \quad (2b)$$

The stochastic processes for excitation and inhibition were defined by the mean conductances, g_{e0} and g_{i0}, the time constants, τ_e and τ_i, and the noise diffusion coefficients, D_e and D_i. The stochastic process for excitation and inhibition also contained a Gaussian white noise random variable, $\chi_1(t)$ and $\chi_2(t)$, respectively, each with zero mean and unit SD. The SD of these stochastic processes is known analytically (Destexhe et al. 2001; Gillespie 1996)

$$\sigma^2 = \frac{D\tau}{2} \quad (3)$$

Throughout all experiments, the SD of excitation, σ_e, and inhibition, σ_i, were matched ($\sigma_e = \sigma_i$). The inhibitory mean, μ_i, was greater than σ_i. The time constants for excitation, τ_e, and inhibition, τ_i, were 2.7 and 10.5 ms, respectively. The mean excitatory conductance, μ_e, and E and I SD ($\sigma_e = \sigma_i$) were varied during the experiments to elicit action potential discharge (Fig. 1). These parameters (μ_e, σ_e, and σ_i) were optimized for each cell to achieve a range of firing rates.

The degree of correlation between the stochastic processes for excitation and inhibition was defined by taking the matrix product of a Gaussian random number, $\chi_1(t)$, and the Cholesky factorization ($C = LL^T$) of the correlation matrix, X. The correlation matrix for generating two noise signals with a correlation of 0.5 is given by

Downloaded from jn.physiology.org on December 22, 2011

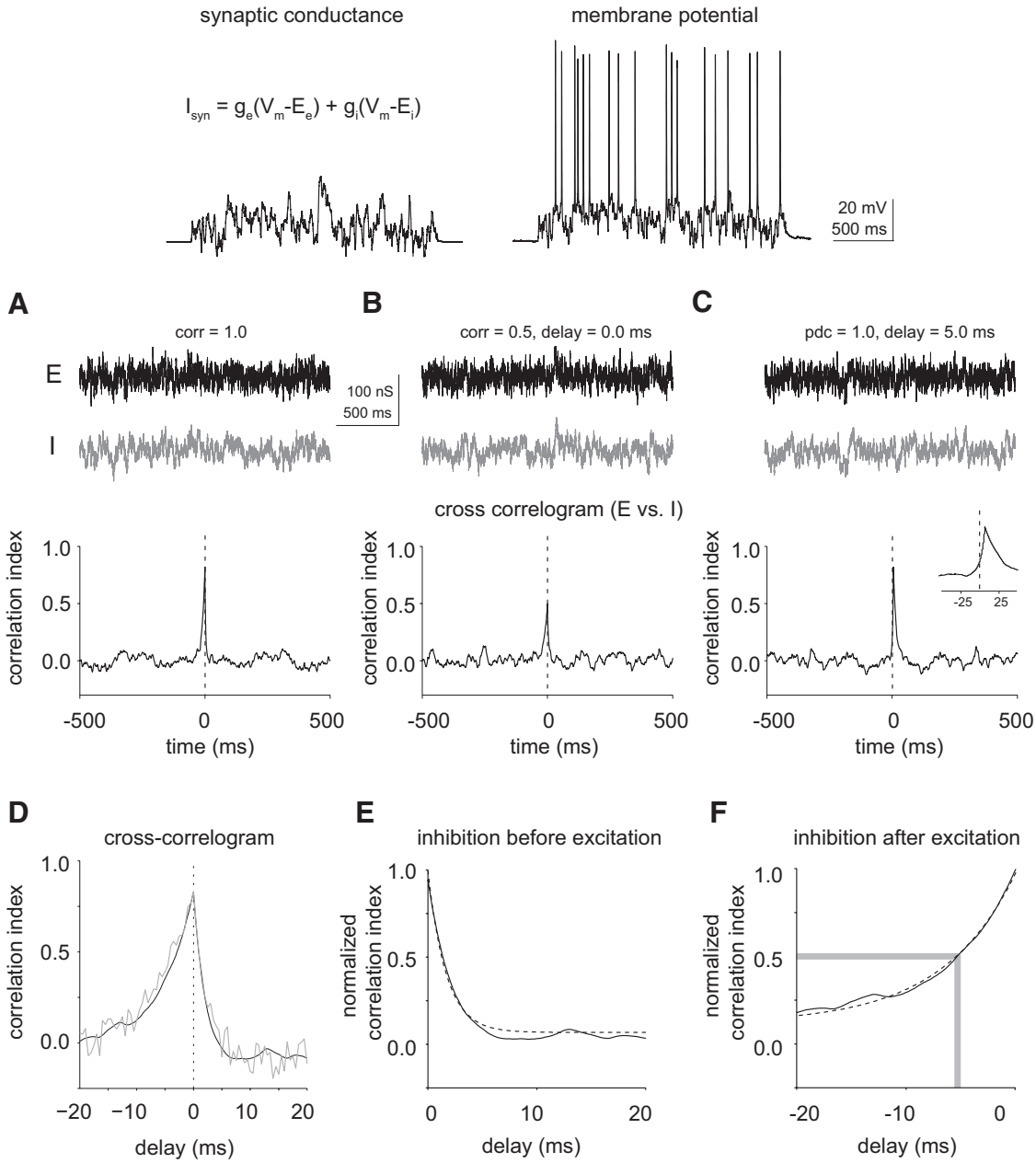

FIG. 1. Statistical interaction between excitation and inhibition. The synaptic current, I_{syn}, was calculated in real time based on the instantaneous membrane potential recoding and the time sampled conductances for excitation and inhibition (top box). Simulated synaptic noise based on the O-U stochastic processes allowed for the independent control of the excitatory and inhibitory mean (μ_e and μ_i) and SD (σ_e and σ_i). Excitation and inhibition were combined such that they were either uncorrelated (data not shown), (*A*) correlated, (*B*) partially correlated with no excitatory to inhibitory balance (EI) delay, or (*C*) correlated with an EI delay. The degree of correlation between excitation and inhibition scales the peak of the cross-correlogram (*A* and *B*, *bottom*). Before temporally shifting the inhibitory synaptic array to generate an EI delay, the correlation between excitation and inhibition, or the predelay correlation (pdc), is 1.0. The EI delay (5 ms) causes the cross-correlation peak to shift from 0 (*C*, *bottom*). (*D*) Plot of correlation as a function of delay to determine the transformation from EI delay to correlation. Conductances defined by a temporal delay between excitation and inhibition display a corresponding correlation, which corresponds to the cross-correlation at time shift zero (vertical dashed line in *C*, see *inset* for expansion of the region around 0). Negative delay values indicate conditions where inhibition preceded excitation (enlarged in *E*), whereas positive delay values represent the condition where inhibition followed excitation (enlarged in *F*). The solid gray curve in *D* shows the correlation resulting from the simulation of excitatory and inhibitory conductances with corresponding delays for a single 2 s-long noise trace. The solid black curves in *D–F* are the average correlation over 20 repeats of the simulation, with unique random sequences for each repeat. Vertical dashed line indicates 0 delay in *D*. Exponential equations (dashed curves in *E* and *F*) were fitted separately to each tail of the normalized correlation transformation function. The fitted parameters of the exponential were used to determine the correlation for a given excitatory to inhibitory relative delay. The thick gray lines indicate the delay value at a correlation of 0.5.

$$X = \begin{bmatrix} 1 & 0.5 \\ 0.5 & 1 \end{bmatrix} \quad (4)$$

Therefore a new random variable, $\chi_2(t)$, was generated with a defined degree of correlation between excitation and inhibition

$$\chi_2 = C \cdot \chi_1 \quad (5)$$

To introduce a time delay, Δt, between excitation and inhibition, $\chi_2(t)$ was shifted Δt time samples to produce a new random variable $\chi_2(t + \Delta t)$. The corresponding excitatory and inhibitory random variables, $\chi_1(t)$ and $\chi_2(t + \Delta t)$, were used to solve for g_e and g_i, respectively. The

Downloaded from jn.physiology.org on December 22, 2011

predelay correlation (*pdc*) is the degree of correlation before a time shift. The time shift decreases the correlation (at time = 0) in a manner that depends on Δt: larger delays decrease the correlation more than smaller delays. Therefore the new EI correlation was calculated for excitatory and inhibitory conductances, $g_e(t)$ and $g_i(t)$, after the imposed time shift. This calculation yields the correlation with an EI delay (see RESULTS and Fig. 1) and permits comparison to unshifted input conductances (i.e., EI synaptic conductances with no delay).

Data analysis

All data analyses were performed using custom-written functions in Matlab R2009a (The Mathworks, Natick, MA) and functions written in C++ under Linux. All statistics are expressed as the median unless otherwise stated. Statistical significance was determined using the Wilcoxon signed rank sum test and analysis of covariance (ANCOVA) where appropriate. Time-locked voltage responses were analyzed to determine spike rates correlated to their corresponding conductance injections. Spikes were analyzed off-line by determining voltage deflections above a threshold (> -10 mV). The correlation, cross-correlation, autocorrelation, and power spectra were calculated using Matlab functions.

Sigmoid, Michaelis-Menten, functions were fitted to the firing rate responses, using nonlinear constrained optimization (fmincon, Matlab function). For response functions where there was a response decrease with an increase in the sampled parameter, x (normalized correlation), or an increase in the sampled parameter, y (conductance), the following sigmoid functions were used

$$R(x) = R_{max} - R_{max}\frac{x^n}{(x^n + c_{50}^n)} + b \tag{6}$$

and

$$R(y) = R_{max}\frac{y^n}{(y^n + c_{50}^n)} + b \tag{7}$$

respectively. The parameters R_{max}, n, b, and c_{50} represent the maximal firing rate, acceleration rate exponent, response offset rate, and the value of x or y that produces one half the maximal response, respectively. The offset, b, was set to the spontaneous firing rate (0 in all cases). The maximal response, R_{max}, was constrained to within ±50% of the empirical maximum response. The half-saturation value, c_{50}, was constrained to the maximum of the sampled parameters, x. The acceleration exponent, n, was constrained to be between 0.1 and 10. The slope of the sigmoid function was calculated as the first derivative of the sigmoid function evaluated at the half-maximal value, c_{50}, or

$$slope = \frac{Rn}{4c_{50}} \tag{8}$$

Conductance-based model neuron

Neuron model simulations were performed using the Matlab software package (Mathworks, Natick, MA). Differential equations for the Hodgkin-Huxley–like model were solved numerically using fourth-order Runge-Kutta. The differential equations were solved for each time step (0.01 ms, 100 kHz) for 2 s of total time. The differential equation used to describe the neuron total current was as follows

$$C_m\frac{dV_m}{dt} = I_{syn} - g_{leak}(V_m - E_{leak}) - I_{Na} - I_K - I_M - I_A - I_H - I_{NaP} \tag{9}$$

where the membrane capacitance, $C_m = 1.3$ nF, the leak conductance, $g_{leak} = 0.01$ μS, and the leak reversal potential, $E_{leak} = -70$ mV. The synaptic current I_{syn}, was defined by

$$I_{syn} = -g_{e_{syn}}(V_m - E_e) - g_{i_{syn}}(V_m - E_i) \tag{10}$$

where the excitatory, g_e, and inhibitory, g_i, conductances were defined by the point conductance model describe above with excitatory synaptic reversal potential, $E_e = 0$ mV and inhibitory synaptic equilibrium potential, $E_i = -80$ mV. The Na^+ and K^+ reversal potentials were calculated through the Nernst equation, where the internal and external concentrations for Na^+ and K^+ were (in mM) 20, 150, 100, and 6, respectively, and the temperature was equal to 30°C.

Action potentials

The spike Na^+ and K^+ currents were defined as

$$I_{Na} = \bar{g}_{Na}(V_m - E_{Na}) \cdot m_{Na}^3 \cdot h_{Na} \tag{11}$$

$$I_K = \bar{g}_K(V_m - E_K) \cdot m_K^4 \tag{12}$$

where the maximal conductance $\bar{g}_{Na} = 50$ μS, sodium reversal $E_{Na} = 50$ mV, $\bar{g}_K = 5$ μS, and $E_K = -72$ mV. The activation and inactivation dynamics were modeled as first order processes, where

$$\tau_m(V_m)\frac{dm}{dt} = m_\infty(V_m) - m \tag{13}$$

and

$$\tau_h(V_m)\frac{dh}{dt} = h_\infty(V_m) - h \tag{14}$$

The steady-state activation (m_∞) and inactivation (h_∞) equations and the time constants, τ_m and τ_h, were defined by Winograd et al. (2008).

Spike-frequency adaptation

The spike-frequency adaptation current I_M was defined as

$$I_M = \bar{g}_M \cdot p \cdot (V_m - E_K) \tag{15}$$

where

$$\frac{dp}{dt} = (p_\infty - p)/\tau_p(V_m) \tag{16}$$

with $\bar{g}_M = 0.13$ μS. The steady-state activation (p_∞) equation for the I_M current and the time constant, τ_p($\tau_{pmax} = 1.1$ s), were defined by Winograd et al. (2008).

The Connors-Stevens current I_A was defined as follows

$$I_A = \bar{g}_A \cdot m^3 \cdot h \cdot (V_m - E_A) \tag{17}$$

where $\bar{g}_A = 0.5$ μS, and the activation and inactivation dynamics were modeled as first-order processes as described above (*Eqs. 13* and *14*), using the steady-state activation (m_∞) and inactivation (h_∞) equations defined by Dayan and Abott (2005).

Hyperpolarization-activated current

The hyperpolarization-activated cationic current I_H was defined as follows

$$I_H = \bar{g}_H \cdot m \cdot (V_m - E_H) \tag{18}$$

where $\bar{g}_H = 0.03$ μS and $E_H = -43$ mV. The activation dynamics were modeled as first-order processes as above (*Eq. 13*) using the steady-state (m_∞) equation defined by Huguenard and McCormick (1992).

Persistent sodium conductance

$$I_{NaP} = \bar{g}_{NaP} \cdot m \cdot h_p \cdot (V_m - E_{Na}) \tag{19}$$

where $\bar{g}_{NaP} = 1.1$ μS and E_{Na} was defined as above. The activation dynamics were modeled as above (*Eq. 13*) and the steady-state (m_∞ and h_∞) equations were as defined by Wu et al. (2005).

Downloaded from jn.physiology.org on December 22, 2011

RESULTS

Construction of in vivo–like synaptic noise barrages with defined statistical properties

To determine the extent to which EI synaptic interactions modulate neuronal response output, we studied neuronal firing rate output in excitatory cortical pyramidal neurons as a function of the statistical interaction between excitatory and inhibitory synaptic inputs, using a dynamic-clamp system (Fig. 1). Noisy synaptic conductances for excitation and inhibition were generated based on the Ornstein-Uhlenbeck (O-U) stochastic point conductance model (see METHODS).

In vivo, neurons receive a variety of inputs from both excitatory and inhibitory neurons, and the correlation between these inputs depends on the circuitry. Correlations are sensitive to both the synchrony and the timing of the inputs. Therefore we examined how neurons respond to correlations between excitatory and inhibitory synaptic conductances using two approaches to vary correlation between E and I. Correlations caused by synchrony of E and I can be simulated using Cholesky factorization to empirically define the degree of correlation (see METHODS). Using this approach, synaptic noise signals were generated that ranged from conditions where excitatory and inhibitory synaptic conductances were completely uncorrelated (corr = 0.0, data not shown) to conditions where excitation and inhibition were completely correlated (corr = 1.0; Fig. 1*A*). Figure 1*B* shows an intermediate level of correlation between excitation and inhibition (corr = 0.5).

To simulate correlations between excitation and inhibition that depend on the relative timing of E and I, correlated excitatory and inhibitory conductance arrays were time shifted relative to each other to produce a given temporal delay (EI delay; Fig. 1*C*). In all cases, excitatory and inhibitory noise used to produce synaptic noise with an EI delay were initially generated with a correlation of 1.0 before time shifting the inhibitory noise array to produce the EI delay. We refer to this initial correlation as the predelay correlation (pdc = 1.0). The delay causes the correlation between E and I to be reduced (Fig. 1*C*). EI delays ranged from 0 to 200 ms. With the exception of Fig. 1, *D* and E, inhibition always followed excitation. For conditions where excitation and inhibition were correlated (Fig. 1*B*) or correlated with an EI delay (Fig. 1*C*), the means and SD of the synaptic conductances were held constant across conditions. This allowed us to isolate the effects of correlation and temporal-delay on firing rate responsiveness independent of EI input statistics.

To directly compare firing rate responses for noise that is systematically varied in EI correlation with no EI delay (e.g., as in Fig. 1, *A* and *B*) to noise with a fixed correlation but with a varying EI delay (e.g., as in Fig. 1*C*), it is necessary to match the responses for actual correlation. For a given temporal delay between excitatory and inhibitory synaptic noise conductances, there is a corresponding correlation measure that depends on the magnitude of the delay (Fig. 1*D*): increasing the EI delay decreases the degree of correlation. To determine the degree of EI correlation in the presence of the EI delay, the cross-correlation of the noise conductances (20 kHz, 2 s; pdc = 1.0) was calculated at a range of EI delays. These EI delays appear as a horizontal shift in the cross-correlation peak (Fig. 1*C*, *bottom*). The correlation for each EI delay corresponds to the cross-correlation of the two time-shifted signals at time = 0 (Fig. 1, *A–C*).

To create a transformation from EI delay to correlation, correlation was plotted as a function of EI delay (gray curve, Fig. 1*D*). The average delay versus correlation function was estimated as the mean correlation for 20 repeats (black curve, Fig. 1*D*). Fitting separate exponential functions (dashed curve, Fig. 1 *E* and *F*) to the average correlation values (solid black curve, Fig. 1*D*) as a function of negative EI delays (inhibition before excitation, Fig. 1*E*) and positive EI delays (inhibition after excitation, Fig. 1*F*) provided a complete description of the transformation from EI delay to correlation. This transformation could be used to determine the correlation of any two noise signals (pdc = 1.0) that contained an EI delay. For example, a 5-ms EI delay between excitatory and inhibitory noise signals yields a correlation of 0.5 (with inhibition following excitation). The values obtained from this transformation then allowed direct comparison of neuronal spike rate responses for two different noise signals with equivalent correlations defined by either *1*) EI delay or *2*) Cholesky factorization without an EI delay.

Effects of EI correlation and timing on neuronal firing rates

To determine whether neurons can detect the EI noise balance statistics between the stimuli constructed as described above, synaptic noise signals were generated and introduced into pyramidal neurons in layer 5 of visual cortical slices using the dynamic-clamp technique, and the resulting neuronal spiking responses were recorded. For a given noise conductance step composed of a combination of excitation and inhibition, conditions where excitation and inhibition were correlated by varying degrees (corr = 0–1) were compared with conditions where excitation and inhibition were completely correlated (pdc = 1.0) but were offset by an EI delay (delay = 0–50 ms) such that inhibition lagged excitation (Fig. 2). The mean and SD of excitation and inhibition were optimized for each recorded neuron to produce a moderate firing rate (7–30 Hz) when excitation and inhibition were uncorrelated with no time delay (corr = 0.0). Each conductance step (2 s, 15-kHz sample rate) was repeated two times, and the firing rates were averaged. Representative mean firing rate responses are shown for three neurons (Fig. 2). Firing rate responses showed a clear dependence on both EI correlation (Fig. 2, *A1–A3*) and EI temporal delay (Fig. 2, *B1–B3*). Response rates were consistently reduced when E and I noise conductances were correlated and contained little temporal delay. Similar dependence on EI correlation and response enhancement for noise containing an EI delay were observed when intracellular calcium was buffered with EGTA in the patch pipette (Supplementary Fig. S1).[1]

To directly compare firing rates for noise steps with and without EI delays, the degree of EI correlation was estimated for EI noise with a temporal delay using the exponential fits of correlation shown in Fig. 1*F*. Neuronal mean firing rate responses for noise with correlations defined by EI delay were plotted as a function of correlation (Fig. 2, *C1–C3*, black). For comparison, spiking responses for noise with equivalent EI correlations but no delay (gray) were overlaid on the delay

[1] The online version of this article contains supplemental data.

Downloaded from jn.physiology.org on December 22, 2011

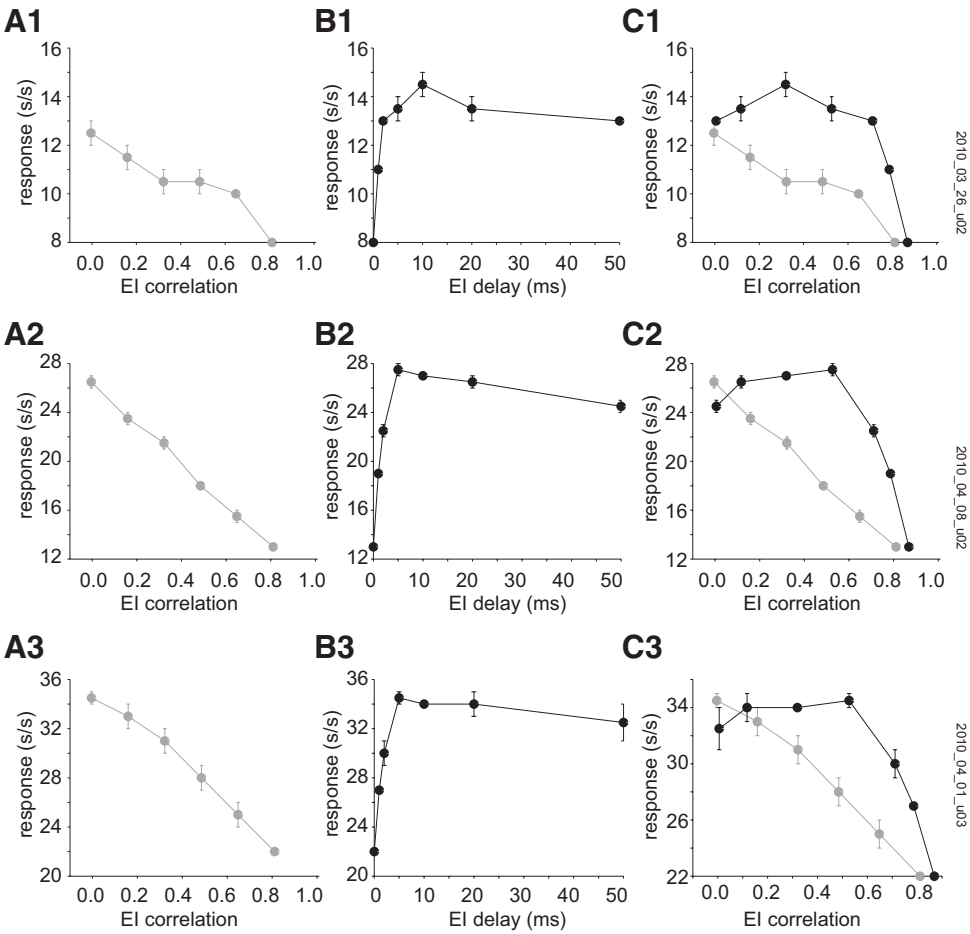

FIG. 2. Background synaptic noise statistics modulate response gain. Representative firing rate response (mean rate) curves as a function of EI synaptic noise statistics are shown for 3 representative neurons (1–3). Conductance injection was a step function of combined excitation and inhibition with either a given EI correlation (corr = 0.0–1.0, gray curves) or a given EI delay (delay = 0–50 ms, black curves). *A1–A3*: firing rate responses (spikes/s) are shown as a function of the degree of EI correlation for correlations defined empirically by Cholesky factorization, as illustrated in Fig. 1, *A* and *B*. *B1–B3*: responses for the same neurons in *A* to varied EI temporal delays are shown in the center column. Inhibition followed excitation, as shown in Fig. 1, *C* and *F*. *C1–C3*: responses to both types of EI noise (i.e., with or without temporal delay) are shown as a function of their corresponding EI correlation. The EI correlation for synaptic noise steps with a temporal delay were estimated from the delay to correlation relationship in Fig. 1*D*. The response gain was greater for synaptic noise signals that contain a temporal delay between excitation and inhibition (black) compared with those with equivalent predefined correlations between excitation and inhibition but no temporal delay (gray).

plots (Fig. 2, *C1–C3*, gray). The change in mean firing rate response as a function of correlation was steeper for noise containing an EI delay and elevated for small EI temporal delay values (<10 ms; Fig. 2, *C1–C3*). Thus in the presence of an EI delay, the response gain was increased at high EI correlations, and responses saturated and stabilized at a high firing rate over a wide range of low EI correlations. In contrast, in the absence of EI delay, responses appeared more linear over the entire range of EI correlations.

Firing rate response curves were fitted with empirical functions. Fits for the same three neurons as shown in Fig. 2 are shown in Fig. 3, *A1–A3*. For EI noise with a temporal delay, firing rate responses as a function of EI correlation were sigmoid shaped and fitted with a sigmoidal, Michaelis-Menten equation (black curves, Fig. 3, *A1–A3*). However, firing rate responses as a function of EI correlation without an EI temporal delay were well fit by a linear regression (gray curves, Fig. 3, *A1–A3*). To make statistical comparisons across the population, parameters were extracted from the fits. For delay data, the maximum response, linear region (c_{50}), and slope of the response function in the linear region were estimated from the sigmoidal fits (see METHODS). For EI noise responses without a temporal delay, comparable measures were extracted from the linear fits.

Across the population of recorded neurons ($n = 29$), the parameters of the sigmoid fits to the response versus EI delay noise steps were compared with the linear fits of the response versus no EI delay steps (Fig. 4). Although the no delay EI steps produced responses that were linear over the range of EI correlations tested, the EI delay responses displayed responses that were linear only near the higher EI correlation values (median $c_{50} = 0.79$; Fig. 4*A*). For very low correlation EI noise (corr = 0.1), the firing rate responses to EI noise with a temporal delay and without an EI delay (Fig. 4, *B* and *C*) were not significantly different [$r^2 = 0.95$, median response % difference (delay – no delay) = 2.9, $P > 0.05$, Wilcoxon rank sum test]. For EI noise steps with moderately correlated EI noise (corr = 0.75; Fig. 4, *D* and *E*), firing rate responses were significantly greater [$r^2 = 0.97$, median response % difference (delay – no delay) = 17.5, $P = 2.8 \times 10^{-6}$, Wilcoxon rank sum test], across the population, for EI noise steps with a temporal delay than with no delay. Therefore on average, response enhancement resulting from EI temporal delay tends to occur from correlated noise (corr = 0.75) rather than essentially uncorrelated noise (corr = 0.1), and the responses are not significantly different for very low correlation EI noise.

The slope of the response versus correlation tuning curves was compared for EI noise with an EI temporal delay (estimated at the c_{50} value, or linear region, for sigmoid fits, see METHODS) to EI noise steps with no delay (linear fits; Fig. 4, *F* and *G*). On average, the slopes were uncorrelated ($r^2 = 0.53$) and significantly greater for EI noise steps with a temporal delay [median slope % difference (delay – no delay) = −61.6, $P = 38 \times 10^{-6}$, Wilcoxon rank sum test]. Overall, there is much greater sensitivity (spike rate per corr, slope) to change

Downloaded from jn.physiology.org on December 22, 2011

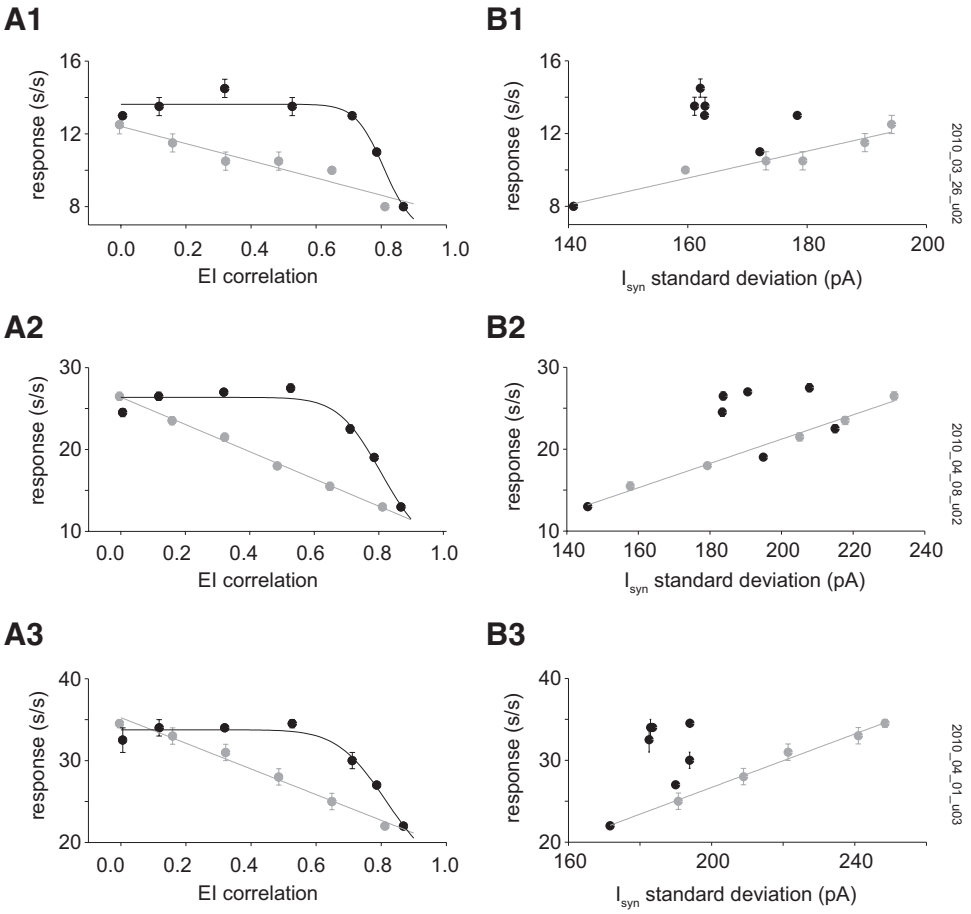

FIG. 3. Representative response vs. EI correlation tuning curves. *A1–A3*: 3 representative neurons (same cells as in Fig. 3) are shown with mean firing rate responses fitted to empirical functions. Response curves evoked with EI noise conductance steps with no EI temporal delay (gray curve) were well fitted with a linear regression. EI delay noise steps were fitted with sigmoidal functions (black curve). *B1–B3*: firing rate responses are shown as a function of the SD of the dynamic clamp command current, I_{syn}, for noise steps with a temporal delay (black) and without an EI temporal delay (gray) next to the corresponding response vs. correlation plots. Gray line is the linear regression of the response vs. I_{syn} SD for the no EI delay condition.

in firing rate as a function of EI correlation when an EI temporal delay is present.

The extent to which the SD of the dynamic clamp command current, I_{syn}, might be responsible for differences in the firing rate observed with and without an EI temporal delay was also examined (Figs. 3, *B1–B3,* and 5). To test this, firing rate responses for stimuli with and without an EI temporal delay were plotted versus the SD of the current injected into each neuron from the combined E and I conductances (I_{syn}, see METHODS; Fig. 3, *B1–B3*). Responses for representative neurons are shown next to their corresponding firing rate versus correlation curves (Fig. 3, *right* and *left columns*, respectively). The mean firing rates for EI noise with a delay (black, Fig. 3, *B1–B3*) were consistently greater compared with responses for stimuli with no EI delay (gray, Fig. 3, *B1–B3*), even for matched I_{syn} SD. To make statistical comparisons across the population of neurons, firing rates as a function of the SD of I_{syn} were fitted with linear regressions (Fig. 3, *B1–B3*). To determine how well the linear model accounts for the data, the best fit r^2 estimate was calculated and compared for both delay and no delay responses (Fig. 5*A*). The responses resulting from correlated EI noise without a delay were well fit with a linear regression, because the goodness of fit was typically high (>0.9) for responses with no EI delay. However, responses with an EI delay were not fit well by a linear model. The goodness of fit was significantly lower when an EI delay was present [median r^2 % difference (delay – no delay) = −13, $P = 1.12 \times 10^{-10}$, Wilcoxcon rank sum test; Fig. 5*B*]. The slopes of both linear regressions were compared. Across the population, the slopes of the linear regression for firing rate versus I_{std} were also not correlated for responses resulting from noise steps with a temporal delay versus with no EI delay (r^2 = 0.23, $P = 0.68$, Wilcoxon rank sum test; Fig. 5). Because the firing rate responses as a function SD of I_{syn} were significantly different between noise steps with an EI temporal delay and with no EI temporal delay, the SD of the command current, I_{syn}, is not sufficient to explain the differences in response.

Effects of EI balance on neuronal firing rates

To determine the effects of synaptic EI noise statistics across a range of EI balances (defined as the ratio of mean excitation to inhibition, μ_e/μ_i), we sampled a range of excitatory mean conductances, μ_e, for a given excitatory SD, σ_e, and a fixed level of mean inhibition, μ_i, with SD, σ_i, (3 repeats of each excitatory mean conductance amplitude; 1-s step at 15 kHz). The response gain function (spike rate vs. mean excitatory conductance) was estimated for conductance steps with no noise (σ_e = 0 nS, μ_i = 15 nS, σ_i = 0 nS), noise with a defined correlation between excitation and inhibition (corr = 0.5, delay = 0 ms; σ_e = 15 nS, μ_i = 15 nS, σ_i = 15 nS) and noise (σ_e = 15 nS, μ_i = 15 nS, σ_i = 15 nS) with an EI delay (delay = 5 ms, corr = 0.5; Fig. 6, *A* and *B*). The correlations of the two random processes were identical (corr = 0.5; see Fig. 1*D*).

Conductance steps with noise that contained an EI delay (○) and with no EI delay (●) were compared with conductance steps (with the same mean conductance) with no noise (Fig. 6, *C–F*). Response functions resulting from conductance steps

Downloaded from jn.physiology.org on December 22, 2011

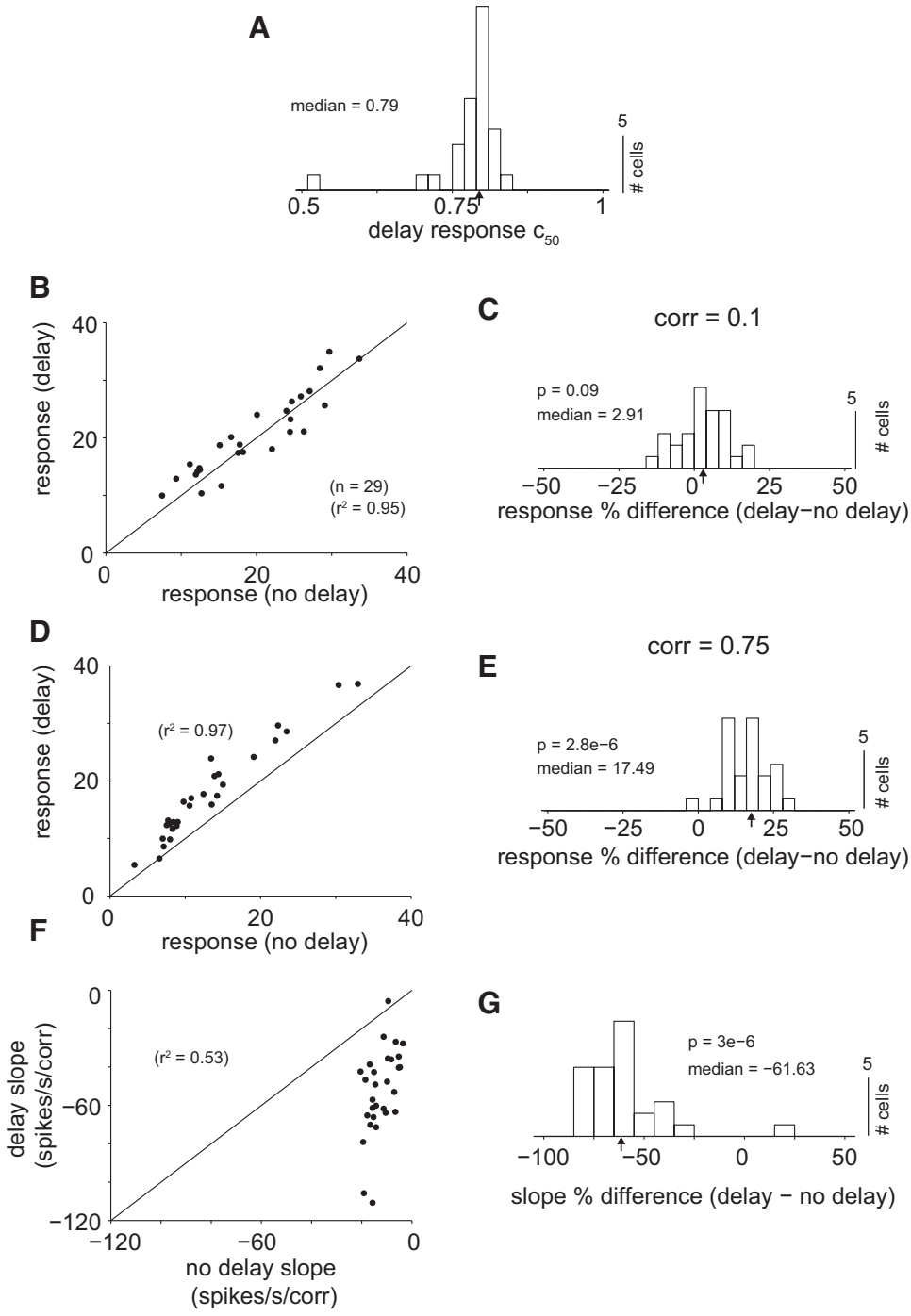

FIG. 4. Population analysis of response vs. EI correlation tuning curves. *A*: for EI noise with a temporal delay, the correlation that produced a half-maximal response, c_{50}, was extracted from the sigmoidal function fits and is shown across the population of cells (median = 0.79, $n = 29$). *B* and *C*: the mean firing rate responses are shown for noise steps with a temporal delay vs. without an EI temporal delay, estimated from the sigmoid and linear regression fits, respectively, at a low EI correlation (corr = 0.1). The responses are highly correlated ($r^2 = 0.95$) and are not significantly different from one another [median response % difference (delay – no delay) = 2.9]. Vertical arrow indicates the median in *C*. *D* and *E*: fitted response estimates are shown for high EI correlation (corr = 0.75). The mean firing rates with and without delay are correlated ($r^2 = 0.97$), and responses are significantly greater ($P = 2.8 \times 10^{-6}$, Wilcoxon rank sum test) for noise steps with an EI temporal delay [median response % difference (delay – no delay) = 17.5]. For scatter plots in *B* and *D*, firing rate responses are shown as spikes/s. *F* and *G*: the response vs. EI noise correlation slopes are shown for noise input with an EI temporal delay vs. no EI delay. The response slopes were estimated from the sigmoid fits and linear regressions, respectively. On average, the response vs. EI correlation slopes were significantly less ($P = 3 \times 10^{-6}$, Wilcoxon rank sum test) for noise steps lacking an EI delay [median slope % difference (delay – no delay) = −61.6] and were not significantly correlated ($r^2 = 0.53$).

with EI noise regardless of the presence of an EI delay (dashed and gray, Fig. 6, *A* and *B*) were shifted to the left and yielded higher firing rates for the same mean conductance compared with conductance steps with no noise (black curve, Fig. 6, *A* and *B*). Across the population ($n = 11$; Fig. 5*C*), there was a significant increase in responsiveness for noise steps both with no EI delay and with an EI delay [median R_{max} % change (noise – no noise) = 7 and 14%; $P = 0.005$ and $P = 0.005$, Wilcoxon signed rank sum test, respectively]. For noise conductance steps with an EI delay, there was a significant leftward shift of the response versus conductance function [median c_{50} % change (noise – no noise) = −10%, $P = 0.04$, Wilcoxon signed rank sum test] and an increase in the slope [median slope % change (noise – no noise) = 8%, $P = 0.01$, Wilcoxon signed rank sum test] compared with noiseless conductance steps (Fig. 6, *D* and *F*).

Synaptic noise composed of correlated excitation and inhibition with an EI delay (delay = 5 ms, corr = 0.5) was compared with correlated noise with no EI delay (corr = 0.5, delay = 0 ms; Figs. 6, *A* and *B*, and 7). Note that these two noise signals have identical EI correlations (corr = 0.5; Fig. 1). Gain response functions with identical correlation, but with or without an EI delay, showed differences in their firing rate responses (dashed vs. gray curve, Fig. 6, *A* and *B*). Across the

Downloaded from jn.physiology.org on December 22, 2011

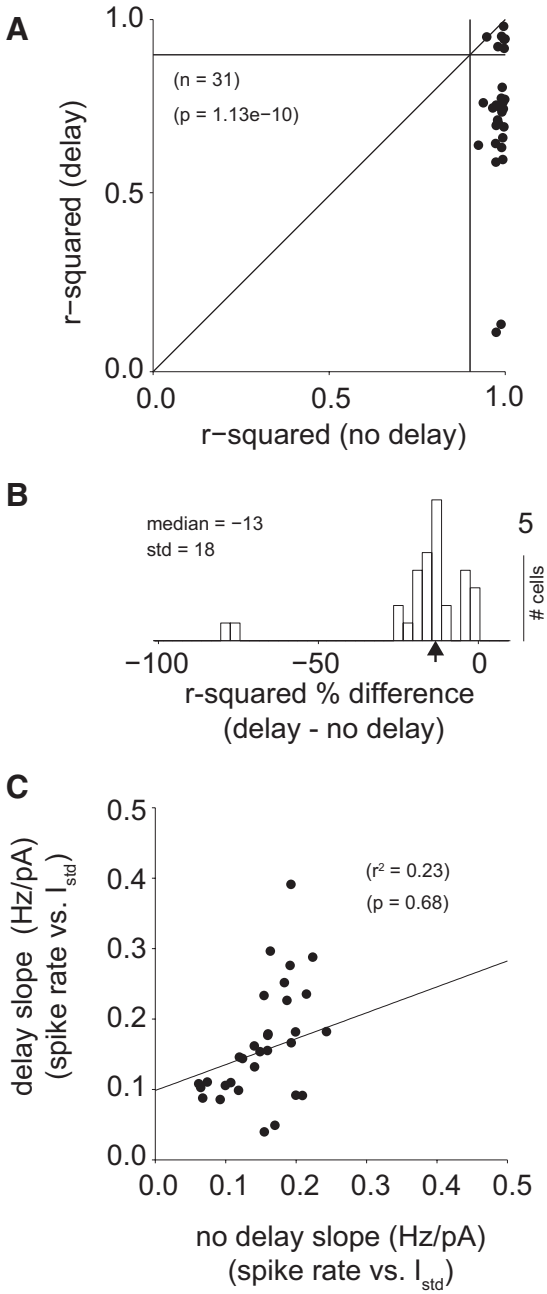

FIG. 5. Population analysis of response vs. command current SD. *A*: across the population of cells ($n = 31$), the response vs. command current SD was fitted with a linear regression. The r^2 goodness of fit was estimated for each curve on a cell by cell basis. Responses resulting from noise steps with no EI delay were well fitted by a linear regression ($r^2 > 0.9$, vertical line), but the majority of responses from noise steps with an EI temporal delay were poorly fitted with a linear regression ($r^2 < 0.9$, horizontal line). *B*: on average, the responses from noise steps with an EI delay produced lower r^2 values [median r^2 % difference (delay – no delay) = −13, vertical arrow]. *C*: the slopes of the linear regressions for firing rate vs. command current SD are shown. The slopes for responses resulting from noise steps with an EI delay were not significantly correlated ($r^2 = 0.23$) with slopes for responses resulting from noise steps with no EI delay.

population of sampled neurons ($n = 11$), the slope (as calculated at the c_{50} value) of the firing rate versus conductance response was significantly higher for noise that contained an EI delay [median slope % change (delay − no delay) = 10.1%, $P = 0.013$, Wilcoxon signed rank sum test; Fig. 7*D*]. EI synaptic noise conductance temporal delay also resulted in a slight but significant change in the maximum response [median R_{max} % change (delay − no delay) = 7%, $P = 0.02$, Wilcoxon signed rank sum test; Fig. 7*A*] and significant leftward shifts in the response functions [median c_{50} % change (delay − no delay) = −4%, $P = 0.014$, Wilcoxon signed rank sum test; Fig. 7*C*]. Therefore an EI delay with equivalent correlation produced response functions that were shifted leftward with an increase in absolute response, causing an increase in response gain or slope (Fig. 7*D*).

Synaptic noise in a Hodgkin-Huxley–like model neuron

To study whether the effects of EI interactions described above can be accounted for by spike currents and/or slow spike-frequency adaptation currents, the responses to background synaptic noise were examined using a conductance-based, Hodgkin-Huxley–like model neuron (see METHODS and Fig. 8). As with the dynamic-clamp recordings, the noisy synaptic conductances for excitation and inhibition were generated using the stochastic O-U model (see METHODS). The model neuron contained Na^+ and K^+ action potential conductances, a leak conductance, spike frequency adaptation conductances (I_M and I_A), the hyperpolarization-activated conductance (I_H), and a persistent sodium conductance (I_{NaP}), with conductance values chosen from estimates of cortical pyramidal neurons in the literature (see METHODS).

Analogous to the patch-clamp experiments, the firing rate of the conductance-based model neuron was quantified for conductance steps where excitatory and inhibitory synaptic conductances were correlated by varying degrees (corr = 0.0–1.0; Fig. 8*A*) to conductance steps where excitatory and inhibitory synaptic conductances were correlated (pdc = 1.0) but contained varying degrees of EI delay (0–200 ms, inhibition follows excitation; Fig. 8*B*). The correlation of EI noise steps containing an EI delay was estimated as described above in Fig. 1, *D* and *F,* and mean firing rates were plotted as a function of correlation. Firing rate responses resulting from stimulation with noise steps with an EI temporal delay were enhanced (black points, Fig. 8*C*) for moderately correlated noise (corr = 0.4–0.6) compared with noise with no EI delay (gray points, Fig. 8*C*).

Next, the data were fitted as described above for neuronal recordings. The response as a function of correlation was linear for noise with no EI delay (gray curve, Fig. 8*C*) and saturating for noise with an EI delay (black curve, Fig. 8*C*), similar to that observed from neuronal recordings. However, when the firing rate was plotted as a function of command current, I_{syn}, SD, the response enhancement was no longer observed (Fig. 8*D*). The linear regression fits of firing rate versus the SD of I_{syn} were statistically identical ($P > 0.05$, ANCOVA). Therefore unlike the neuronal recordings, the difference in response between noise steps with an EI delay and with no delay can be accounted for by differences in the SD of the synaptic current that result from the summed EI conductances. These modeled conductances are therefore insufficient to account for the observed firing rate properties in the presence of delayed inhibition. These results suggest that there are at least two mechanisms that contribute to neuronal responses to correlated E-I noise with a delay: one mechanism that is sensitive to the SD of the synaptic currents and

Downloaded from jn.physiology.org on December 22, 2011

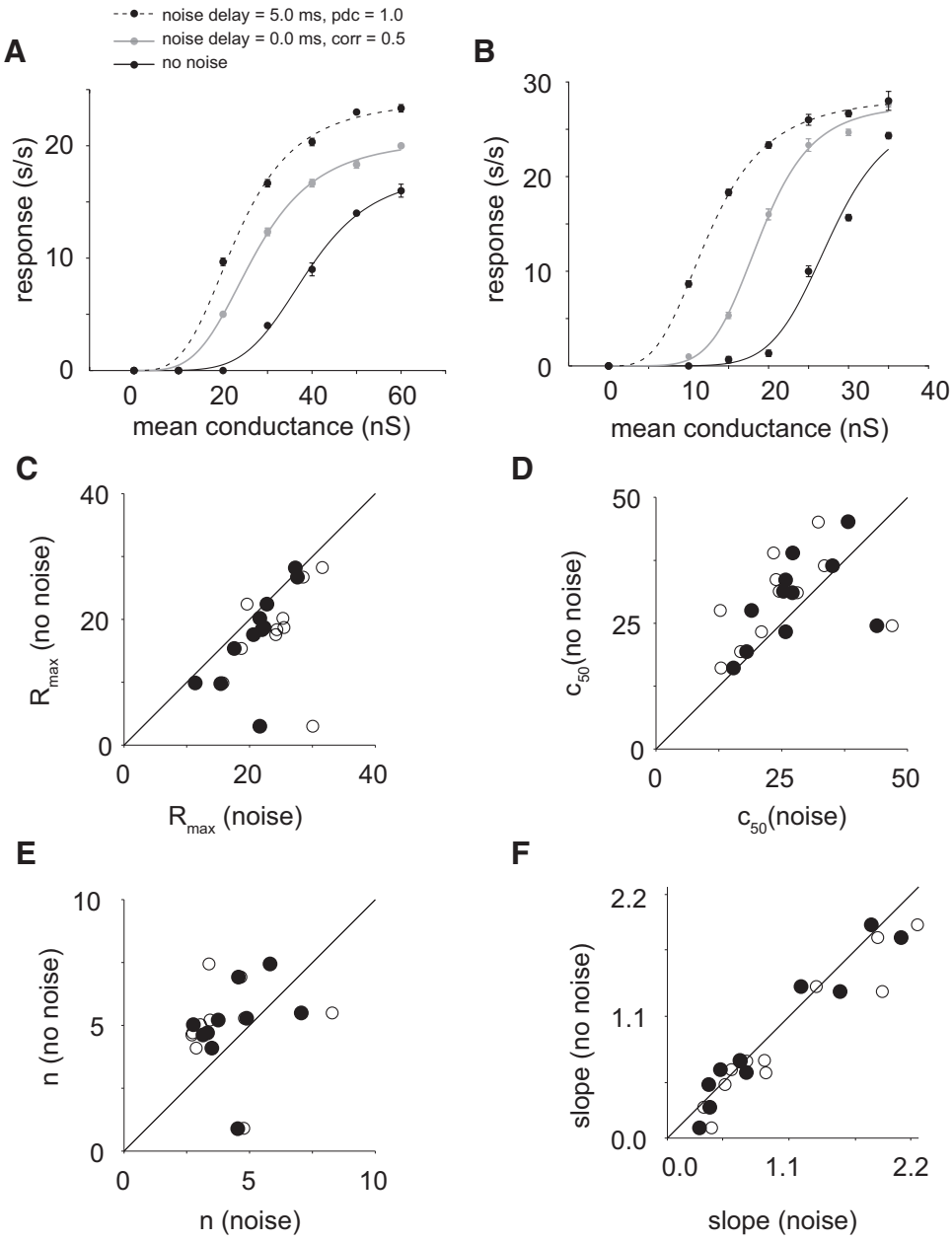

FIG. 6. Noise modulates the response gain as a function of the statistical balance between excitation and inhibition. *A* and *B*: the firing rate (Hz) response as a function of injected conductance mean is shown for 2 representative neurons. Black curves indicate conductance steps with no noise. Gray curves indicate conductance steps with the same mean conductance as the corresponding black curve with the addition of a synaptic noise (σ_e = 15 nS, σ_i = 15 nS, μ_i = 15 nS, μ_e = conductance step) composed of excitatory and inhibitory conductances with correlation of 0.5 and no EI delay. Dashed curves indicate response functions with mean conductance equal to the corresponding black curve with the addition of a synaptic noise (σ_e = 15 nS, σ_i = 15 nS, μ_i = 15 nS, and μ_e = conductance step) composed of excitatory and inhibitory synaptic conductances with a correlation of 0.5 (pdc = 1.0, delay = 5 ms; Fig. 1). *C–F*: across the population (n = 11), synaptic noise increased the firing rate responsiveness. Individual function fitted parameters (see METHODS), R_{max}, n, and c_{50}, and the calculated slope were compared for conductance injection steps with noise vs. no noise. Open circles represent parameter estimates from response curves with no noise compared with conductance steps with synaptic noise composed of EI conductances with an EI delay (5 ms) and a correlation of 0.5. Solid points represent estimates from response curves with no noise compared with conductance steps with synaptic noise composed of EI conductances with no EI delay and a correlation of 0.5.

can be generated by activation of conductances present in the model and a second mechanism that depends on additional channels or properties.

DISCUSSION

Previous studies have shown that barrages of synaptic activity shape the time constants and integrative properties of neocortical neurons (Borg-Graham et al. 1998; Destexhe et al. 2003; Leger et al. 2005; Shu et al. 2003; Wehr and Zador 2003; Zsiros and Hestrin 2005). The effects of barrages of synaptic conductances have been observed both in vitro and in response to visual stimulation in vivo (Destexhe et al. 2003; Douglas and Martin 2004; Leger et al. 2005; Shu et al. 2003). Therefore subthreshold synaptic conductances play a crucial nonlinear role in synaptic integration and in shaping network behavior by affecting response properties of individual neurons.

Diverse effects have been reported for the modulation of firing rate from the combination of DC steps and noisy background synaptic input conductances delivered through the dynamic-clamp system. Some have reported a divisive effect from background synaptic noise (Chance et al. 2002; Mitchell and Silver 2003; Prescott and De Koninck 2003), whereas others have shown either a multiplicative effect or a mixture of effects across cell types (Higgs et al. 2006; Murphy and Miller 2003). Barrages of synaptic activity as seen in vivo would induce conductance changes without additional DC current steps (Graham and Schramm 2009). Therefore we measured the response gain resulting from noisy conductance steps without an additional DC step to simulate biologically realistic synaptic stimulation. We found that noise has a multiplicative rather than divisive effect on response gain, consistent with observations by Higgs et al. (2006) from neocortical pyramidal cells in vitro, as well as model results (Murphy and Miller 2003).

Downloaded from jn.physiology.org on December 22, 2011

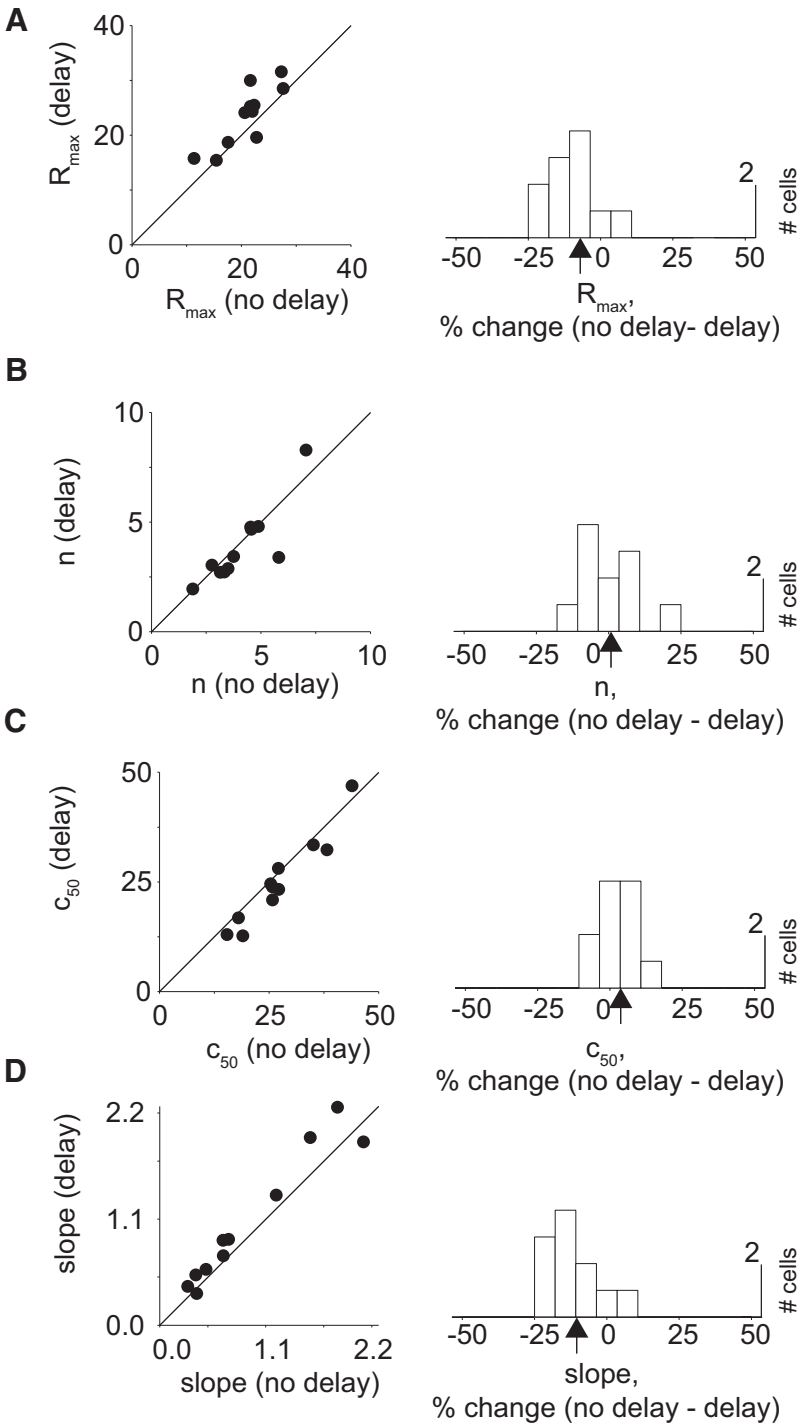

FIG. 7. Population analysis of modulation of response gain by EI balance noise statistics. Correlated excitation and inhibition that contained a temporal delay (inhibition lagging excitation) had a greater effect of increasing response gain than noise with an equivalent correlation (corr = 0.5), which lacked a temporal delay. Individual sigmoid function fitted parameters (see METHODS), R_{max}, n, and c_{50}, and the calculated slope were compared. Parameters for response rate vs. injected mean conductance curves for cases where the injected conductance contained synaptic noise defined by correlated excitatory and inhibitory synaptic conductances with a temporal delay (delay = 5 ms, corr = 0.5) to those with an equivalent correlation (corr = 0.5) and no temporal delay. Vertical arrow indicates parameter median. Response slope and maximal response, R_{max}, showed significantly greater values for conditions where there is a temporal delay compared with no delay ($P = 0.02$ and 0.014, respectively, Wilcoxon signed rank sum test).

The results presented here showed that the firing rates of individual excitatory pyramidal cortical neurons are modulated by the statistical properties of the synaptic noise conductance that they receive. Specifically, individual neurons showed response gain enhancement for synaptic noise conductance steps where inhibition was delayed relative to excitation for correlated O-U processes compared with noisy conductance steps where excitation and inhibition have a comparable degree of correlation but lacked an EI delay. Comparing firing rate as a function of EI delay indicated that such responsiveness enhancement occurs when correlated (corr = 1.0) inhibition follows excitation within the range of 1–10 ms. These temporal delays are consistent with EI temporal interactions as short as a single monosynaptic delay. Such delays might result from either feed-forward inhibition or recurrent lateral interactions and have been observed during spontaneous activity (Douglas and Martin 2004; Okun and Lampl 2008; Thomson et al. 2002a).

Firing rate responses to noise steps with an EI delay showed enhanced firing rates relative to no EI delay even when plotted as a function of the SD of the dynamic clamp command, I_{syn}. Firing rate as a function of I_{syn} SD was linear over the range of

Downloaded from jn.physiology.org on December 22, 2011

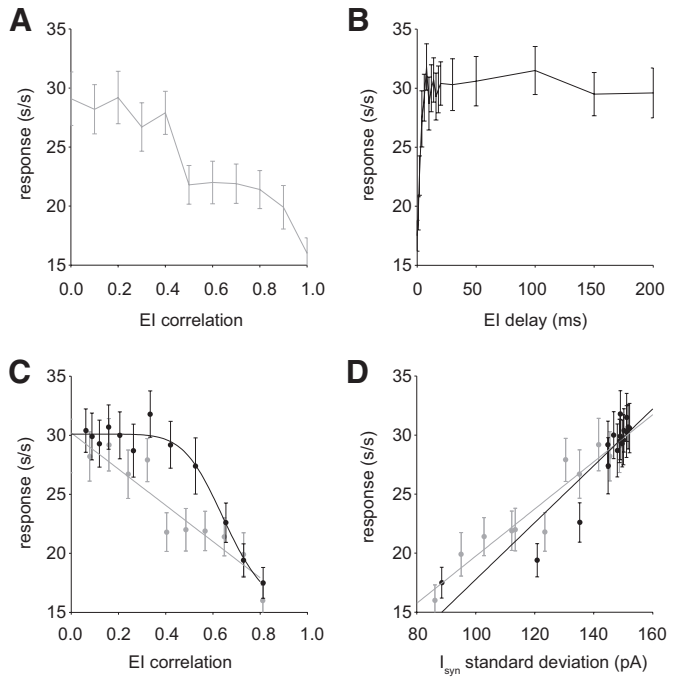

FIG. 8. Effects of synaptic noise in a conductance-based model simulation. *A–C*: firing rate responses are shown as a function of the EI correlation for noise conductance steps. Responses were averaged over 10 repeats.Firing rate is shown as a function of the EI correlation (*A*) and as a function of EI temporal delay (*B*). *C*: the firing rate responses for EI noise with a temporal delay (black points) are elevated relative to responses with no EI temporal delay (gray points). The solid black and gray curves represent sigmoid and linear fits to the data, respectively. *D*: the firing rate response from *C* are shown plotted as a function of the SD of the model current drive, I_{syn}. Unlike the neuron recordings, both the responses from the noise steps with a temporal delay (black points) and with no delay (gray points) are well fit by the same linear regression (ANCOVA).

EI correlations (0–1), whereas the same relation was not well fit by a linear regression when an EI temporal delay was present. The slope of the linear regression for the response versus I_{syn} SD was also not correlated between the delay and no delay step responses. Therefore the firing rate response enhancement resulting from the presence of an EI temporal delay was not explained by the command current, I_{syn}, SD.

Near spike threshold for these neurons (approximately −40 mV), the combined EI synaptic noise current [$I_{syn} = g_e(V_m - E_e) - g_i(V_m - E_i)$] used in our study shows distinct properties of the autocorrelation function (Supplementary Fig. S2*A*) and power spectrum (Supplementary Fig. S2*B*) for noise with an EI delay (5 ms, black traces) compared with no EI delay (gray traces). The power spectrum of the combined EI noise indicated that high-frequency oscillations were present when an EI delay was present (Supplementary Fig. S2*B*). Previous reports have shown that neurons are able to track transients ≤200 Hz with no attenuation, well above that predicted from the cut-off from passive membrane properties (Kondgen et al. 2008). Therefore it is possible that such oscillations were responsible for the response gain enhancement observed with noise containing an EI delay. The oscillation frequencies were within the range of cortical oscillations induced by cortical network activity observed in vivo (Fries et al. 2007).

The statistical interactions between excitation and inhibition used to define the fluctuating synaptic conductances in our study correspond to biologically realistic circuitry. We used the O-U model to simulate the summed activity of a barrage of either glutamatergic or GABAergic synaptic inputs. The correlation between the excitatory and inhibitory inputs simulated the circuitry behind the converging synaptic inputs of a given recorded neuron. Uncorrelated EI synaptic noise would correspond to independent excitation and inhibition, whereas correlated EI noise would correspond to circuitry with a common input for excitation and inhibition (Fig. 9). EI noise with delayed inhibition could result from disynaptic (or polysynaptic) inhibition from a common input source. Such canonical circuits have been described for neocortical pyramidal neurons and therefore reflect realistic and plausible synaptic drive (Douglas and Martin 2004; Ferster and Miller 2000; Wehr and Zador 2003).

Cortical responses in vivo are driven by dynamic changes in the balance of excitation to inhibition. In vivo whole cell recordings of visually evoked activity have shown that the ratio of excitation to inhibition depends on the visual stimulus and the level of network activity (Azouz and Gray 2008; Monier et al. 2008). Stimulus selective spiking arises through changes in the EI balance, relative timing, and degree of synchrony for optimal and nonoptimal stimuli (Anderson et al. 2001; Azouz and Gray 2008; Borg-Graham et al. 1998; Monier et al. 2008). Although it is well established that the relative strength and timing of E and I vary during visual stimulation, it is not clear how EI timing and synchrony control the firing rates. Spatially extended visual stimuli induce a reduction in spike rates

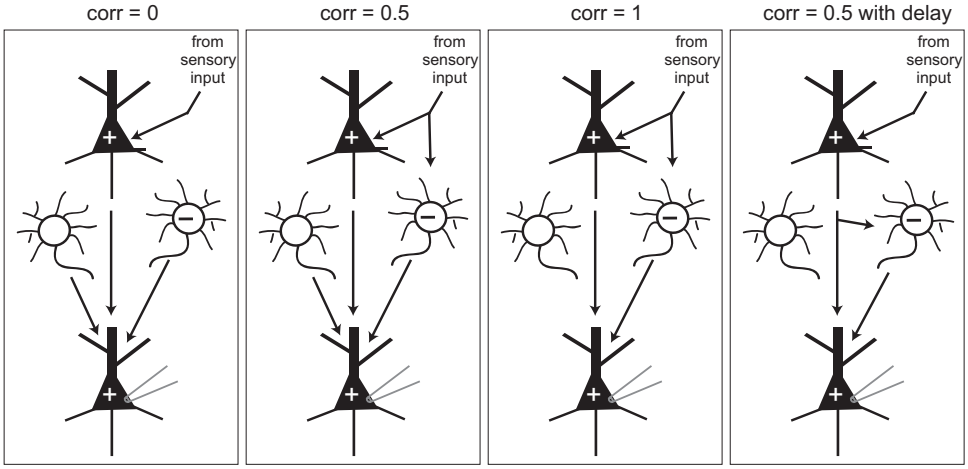

FIG. 9. Correlation statistics and corresponding circuit models. The degree of correlation between excitation and inhibition depends in part on whether excitation and inhibition have a common input. Excitation with no common input, partial common input, or complete common input would correspond to corr = 0.0, 0.5, and 1.0, respectively. Correlated excitation and inhibition with a temporal delay would result from disynaptic inhibition with a common input.

Downloaded from jn.physiology.org on December 22, 2011

through surround suppression (Anderson et al. 2001; Sceniak et al. 1999). This spike rate reduction results from a concomitant increase in synaptically driven inhibition and decrease in excitation (Anderson et al. 2001). During spontaneous high-conductance UP-states in vivo, it has also been shown that the balance of excitation to inhibition varies throughout the UP state (Haider et al. 2006; Rudolph et al. 2007).

Not only is the excitatory to inhibitory balance dynamically modulated by stimulus drive, the history of this activity alters the circuit through plasticity. For example, the balance between excitation and inhibition is dynamically shifted by differential sensitivity of excitation and inhibition to synaptic depression, adaptation, and homeostatic plasticity (Heiss et al. 2008; Maffei et al. 2006; Varela et al. 1999). In addition, plasticity could alter the relative EI timing and correlation through activity-dependent changes in local circuitry. In somatosensory cortex, trains of stimuli induce adaption of feedforward connections from the thalamus but do not alter intracortical synaptic responses (Chung et al. 2002). In other experiments, it has been shown that, although depression of EPSCs in feedforward and feedback pathways within the cortex exhibit similar dependencies on the frequency of stimulation, inhibitory synapses from feedback pathways are more depressed than those from feedforward pathways when stimulated at high frequencies (Dong et al. 2004).

Our results indicate that an EI noise temporal delay modulates response gain for a single excitatory pyramidal neuron. More complex models will need to be tested that take into account the spatial arrangement of synaptic inputs as well as synaptic plasticity (Azouz 2005). It will be important to examine whether the effects observed here are present in other types of cortical neurons, such as various classes of inhibitory neurons, because different cell types likely have unique statistical patterns of synaptic input for excitation and inhibition. In addition, a recent study showed that subthreshold membrane potential fluctuations from synaptic inputs reflect the sensory drive and degree of network correlation (El Boustani et al. 2009). Further studies will be needed to measure the full range of synaptic input statistics present in vivo. In particular, determining the impact of synaptic patterns that arise from specific visual stimuli will be important for characterizing the relevance of neuronal sensitivity to EI temporal interactions to visual processing.

Understanding the modulatory effects of synaptic background noise on response properties of neocortical neurons is a necessary component to decoding cortical processing. It will be essential to consider these effects to form accurate models of cortical function. Not only is our understanding of the effects of EI interactions on cortical responses important for the understanding of normal cortical function, it is also expected to provide insight into the mechanisms of diseases linked to cortical dysfunction (Uhlhaas and Singer 2006).

ACKNOWLEDGMENTS

We thank the RTXI project (www.rtxi.org) for generous sharing of software. We also thank J. Bettencourt for helpful assistance with programming RTXI models and setup.

DISCLOSURES

No conflicts of interest, financial or otherwise, are declared by the authors.

REFERENCES

Anderson JS, Lampl I, Gillespie DC, Ferster D. Membrane potential and conductance changes underlying length tuning of cells in cat primary visual cortex. *J Neurosci* 21: 2104–2112, 2001.

Azouz R. Dynamic spatiotemporal synaptic integration in cortical neurons: neuronal gain, revisited. *J Neurophysiol* 94: 2785–2796, 2005.

Azouz R, Gray CM. Stimulus-selective spiking is driven by the relative timing of synchronous excitation and disinhibition in cat striate neurons in vivo. *Eur J Neurosci* 28: 1286–1300, 2008.

Borg-Graham LJ, Monier C, Fregnac Y. Visual input evokes transient and strong shunting inhibition in visual cortical neurons. *Nature* 393: 369–373, 1998.

Chance FS, Abbott LF, Reyes AD. Gain modulation from background synaptic input. *Neuron* 35: 773–782, 2002.

Chung S, Li X, Nelson SB. Short-term depression at thalamocortical synapses contributes to rapid adaptation of cortical sensory responses in vivo. *Neuron* 34: 437–446, 2002.

Connors BW, Malenka RC, Silva LR. Two inhibitory postsynaptic potentials, and GABAA and GABAB receptor-mediated responses in neocortex of rat and cat. *J Physiol* 406: 443–468, 1988.

Dani VS, Chang Q, Maffei A, Turrigiano GG, Jaenisch R, Nelson SB. Reduced cortical activity due to a shift in the balance between excitation and inhibition in a mouse model of Rett syndrome. *Proc Natl Acad Sci USA* 102: 12560–12565, 2005.

Dayan P, Abbott L. *Theoretical Neuroscience: Computational and Mathematical Modeling of Neural Systems.* Cambridge, MA: MIT Press, 2005.

de la Rocha J, Doiron B, Shea-Brown E, Josic K, Reyes A. Correlation between neural spike trains increases with firing rate. *Nature* 448: 802–806, 2007.

Destexhe A, Rudolph M, Fellous JM, Sejnowski TJ. Fluctuating synaptic conductances recreate in vivo-like activity in neocortical neurons. *Neuroscience* 107: 13–24, 2001.

Destexhe A, Rudolph M, Pare D. The high-conductance state of neocortical neurons in vivo. *Nat Rev Neurosci* 4: 739–751, 2003.

Dong H, Shao Z, Nerbonne JM, Burkhalter A. Differential depression of inhibitory synaptic responses in feedforward and feedback circuits between different areas of mouse visual cortex. *J Comp Neurol* 475: 361–373, 2004.

Dorval AD, Christini DJ, White JA. Real-time linux dynamic clamp: a fast and flexible way to construct virtual ion channels in living cells. *Ann Biomed Eng* 29: 897–907, 2001.

Douglas RJ, Martin KA. A functional microcircuit for cat visual cortex. *J Physiol* 440: 735–769, 1991.

Douglas RJ, Martin KA. Neuronal circuits of the neocortex. *Annu Rev Neurosci* 27: 419–451, 2004.

Douglas RJ, Martin KA, Whitteridge D. An intracellular analysis of the visual responses of neurones in cat visual cortex. *J Physiol* 440: 659–696, 1991.

El Boustani S, Marre O, Behuret S, Baudot P, Yger P, Bal T, Destexhe A, Fregnac Y. Network-state modulation of power-law frequency-scaling in visual cortical neurons. *PLoS Comput Biol* 5: e1000519, 2009.

Fellous JM, Rudolph M, Destexhe A, Sejnowski TJ. Synaptic background noise controls the input/output characteristics of single cells in an in vitro model of in vivo activity. *Neuroscience* 122: 811–829, 2003.

Ferster D, Jagadeesh B. EPSP-IPSP interactions in cat visual cortex studied with in vivo whole-cell patch recording. *J Neurosci* 12: 1262–1274, 1992.

Ferster D, Miller KD. Neural mechanisms of orientation selectivity in the visual cortex. *Annu Rev Neurosci* 23: 441–471, 2000.

Frégnac Y, Monier C, Chavane F, Baudot P, Graham L. Shunting inhibition, a silent step in visual cortical computation. *J Physiol Paris* 97: 441–451, 2003.

Fries P, Nikolic D, Singer W. The gamma cycle. *Trends Neurosci* 30: 309–316, 2007.

Gillespie DT. Exact numerical simulation of the Ornstein-Uhlenbeck process and its integral. *Phys Rev E Stat Phys Plasmas Fluids Relat Interdiscip Topics* 54: 2084–2091, 1996.

Graham LJ, Schramm A. In vivo dynamic-clamp manipulation of extrinsic and intrinsic conductances: functional roles of shunting inhibition and IBK in rat and cat cortex. In: *Dynamic-Clamp: From Principles to Applications*, edited by Destexhe A, Bal T. New York: Springer Press, 2009, p. 141–163.

Haider B, Duque A, Hasenstaub AR, McCormick DA. Neocortical network activity in vivo is generated through a dynamic balance of excitation and inhibition. *J Neurosci* 26: 4535–4545, 2006.

Downloaded from jn.physiology.org on December 22, 2011

Heiss JE, Katz Y, Ganmor E, Lampl I. Shift in the balance between excitation and inhibition during sensory adaptation of S1 neurons. *J Neurosci* 28: 13320–13330, 2008.

Higgs MH, Slee SJ, Spain WJ. Diversity of gain modulation by noise in neocortical neurons: regulation by the slow afterhyperpolarization conductance. *J Neurosci* 26: 8787–8799, 2006.

Hirsch JA, Martinez LM. Circuits that build visual cortical receptive fields. *Trends Neurosci* 29: 30–39, 2006.

Huguenard JR, McCormick DA. Simulation of the currents involved in rhythmic oscillations in thalamic relay neurons. *J Neurophysiol* 68: 1373–1383, 1992.

Kondgen H, Geisler C, Fusi S, Wang XJ, Luscher HR, Giugliano M. The dynamical response properties of neocortical neurons to temporally modulated noisy inputs in vitro. *Cereb Cortex* 18: 2086–2097, 2008.

Leger JF, Stern EA, Aertsen A, Heck D. Synaptic integration in rat frontal cortex shaped by network activity. *J Neurophysiol* 93: 281–293, 2005.

Maffei A, Nataraj K, Nelson SB, Turrigiano GG. Potentiation of cortical inhibition by visual deprivation. *Nature* 443: 81–84, 2006.

Maffei A, Nelson SB, Turrigiano GG. Selective reconfiguration of layer 4 visual cortical circuitry by visual deprivation. *Nat Neurosci* 7: 1353–1359, 2004.

Mitchell SJ, Silver RA. Shunting inhibition modulates neuronal gain during synaptic excitation. *Neuron* 38: 433–445, 2003.

Monier C, Fournier J, Fregnac Y. In vitro and in vivo measures of evoked excitatory and inhibitory conductance dynamics in sensory cortices. *J Neurosci Methods* 169: 323–365, 2008.

Murphy BK, Miller KD. Multiplicative gain changes are induced by excitation or inhibition alone. *J Neurosci* 23: 10040–10051, 2003.

Nirenberg S, Latham PE. Decoding neuronal spike trains: how important are correlations? *Proc Natl Acad Sci USA* 100: 7348–7353, 2003.

Okun M, Lampl I. Instantaneous correlation of excitation and inhibition during ongoing and sensory-evoked activities. *Nat Neurosci* 11: 535–537, 2008.

Ozeki H, Finn IM, Schaffer ES, Miller KD, Ferster D. Inhibitory stabilization of the cortical network underlies visual surround suppression. *Neuron* 62: 578–592, 2009.

Pillow JW, Shlens J, Paninski L, Sher A, Litke AM, Chichilnisky EJ, Simoncelli EP. Spatio-temporal correlations and visual signalling in a complete neuronal population. *Nature* 454: 995–999, 2008.

Prescott SA, De Koninck Y. Gain control of firing rate by shunting inhibition: roles of synaptic noise and dendritic saturation. *Proc Natl Acad Sci USA* 100: 2076–2081, 2003.

Rauch A, La Camera G, Luscher HR, Senn W, Fusi S. Neocortical pyramidal cells respond as integrate-and-fire neurons to in vivo-like input currents. *J Neurophysiol* 90: 1598–1612, 2003.

Rudolph M, Pospischil M, Timofeev I, Destexhe A. Inhibition determines membrane potential dynamics and controls action potential generation in awake and sleeping cat cortex. *J Neurosci* 27: 5280–5290, 2007.

Sceniak MP, Maciver MB. Cellular actions of urethane on rat visual cortical neurons in vitro. *J Neurophysiol* 95: 3865–3874, 2006.

Sceniak MP, Maciver MB. Slow GABA(A) mediated synaptic transmission in rat visual cortex. *BMC Neurosci* 9: 8, 2008.

Sceniak MP, Ringach DL, Hawken MJ, Shapley R. Contrast's effect on spatial summation by macaque V1 neurons. *Nat Neurosci* 2: 733–739, 1999.

Series P, Lorenceau J, Fregnac Y. The "silent" surround of V1 receptive fields: theory and experiments. *J Physiol Paris* 97: 453–474, 2003.

Shu Y, Hasenstaub A, Badoual M, Bal T, McCormick DA. Barrages of synaptic activity control the gain and sensitivity of cortical neurons. *J Neurosci* 23: 10388–10401, 2003.

Stepanyants A, Martinez LM, Ferecsko AS, Kisvarday ZF. The fractions of short- and long-range connections in the visual cortex. *Proc Natl Acad Sci USA* 106: 3555–3560, 2009.

Thomson AM, Bannister AP, Mercer A, Morris OT. Target and temporal pattern selection at neocortical synapses. *Philos Trans R Soc Lond B Biol Sci* 357: 1781–1791, 2002a.

Thomson AM, West DC, Wang Y, Bannister AP. Synaptic connections and small circuits involving excitatory and inhibitory neurons in layers 2–5 of adult rat and cat neocortex: triple intracellular recordings and biocytin labelling in vitro. *Cereb Cortex* 12: 936–953, 2002b.

Trevelyan AJ, Watkinson O. Does inhibition balance excitation in neocortex? *Prog Biophys Mol Biol* 87: 109–143, 2005.

Uhlhaas PJ, Singer W. Neural synchrony in brain disorders: relevance for cognitive dysfunctions and pathophysiology. *Neuron* 52: 155–168, 2006.

Varela JA, Song S, Turrigiano GG, Nelson SB. Differential depression at excitatory and inhibitory synapses in visual cortex. *J Neurosci* 19: 4293–4304, 1999.

Wehr M, Zador AM. Balanced inhibition underlies tuning and sharpens spike timing in auditory cortex. *Nature* 426: 442–446, 2003.

Winograd M, Destexhe A, Sanchez-Vives MV. Hyperpolarization-activated graded persistent activity in the prefrontal cortex. *Proc Natl Acad Sci USA* 105: 7298–7303, 2008.

Wu N, Enomoto A, Tanaka S, Hsiao CF, Nykamp DQ, Izhikevich E, Chandler SH. Persistent sodium currents in mesencephalic v neurons participate in burst generation and control of membrane excitability. *J Neurophysiol* 93: 2710–2722, 2005.

Xing J, Gerstein GL. Networks with lateral connectivity. I. Dynamic properties mediated by the balance of intrinsic excitation and inhibition. *J Neurophysiol* 75: 184–199, 1996.

Zsiros V, Hestrin S. Background synaptic conductance and precision of EPSP-spike coupling at pyramidal cells. *J Neurophysiol* 93: 3248–3256, 2005.

Downloaded from jn.physiology.org on December 22, 2011

Articles in PresS. J Neurophysiol (August 25, 2010). doi:10.1152/jn.00023.2010

Modulation of firing rate by background synaptic noise statistics in rat visual cortical neurons.

Michael P. Sceniak and Shasta L. Sabo
Neuroscience & Pharmacology,
Case Western Reserve University, Cleveland, OH 44116

August 4, 2010

Corresponding author:
Michael P. Sceniak
Case Western Reserve University
Department of Pharmacology
Wood Bldg. W343
2109 Adelbert Rd.
Cleveland, OH 44106
michael.sceniak@case.edu

Copyright © 2010 by the American Physiological Society.

Title: Modulation of response gain by background synaptic noise statistics in rat visual cortical neurons.

Authors: Michael P. Sceniak and Shasta L. Sabo

Abstract:

It has been shown previously that background synaptic noise modulates the response gain of neocortical neurons. However, the role of the statistical properties of the noise in modulating firing rate is not known. Here, the dependence of firing rate on the statistical properties of the excitatory to inhibitory balance (EI) in cortical pyramidal neurons was investigated. Excitatory glutamatergic and inhibitory GABA-ergic synaptic conductances were simulated as two stochastic processes and injected into individual neurons *in vitro* through use of the dynamic-clamp system. Response gain was significantly modulated as a function of the statistical interactions between excitatory and inhibitory synaptic conductances. Firing rates were compared for noisy synaptic conductance steps by varying either the EI correlation or the relative delay between correlated E and I. When inhibitory synaptic conductances exhibited a short temporal delay (5 ms) relative to correlated excitatory synaptic conductances, the response gain was increased compared to noise with no temporal delay but with an equivalent degree of correlation. The dependence of neuronal firing rate on the EI delay of the noisy background synaptic conductance suggests that individual excitatory pyramidal neurons are sensitive to the EI balance of the synaptic conductance. Therefore, the statistical EI interactions encoded within the synaptic subthreshold membrane fluctuations are able to modulate neuronal firing properties.

keywords: visual cortex, correlation, synapse, GABA, glutamate, dynamic-clamp, whole-cell patch clamp, in vitro, neocortex, firing rate, action potential, spikes.

INTRODUCTION:

Interactions of excitatory and inhibitory (EI) synaptic inputs are crucial for cortical circuit function. EI interactions have been shown to play a crucial role in regulating and establishing cortical receptive field properties (Borg-Graham et al. 1998; Connors et al. 1988; Douglas and Martin 2004; Douglas et al. 1991; Ferster and Jagadeesh 1992; Hirsch and Martinez 2006; Ozeki et al. 2009). Recent studies have suggested that EI balance, or the ratio of excitatory to inhibitory synaptic inputs, is one form of EI interaction that helps establish the intrinsic excitability of the cortex (Leger et al. 2005; Maffei et al. 2004; Trevelyan and Watkinson 2005; Xing and Gerstein 1996). It has been shown that correlated activity within the cortical network critically influences the response of individual neurons within the network (de la Rocha et al. 2007; Destexhe et al. 2001; Fellous et al. 2003; Nirenberg and Latham 2003; Pillow et al. 2008; Rauch et al. 2003). Besides the EI balance, other possible EI interactions exist within the cortical network that might regulate neuronal information processing such as the correlated firing and relative timing of excitation and inhibition. Such interactions have implications for neuronal processing where global network activity appears to modulate receptive field properties of individual neurons (Sceniak et al. 1999; Series et al. 2003).

Recent studies have shown that noisy background synaptic activity modulates the responsiveness of cortical neurons relative to a quiescent state (Chance et al. 2002; Fellous et al. 2003; Higgs et al. 2006; Mitchell and Silver 2003; Prescott and De Koninck 2003). Noisy background synaptic activity composed of excitatory and inhibitory synaptic conductances, simulated using the dynamic-clamp technique, have been shown to modulate response firing rate gain. Whether or not individual neurons are capable of detecting particular EI statistical interactions embedded within the noisy background signals has not been addressed previously.

A given excitatory pyramidal cortical neuron receives thousands of synaptic inputs from many

neurons within the circuit (Douglas and Martin 1991; 2004; Thomson et al. 2002b). The pattern of activity converging on a given pyramidal neuron contains the sum of these synaptic inputs. Background synaptic activity can originate from either feed-forward or recurrent feedback drive from either excitatory or inhibitory neurons or a combination of these sources (Douglas and Martin 2004; Stepanyants et al. 2009). By simulating the pattern of activity converging on a given neuron, the interactions and statistics of excitatory and inhibitory synaptic conductance inputs can be controlled to determine their effects on firing rate. Such patterns of activity represent the relative correlation and synchrony of excitation and inhibition.

This study addresses to what extent the firing rate encoding of individual neurons is modulated by the EI interactions which define the background synaptic noise conductance. The EI interactions tested include the degree of correlation between excitation and inhibition and the relative temporal delay or phase between correlated excitation and inhibition. Using the dynamic-clamp system and a stochastic model to simulate *in vivo*-like synaptic conductances (Destexhe et al. 2001; Destexhe et al. 2003; Fellous et al. 2003), we were able to design particular synaptic conductance stimuli which isolated the effects of these particular EI interactions. Synaptic noise signals with identical mean, standard deviation and EI correlation were generated that differed in whether there was a relative delay between excitation and inhibition.

Understanding the effects of global network activity on the information processing of individual neurons is a necessary component to determining how network states contribute to perception and sensation (Fregnac, 2003; de la Rocha, 2007; El Boustani, 2009). Classifying the population of synaptic inputs from the cortical network according to the statistical interactions between the excitatory and inhibitory synaptic inputs that make up the network allows us to determine the response modulation from network activity in a reduced model system. Given the complexity of cortical

networks, this allows one to reduce the problem to manageable comparisons and more straight-forward interpretations. Our results indicate that neurons are sensitive to these subtle statistical interactions between excitation and inhibition and need to be considered in models of cortical function.

METHODS:

All procedures and protocols used in this study adhere to published guidelines of the National Institutes of Health and were approved by the Institutional Animal Care and Use Committee at Case Western Reserve University. Rat brain slices were cut from dissected visual cortex of young adult (28-32 days postnatal) Long-Evans rats (Charles River Laboratories, Wilmington, MA). Animals used for the data in Figures 6 & 7were 14-21 days old. Initially, rats were anesthetized with isoflurane (4%). The brain was dissected and temporarily (< 30 s) placed in ice-cold (1-4 ºC) oxygenated (95% O_2, 5% CO_2) artificial cerebral spinal fluid (ACSF), composed of the following (in mM): 126 NaCl, 1 NaH_2PO_4, 25 $NaHCO_3$, 25 dextrose, 3 KCl, 2 $MgSO_4$ and 2 $CaCl_2$. Brain slices were cut in oxygenated ice-cold ASCF into 350 µm slices and placed in a holding chamber with 30-35 ºC ACSF that gradually (<30 min) equilibrated to room temperature (25 ºC).

Brain slices were transferred from the holding chamber after 1-2 hrs and placed in a submersion-recording chamber with a heated water jacket (Warner Instruments, Hamden, CT). Slices were perfused with oxygenated 30-35 ºC gravity-fed ACSF (2-4 ml/min). ASCF temperature was maintained with a ThermoClamp-1 (Automate Scientific, Berkeley, CA) inline heater and temperature controller. Neurons were visualized with an Olympus BX51WI microscope (Olympus America, Central Valley, PA) equipped with a water immersion objective (20X with 2X post magnification) with near-infrared wavelength illumination, differential interference contrast optics (DIC) and a CCD camera (OLY-150, Olympus America, Central Valley, PA) with contrast enhancement.

Electrophysiology:

Membrane potentials and currents were collected using a Multi-clamp 700B patch clamp amplifier

(Axon Instruments, Foster City, CA) and digitized with a Digidata 1440A analog to digital converter which was controlled by the pClamp 10.2 software package (Axon Instruments). Recording electrodes were filled with a K-gluconate-based internal solution composed of the following (in mM): 100 K-gluconate, 20 KCl, 10 phosphocreatine, 5 $MgCl_2$, 10 HEPES, 4 Na-ATP, 0.3 Na-GTP (pH 7.3 and 290-300 mOsm). Some experiments (Figures 6 & 7) were performed with the following internal electrode solution (in mM): 100 K-gluconate, 1 EGTA, 5 $MgCl_2$, 40 HEPES, 2 Na-ATP, 0.3 Na-GTP (pH 7.3 and 290-300 mOsm). Electrode resistance ranged from 4-8 MΩ and whole-cell patch recordings were made with seal resistances of 1-3 GΩ. Successful whole-cell recordings had resting membrane potentials of -57 mV or more negative. Average electrode series resistance ranged from 10-30 MΩ after whole-cell patching. Recordings with seals < 1GΩ or resting potentials greater than -57 mV were not included in the analysis.

Excitatory pyramidal neurons were selected from within rat primary visual cortical layer 5. Pyramidal neurons were selected to establish the most homogeneous population possible. Pyramidal neurons were selected initially based on spiking and intrinsic electrical membrane properties and confirmed through histological reconstructions using biocytin fills (Sceniak and Maciver 2006; 2008).

Dynamic Clamp:

Conductance injection was accomplished through use of a computer-based dynamic-clamp system. The computer contained an Intel-based motherboard running the real-time Linux operating system (RTAI, www.rtai.org), with an open source data acquisition hardware driver (COMEDI, www.comedi.org) and open source dynamic-clamp software (RTXI, (Dorval et al. 2001)). Data acquisition and control was accomplished through a National Instruments data acquisition board (PCI-6251, Austin, TX) and interface breakout box (BNC-2090, National Instruments). The dynamic-clamp

system sampled voltage measures at 15 kHz. The computer used for the dynamic-clamp system contained a dual microprocessor-based motherboard (Intel, Core 2 Duo; Santa Clara, CA) running at 2.53 GHz. Stimuli were constructed and delivered via custom written RTXI modules according to the equations described below.

Point conductance model:

The synaptic conductance injected into the soma of each cell was generated from the point conductance model to simulate noisy background synaptic activity (Destexhe et al. 2001; Destexhe et al. 2003; Fellous et al. 2003). Excitatory and inhibitory synaptic conductances were combined by Ohm's law and Kirchhoff's current law to produce a total synaptic current to drive individual neurons to produce action potentials (Figure 1). The total synaptic current, I_{syn}, was calculated in real-time from the instantaneous membrane potential measure, V_m, and the time dependent excitatory, $g_e(t)$, and inhibitory, $g_i(t)$ synaptic conductances.

$$I_{syn} = g_e(t)(V_m - E_e) + g_i(t)(V_m - E_i) \quad (1)$$

The reversal potential for glutamatergic excitation and GABAergic inhibition were E_e = 0 mV and E_i = -75 mV respectively (Figure 1), consistent with previous reports (Chance et al., 2002; Fellous et al., 2003).

The excitatory and inhibitory conductances used to simulate noisy background synaptic activity were defined by two stochastic processes based on the Ornstein-Uhlenbeck process originally introduced to describe Brownian motion (Destexhe et al. 2001). The time-dependent equations for these two processes for excitation, $g_e(t)$, and inhibition, $g_i(t)$, were as follows:

$$\frac{dg_e(t)}{dt} = \frac{1}{\tau_e}[\, g_e(t) - g_{e0}] + \sqrt{D_e}\chi_1(t) \quad (2a)$$

$$\frac{dg_i(t)}{dt} = \frac{1}{\tau_i}[\, g_i(t) - g_{i0}] + \sqrt{D_i}\chi_2(t) \ . \quad (2b)$$

The stochastic processes for excitation and inhibition were defined by the mean conductances, g_{e0} and g_{i0}, the time constants, τ_e and τ_i, and the noise 'diffusion' coefficients, D_e and D_i. The stochastic process for excitation and inhibition also contained a Gaussian white noise random variable, $\chi_1(t)$ and $\chi_2(t)$ respectively, each with zero mean and unit standard deviation. The standard deviation of these stochastic processes is known analytically (Destexhe et al. 2001; Gillespie 1996):

$$\sigma^2 = \frac{D\tau}{2}. \quad (3)$$

Throughout all experiments, the standard deviation of excitation, σ_e, and inhibition, σ_i, were matched ($\sigma_e = \sigma_i$). The inhibitory mean, μ_i, was greater than σ_i. The time constants for excitation, τ_e, and inhibition, τ_i, were 2.7 ms and 10.5 ms, respectively. The mean excitatory conductance, μ_e, and E and I standard deviations ($\sigma_e = \sigma_i$) were varied during the experiments to elicit action potential discharge (Figure 1). These parameters (μ_e, σ_e and σ_i) were optimized for each cell to achieve a range of firing rates.

The degree of correlation between the stochastic processes for excitation and inhibition was defined by taking the matrix product of a Gaussian random number, $\chi_1(t)$, and the Cholesky factorization ($C = LL^T$) of the correlation matrix, X. The correlation matrix for generating two noise signals with a correlation of 0.5 is given by:

$$X = \begin{bmatrix} 1 & 0.5 \\ 0.5 & 1 \end{bmatrix}. \quad (4)$$

Therefore, a new random variable, $\chi_2(t)$, was generated with a defined degree of correlation between excitation and inhibition:

$$\chi_2 = C \cdot \chi_1. \quad (5)$$

In order to introduce a time delay, Δt, between excitation and inhibition, $\chi_2(t)$, was shifted Δt time samples to produce a new random variable $\chi_2(t + \Delta t)$. The corresponding excitatory and inhibitory

212 random variables, $\chi_1(t)$ and $\chi_2(t+\Delta t)$, were then used to solve for g_e and g_i, respectively. The pre-delay
213 correlation (*pdc*) is the degree of correlation before a time shift. The time shift then decreases the
214 correlation (at time = 0) in a manner that depends on Δt: larger delays decrease the correlation more
215 than smaller delays. Therefore, the new EI correlation was calculated for excitatory and inhibitory
216 conductances, $g_e(t)$ and $g_i(t)$, after the imposed time shift. This calculation yields the correlation with an
217 EI delay (see Results and Figure 1) and permits comparison to unshifted input conductances (i.e. EI
218 synaptic conductances with no delay).

219 *Data Analysis:*

220 All data analyses were performed using custom-written functions in Matlab R2009a (The Mathworks,
221 Natick, MA) and functions written in C++ under Linux. All statistics are expressed as the median
222 unless otherwise stated. Statistical significance was determined using the Wilcoxon signed rank sum
223 test and analysis of covariance (ANOCOVA) where appropriate. Time-locked voltage responses were
224 analyzed to determine spike rates correlated to their corresponding conductance injections. Spikes were
225 analyzed offline by determining voltage deflections above a threshold (> -10 mV). The correlation,
226 cross-correlation, autocorrelation and power spectra were calculated using Matlab functions.

227 Sigmoid, Michaelis-Menten, functions were fitted to the firing rate responses, using nonlinear
228 constrained optimization (fmincon, Matlab function). For response functions where there was a
229 response decrease with an increase in the sampled parameter, x (normalized correlation), or an increase
230 in the sampled parameter, y (conductance), the following sigmoid functions were used:

231 $$R(x) = R_{max} - R_{\max}\frac{x^n}{(x^n + {c_{50}}^n)} + b\ , \tag{6}$$

232 $$R(y) = R_{\max}\frac{y^n}{(y^n + {c_{50}}^n)} + \mathrm{b}, \tag{7}$$

233 respectively. The parameters R_{max}, n, b and c_{50} represent the maximal firing rate, acceleration rate

exponent, response offset rate, and the value of x or y which produces half the maximal response, respectively. The offset, b, was set to the spontaneous firing rate (0 in all cases). The maximal response, R_{max}, was constrained to within ±50% of the empirical maximum response. The half-saturation value, c_{50}, was constrained to the maximum of the sampled parameters, x. The acceleration exponent, n, was constrained to be between 0.1 and 10. The slope of the sigmoid function was calculated as the first derivative of the sigmoid function evaluated at the half-maximal value, c_{50}, or

$$slope = \frac{Rn}{4c_{50}}. \quad (8)$$

Conductance-based model neuron:

Neuron model simulations were performed using the Matlab software package (Mathworks, Natick, MA). Differential equations for the Hodgkin-Huxley-like model were solved numerically using 4th order Runge-Kutta. The differential equations were solved for each time step (0.01 ms, 100 kHz) for 2 s of total time. The differential equation used to describe the neuron total current was as follows:

$$C_m \frac{dV_m}{dt} = I_{syn} - g_{leak}(V_m - E_{leak}) - I_{Na} - I_K - I_M - I_A - I_H - I_{NaP,} \quad (9)$$

where the membrane capacitance, C_m = 1.3 nF, the leak conductance, g_{leak} = 0.01 µS and the leak reversal potential, E_{leak} = -70 mV. The synaptic current I_{syn}, was defined by

$$I_{syn} = -g_{e_{syn}}(V_m - E_e) - g_{i_{syn}}(V_m - E_i)\ , \quad (10)$$

where the excitatory, g_e, and inhibitory, g_i, conductances were defined by the point conductance model describe above with excitatory synaptic reversal potential, E_e = 0 mV and inhibitory synaptic equilibrium potential, E_i = -80 mV. The Na^+ and K^+ reversal potentials were calculated through the Nernst equation where the internal and external concentrations for Na^+ and K^+ were (in mM) 20, 150, 100 and 6 (respectively) and the temperature was equal to 30 ºC.

Action Potentials:

The spike Na+ and K+ currents were defined as

$$I_{Na} = \bar{g}_{Na}(V_m - E_{Na}) \cdot {m_{Na}}^3 \cdot h_{Na} \quad (11)$$

$$I_K = \bar{g}_K(V_m - E_K) \cdot {m_K}^4 \quad , \quad (12)$$

where the maximal conductance $\bar{g}_{Na}$= 50 µS, sodium reversal E_{Na} = 50 mV, $\bar{g}_K$ = 5 µS and E_K = -72 mV. The activation and inactivation dynamics were modeled as first order processes, where

$$\tau_m(V_m)\frac{dm}{dt} = m_\infty(V_m) - m \quad (13)$$

and

$$\tau_h(V_m)\frac{dh}{dt} = h_\infty(V_m) - h \; . \quad (14)$$

The steady-state activation (m_∞) and inactivation (h_∞) equations and the time constants, τ_m and τ_h, were defined by Winograd and colleagues (Winograd et al. 2008).

Spike-frequency adaptation:

The spike-frequency adaptation current I_M was defined as

$$I_M = \bar{g}_M \cdot p \cdot (V_m - E_K) \quad (15)$$

where

$$\frac{dp}{dt} = (p_\infty - p)/\tau_p(V_m), \quad (16)$$

with $\bar{g}_M$= 0.13 µS. The steady-state activation (p_∞) equation for the I_M current and the time constant, τ_p (τ_{pmax} = 1.1s), were defined by Winograd and colleagues (Winograd et al. 2008).

The Connors-Stevens current I_A was defined as follows:

$$I_A = \bar{g}_A \cdot m^3 \cdot h \cdot (V_m - E_A) \quad (17)$$

where $\bar{g}_A$= 0.5 µS and the activation and inactivation dynamics were modeled as first order processes as described above (eqs. 13-14), using the steady-state activation (m_∞) and inactivation (h_∞) equations defined by Dayan and Abott (Dayan and Abbott 2005).

278 *Hyperpolarization-activated current:*

279 The hyperpolarization-activated cationic current I_H was defined as follows:

280 $$I_H = \bar{g}_H \cdot m \cdot (V_m - E_H), \quad (18)$$

281 where $\bar{g}_H$ = 0.03 µS and E_H = -43 mV. The activation dynamics were modeled as first order processes

282 as above (eq. 13) using the steady-state (m_∞) equation defined by Huguenard and McCormick (1992).

283 *Persistent sodium conductance:*

284 $$I_{NaP} = \bar{g}_{NaP} \cdot m \cdot h_p \cdot (V_m - E_{Na}) , \quad (19)$$

285 where $\bar{g}_{NaP}$= 1.1 µS and E_{Na} was defined as above. The activation dynamics were modeled as above

286 (eq. 13) and the steady state (m_∞ and h_∞) equations were as defined by Wu et al. (2005).

287

288

289

RESULTS:

Construction of *in vivo*-like synaptic noise barrages with defined statistical properties.

In order to determine the extent to which EI synaptic interactions modulate neuronal response output, we investigated neuronal firing rate output in excitatory cortical pyramidal neurons as a function of the statistical interaction between excitatory and inhibitory synaptic inputs, using a dynamic-clamp system (Figure 1). Noisy synaptic conductances for excitation and inhibition were generated based on the Ornstein-Uhlenbeck (O-U) stochastic point conductance model (see Methods).

In vivo, neurons receive a variety of inputs from both excitatory and inhibitory neurons, and the correlation between these inputs depends on the circuitry. Correlations are sensitive to both the synchrony and the timing of the inputs. Therefore, we examined how neurons respond to correlations between excitatory and inhibitory synaptic conductances using two approaches to vary correlation between E and I. Correlations due to synchrony of E and I can be simulated using Cholesky factorization to empirically define the degree of correlation (see Methods). Using this approach, synaptic noise signals were generated that ranged from conditions where excitatory and inhibitory synaptic conductances were completely uncorrelated (corr = 0.0, not shown) to conditions where excitation and inhibition were completely correlated (corr = 1.0, Figure 1A). Figure 1B shows an intermediate level of correlation between excitation and inhibition (corr = 0.5).

To simulate correlations between excitation and inhibition that depend on the relative timing of E and I, correlated excitatory and inhibitory conductance arrays were time shifted relative to each other to produce a given temporal delay (EI delay, Figure 1C). In all cases, excitatory and inhibitory noise used to produce synaptic noise with an EI delay were initially generated with a correlation of 1.0 prior to time shifting the inhibitory noise array to produce the EI delay. We refer to this initial correlation as the

pre-delay correlation (pdc = 1.0). The delay causes the correlation between E and I to be reduced (Figure 1C). EI delays ranged from 0 ms to 200 ms. With the exception of Figure 1D & E, inhibition always followed excitation. For conditions where excitation and inhibition were correlated (Figure 1B) or correlated with an EI delay (Figure 1C), the means and standard deviations of the synaptic conductances were held constant across conditions. This allowed us to isolate the effects of correlation and temporal-delay on firing rate responsiveness independent of EI input statistics.

In order to directly compare firing rate responses for noise which is systematically varied in EI correlation with no EI delay (e.g. as in Figure 1A&B) to noise with a fixed correlation but with a varying EI delay (e.g. as in Figure 1C), it is necessary to match the responses for actual correlation. For a given temporal delay between excitatory and inhibitory synaptic noise conductances, there is a corresponding correlation measure that depends on the magnitude of the delay (Figure 1D): increasing the EI delay decreases the degree of correlation. To determine the degree of EI correlation in the presence of the EI delay, the cross-correlation of the noise conductances (20 kHz, 2 s; pdc = 1.0) was calculated at a range of EI delays. These EI delays appear as a horizontal shift in the cross-correlation peak (Figure 1C, bottom panel). The correlation for each EI delay then corresponds to the cross-correlation of the two time-shifted signals at time = 0 (Figure 1A-C).

To create a transformation from EI delay to correlation, correlation was plotted as a function of EI delay (gray curve, Figure 1D). The average delay versus correlation function was estimated as the mean correlation for 20 repeats (black curve, Figure 1D). Fitting separate exponential functions (dashed curve, Figure 1E&F) to the average correlation values (solid black curve, Figure 1D) as a function of negative EI delays (inhibition before excitation, Figure 1E) and positive EI delays (inhibition after excitation, Figure 1F) provided a complete description of the transformation from EI delay to correlation. This transformation could then be used to determine the correlation of any two

noise signals (pdc = 1.0) that contained an EI delay. For example, a 5 ms EI delay between excitatory and inhibitory noise signals yields a correlation of 0.5 (with inhibition following excitation). The values obtained from this transformation then allowed direct comparison of neuronal spike rate responses for two different noise signals with equivalent correlations defined by either (i) EI delay or (ii) Cholesky factorization without an EI delay.

Effects of EI correlation and timing on neuronal firing rates.

To determine whether neurons can detect the EI noise balance statistics between the stimuli constructed as described above, synaptic noise signals were generated and introduced into pyramidal neurons in layer 5 of visual cortical slices using the dynamic-clamp technique and the resulting neuronal spiking responses were recorded. For a given noise conductance step composed of a combination of excitation and inhibition, conditions where excitation and inhibition were correlated by varying degrees (corr = 0 to 1) were compared to conditions where excitation and inhibition were completely correlated (pdc = 1.0) but were offset by an EI delay (delay = 0 to 50 ms) such that inhibition lagged excitation (Figure 2). The mean and standard deviation of excitation and inhibition were optimized for each recorded neuron to produce a moderate firing rate (7 to 30 Hz) when excitation and inhibition were uncorrelated with no time delay (corr = 0.0). Each conductance step (2 s, 15 kHz sample rate) was repeated 2 times, and the firing rates were averaged. Representative mean firing rate responses are shown for three neurons (Figure 2). Firing rate responses showed a clear dependence on both EI correlation (Figure 2A1-A3) and EI temporal delay (Figure 2B1-B3). Response rates were consistently reduced when E and I noise conductances were correlated and contained little temporal delay. Similar dependence on EI correlation and response enhancement for noise containing an EI delay were observed when intracellular calcium was buffered with EGTA in the patch pipette

(Supplementary Figure 1).

In order to directly compare firing rates for noise steps with and without EI delays, the degree of EI correlation was estimated for EI noise with a temporal delay using the exponential fits of correlation shown in Figure 1F. Neuronal mean firing rate responses for noise with correlations defined by EI delay were then plotted as a function of correlation (Figure 2C1-3, black). For comparison, spiking responses for noise with equivalent EI correlations but no delay (grey) were overlaid on the delay plots (Figure 2C1-3, grey). The change in mean firing rate response as a function of correlation was steeper for noise containing an EI delay and elevated for small EI temporal delay values (< 10 ms, Figure 2C1-3). Thus, in the presence of an EI delay, the response gain was increased at high EI correlations, and responses saturated and stabilized at a high firing rate over a wide range of low EI correlations. In contrast, in the absence of EI delay, responses appeared more linear over the entire range of EI correlations.

Firing rate response curves were then fitted with empirical functions. Fits for the same 3 neurons as shown in Figure 2 are illustrated in Figure 3A1-3. For EI noise with a temporal delay, firing rate responses as a function of EI correlation were sigmoid shaped and fitted with a sigmoidal, Michaelis–Menten equation (black curves, Figure 3A1-3). However, firing rate responses as a function of EI correlation without an EI temporal delay were well fit by a linear regression (gray curves, Figure 3A1-3). In order to make statistical comparisons across the population, parameters were extracted from the fits. For delay data, the maximum response, linear region (c_{50}), and slope of the response function in the linear region were estimated from the sigmoidal fits (see Methods). For EI noise responses without a temporal delay, comparable measures were extracted from the linear fits.

Across the population of recorded neurons (n = 29), the parameters of the sigmoid fits to the response vs. EI delay noise steps were compared to the linear fits of the response vs. no EI delay steps

(Figure 4). While the no delay EI steps produced responses that were linear over the range of EI correlations tested, the EI delay responses displayed responses that were linear only near the higher EI correlation values (median c_{50} = 0.79, Figure 4A). For very low correlation EI noise (corr = 0.1), the firing rate responses to EI noise with a temporal delay and without an EI delay (Figure 4B,C) were not significantly different (r^2 = 0.95, median *response* % difference (delay – no delay) = 2.9, p > 0.05, Wilcoxon rank sum test). For EI noise steps with moderately correlated EI noise (corr = 0.75, Figure 4D,E), firing rate responses were significantly greater (r^2 = 0.97, median *response* % difference (delay – no delay) = 17.5, p = 2.8e-6, Wilcoxon rank sum test), across the population, for EI noise steps with a temporal delay than with no delay. Therefore, on average, response enhancement resulting from EI temporal delay tends to occur from correlated noise (corr = 0.75) rather than essentially uncorrelated noise (corr = 0.1), and the responses are not significantly different for very low correlation EI noise.

The slope of the response vs. correlation tuning curves was compared for EI noise with an EI temporal delay (estimated at the c_{50} value, or linear region, for sigmoid fits, see Methods) to EI noise steps with no delay (linear fits, Figure 4F,G). On average, the slopes were uncorrelated (r^2 = 0.53) and significantly greater for EI noise steps with a temporal delay (median *slope* % difference (delay – no delay) = -61.6, p = 3e-6, Wilcoxon rank sum test). Overall, there is much greater sensitivity (spike rate per corr, slope) to change in firing rate as a function of EI correlation when an EI temporal delay is present.

The extent to which the standard deviation of the dynamic clamp command current, I_{syn}, might be responsible for differences in the firing rate observed with and without an EI temporal delay was also examined (Figure 3B1-3 & Figure 5). To test this, firing rate responses for stimuli with and without an EI temporal delay were plotted vs. the standard deviation of the current injected into each neuron from the combined E and I conductances (I_{syn}, see Methods; Figure 3B1-3). Responses for representative

neurons are shown next to their corresponding firing rate vs. correlation curves (Figure 3 right and left columns, respectively). The mean firing rates for EI noise with a delay (black, Figure 3B1-3) were consistently greater when compared to responses for stimuli with no EI delay (grey, Figure 3B1-3), even for matched I_{syn} standard deviations. In order to make statistical comparisons across the population of neurons, firing rates as a function the standard deviation of I_{syn}were fitted with linear regressions (Figure 3B1-3). To determine how well the linear model accounts for the data, the best fit r-squared estimate was calculated and compared for both delay and no delay responses (Figure 5A). The responses resulting from correlated EI noise without a delay were well fit with a linear regression, since the goodness of fit was typically high (> 0.9) for responses with no EI delay. However, responses with an EI delay were not fit well by a linear model. The goodness of fit was significantly lower when an EI delay was present (median *r-squared* % difference (delay – no delay) = -13, p = 1.12e-10, Wilcoxcon rank sum test, Figure 5B). The slopes of both linear regressions were then compared. Across the population, the slopes of the linear regression for firing rate vs. I_{std} were also not correlated for responses resulting from noise steps with a temporal delay vs. with no EI delay ($r^2 = 0.23$, p = 0.68, Wilcoxon rank sum test, Figure 5). Because the firing rate responses as a function standard deviation of I_{syn} were significantly different between noise steps with an EI temporal delay and with no EI temporal delay, the standard deviation of the command current, I_{syn}, is not sufficient to explain the differences in response.

Effects of EI balance on neuronal firing rates.

In order to determine the effects of synaptic EI noise statistics across a range of EI balances (defined as the ratio of mean excitation to inhibition, μ_e/μ_i), we sampled a range of excitatory mean conductances, μ_e, for a given excitatory standard deviation, σ_e, and a fixed level of mean inhibition, μ_i,

with standard deviation, $\sigma_{i,}$ (3 repeats of each excitatory mean conductance amplitude; 1 s step at 15 kHz),. The response gain function (spike rate vs. mean excitatory conductance) was estimated for conductance steps with no noise (σ_e = 0 nS, μ_i = 15 nS, σ_i = 0 nS), noise with a defined correlation between excitation and inhibition (corr = 0.5, delay = 0 ms ; σ_e = 15 nS, μ_i = 15 nS, σ_i = 15 nS) and noise (σ_e = 15 nS, μ_i = 15 nS, σ_i = 15 nS) with an EI delay (delay = 5 ms, corr = 0.5; Figure 6A-B). The correlations of the two random processes were identical (corr = 0.5; see Figure 1D).

Conductance steps with noise that contained an EI delay (open circles) and with no EI delay (closed circles) were compared to conductance steps (with the same mean conductance) with no noise (Figure 6C-F). Response functions resulting from conductance steps with EI noise regardless of the presence of an EI delay (dashed and gray, Figure 6A,B) were shifted to the left and yielded higher firing rates for the same mean conductance when compared to conductance steps with no noise (black curve, Figure 6A-B). Across the population (n = 11, Figure 5C), there was a significant increase in responsiveness for noise steps both with no EI delay and with an EI delay (median R_{max} % change [noise – no noise] = 7% and 14%; p = 0.005 and p = 0.005, Wilcoxon signed rank sum test, respectively). For noise conductance steps with an EI delay, there was a significant leftward shift of the response versus conductance function (median c_{50} % change [noise – no noise] = -10 %, p = 0.04, Wilcoxon signed rank sum test) and an increase in the slope (median *slope* % change [noise – no noise] = 8%, p = 0.01, Wilcoxon signed rank sum test) compared to noiseless conductance steps (Figure 6D&F).

Synaptic noise composed of correlated excitation and inhibition with an EI delay (delay = 5 ms, corr = 0.5) was compared to correlated noise with no EI delay (corr = 0.5, delay = 0 ms; Figure 6A-B and 7). Note that these two noise signals have identical EI correlations (corr = 0.5, Figure 1). Gain response functions with identical correlation, but with or without an EI delay, showed differences in their firing rate responses (dashed vs. gray curve, Figure 6A-B). Across the population of sampled neurons (n =

11), the slope (as calculated at the c_{50} value) of the firing rate vs. conductance response was significantly higher for noise that contained an EI delay (median *slope* % change [delay - no delay] = 10.1 %, p = 0.013, Wilcoxon signed rank sum test; Figure 7D). EI synaptic noise conductance temporal delay also resulted in a slight but significant change in the maximum response (median R_{max} % change [delay - no delay] = 7%, p = 0.02, Wilcoxon signed rank sum test; Figure 7A) and significant leftward shifts in the response functions (median c_{50} % change [delay - no delay] = -4%, p = 0.014, Wilcoxon signed rank sum test; Figure 7C). Therefore an EI delay with equivalent correlation produced response functions that were shifted leftward with an increase in absolute response, causing an increase in response gain or slope (Figure 7D).

Synaptic noise in a Hodgkin-Huxley-like model neuron.

To investigate whether the effects of EI interactions described above can be accounted for by spike currents and/or slow spike-frequency adaptation currents, the responses to background synaptic noise were examined using a conductance-based, Hodgkin-Huxley-like model neuron (see Methods, Figure 8). As with the dynamic-clamp recordings, the noisy synaptic conductances for excitation and inhibition were generated using the stochastic Ornstein-Uhlenbeck model (see Methods). The model neuron contained Na+ and K+ action-potential conductances, a leak conductance, spike-frequency-adaptation conductances (I_M and I_A), the hyperpolarization-activated conductance (I_H), and a persistent sodium conductance (I_{NaP}), with conductance values chosen from estimates of cortical pyramidal neurons in the literature (see Methods).

Analogous to the patch-clamp experiments, the firing rate of the conductance-based model neuron was quantified for conductance steps where excitatory and inhibitory synaptic conductances were correlated by varying degrees (corr = 0.0 to 1.0; Figure 8A) to conductance steps where excitatory and inhibitory synaptic conductances were correlated (pdc = 1.0) but contained varying degrees of EI delay

(0 to 200 ms, inhibition follows excitation; Figure 8B). The correlation of EI noise steps containing an EI delay was estimated as described above in Figure 1D and F then mean firing rates were plotted as a function of correlation. Firing rate responses resulting from stimulation with noise steps with an EI temporal delay were enhanced (black points, Figure 8C) for moderately correlated noise (corr = 0.4-0.6) compared to noise with no EI delay (gray points, Figure 8C).

Next, the data were fitted as described above for neuronal recordings. The response as a function of correlation was linear for noise with no EI delay (gray curve, Figure 8C) and saturating for noise with an EI delay (black curve, Figure 8C), similar to that observed from neuronal recordings. However, when the firing rate was plotted as a function of command current, I_{syn}, standard deviation, the response enhancement was no longer observed (Figure 8D). The linear regression fits of firing rate vs. the standard deviation of I_{syn} were statistically identical ($p > 0.05$, ANACOVA). Therefore, unlike the neuronal recordings, the difference in response between noise steps with an EI delay and with no delay can be accounted for by differences in the standard deviation of the synaptic current that result from the summed EI conductances. These modeled conductances are therefore insufficient to account for the observed firing rate properties in the presence of delayed inhibition. These results suggest that there are at least two mechanisms that contribute to neuronal responses to correlated E-I noise with a delay: one mechanism is a sensitive to the standard deviation of the synaptic currents and can be generated by activation of conductances present in the model, and a second mechanism that depends on additional channels or properties.

DISCUSSION:

Previous studies have shown that barrages of synaptic activity shape the time constants and integrative properties of neocortical neurons (Borg-Graham et al. 1998; Destexhe et al. 2003; Leger et al. 2005; Shu et al. 2003; Wehr and Zador 2003; Zsiros and Hestrin 2005). The effects of barrages of synaptic conductances have been observed both *in vitro* and in response to visual stimulation *in vivo* (Destexhe et al. 2003; Douglas and Martin 2004; Leger et al. 2005; Shu et al. 2003). Therefore, subthreshold synaptic conductances play a crucial non-linear role in synaptic integration and in shaping network behavior by affecting response properties of individual neurons.

Diverse effects have been reported for the modulation of firing rate from the combination of DC steps and noisy background synaptic input conductances delivered through the dynamic-clamp system. Some have reported a divisive effect from background synaptic noise (Chance et al. 2002; Mitchell and Silver 2003; Prescott and De Koninck 2003), while others have shown either a multiplicative effect or a mixture of effects across cell types (Higgs et al. 2006; Murphy and Miller 2003). Barrages of synaptic activity as seen *in vivo* would induce conductance changes without additional DC current steps (Graham and Schramm 2009). Therefore, we measured the response gain resulting from noisy conductance steps without an additional DC step to simulate biologically realistic synaptic stimulation. We find that noise has a multiplicative rather than divisive effect on response gain, consistent with observations by Higgs and colleagues (Higgs et al. 2006) from neocortical pyramidal cells *in vitro* as well as model results (Murphy and Miller 2003).

The results presented here demonstrate that the firing rates of individual excitatory pyramidal cortical neurons are modulated by the statistical properties of the synaptic noise conductance that they receive. Specifically, individual neurons showed response gain enhancement for synaptic noise conductance steps where inhibition was delayed relative to excitation for correlated O-U processes

519 compared to noisy conductance steps where excitation and inhibition have a comparable degree of
520 correlation, but lacked an EI delay. Comparing firing rate as a function of EI delay indicated that such
521 responsiveness enhancement occurs when correlated (corr = 1.0) inhibition follows excitation within
522 the range of 1 to 10 ms. These temporal delays are consistent with EI temporal interactions as short as a
523 single monosynaptic delay. Such delays might result from either feed-forward inhibition or recurrent
524 lateral interactions and have been observed during spontaneous activity (Douglas and Martin 2004;
525 Okun and Lampl 2008; Thomson et al. 2002a).

526 Firing rate responses to noise steps with an EI delay showed enhanced firing rates relative to no EI
527 delay even when plotted as a function of the standard deviation of the dynamic clamp command, I_{syn}.
528 Firing rate as a function of I_{syn} standard deviation was linear over the range of EI correlations (0-1),
529 while the same relation was not well fit by a linear regression when an EI temporal delay was present.
530 The slope of the linear regression for the response vs. I_{syn} standard deviation was also not correlated
531 between the delay and no delay step responses. Therefore, the firing rate response enhancement
532 resulting from the presence of an EI temporal delay was not explained by the command current, I_{syn},
533 standard deviation.

534 Near spike threshold for these neurons (approximately -40mV), the combined EI synaptic noise
535 current ($I_{syn} = g_e(V_m-E_e)-g_i(V_m-E_i)$) used in our study shows distinct properties of the autocorrelation
536 function (Supplementary Figure 2A) and power spectrum (Supplementary Figure2B) for noise with an
537 EI delay (5 ms, black traces) compared to no EI delay (gray traces). The power spectrum of the
538 combined EI noise indicated that high frequency oscillations were present when an EI delay was
539 present (Supplementary Figure 2B). Previous reports have shown that neurons are able to track
540 transients up to 200 Hz with no attenuation, well above that predicted from the cut-off from passive
541 membrane properties (Kondgen et al. 2008). Therefore, it is possible that such oscillations were

responsible for the response gain enhancement observed with noise containing an EI delay. The oscillation frequencies were within the range of cortical oscillations induced by cortical network activity observed *in vivo* (Fries et al. 2007).

The statistical interactions between excitation and inhibition used to define the fluctuating synaptic conductances in our study correspond to biologically realistic circuitry. We used the O-U model to simulate the summed activity of a barrage of either glutamatergic or GABAergic synaptic inputs. The correlation between the excitatory and inhibitory inputs simulated the circuitry behind the converging synaptic inputs of a given recorded neuron. Uncorrelated EI synaptic noise would correspond to independent excitation and inhibition, while correlated EI noise would correspond to circuitry with a common input for excitation and inhibition (Figure 9). EI noise with delayed inhibition could result from disynaptic (or polysynaptic) inhibition from a common input source. Such canonical circuits have been described for neocortical pyramidal neurons and therefore reflect realistic and plausible synaptic drive (Douglas and Martin 2004; Ferster and Miller 2000; Wehr and Zador 2003).

Cortical responses *in vivo* are driven by dynamic changes in the balance of excitation to inhibition. *In vivo* whole-cell recordings of visually evoked activity have shown that the ratio of excitation to inhibition depends on the visual stimulus and the level of network activity (Azouz and Gray 2008; Monier et al. 2008). Stimulus selective spiking arises through changes in the EI balance, relative timing and degree of synchrony for optimal and non-optimal stimuli (Anderson et al. 2001; Azouz and Gray 2008; Borg-Graham et al. 1998; Monier et al. 2008). Although it is well established that the relative strength and timing of E and I vary during visual stimulation, it is not clear how EI timing and synchrony control the firing rates. Spatially extended visual stimuli induce a reduction in spike rates through surround suppression (Anderson et al. 2001; Sceniak et al. 1999). This spike rate reduction results from a concomitant increase in synaptically driven inhibition and decrease in excitation

565 (Anderson et al. 2001). During spontaneous high-conductance UP-states *in vivo*, it has also been shown
566 that the balance of excitation to inhibition varies throughout the UP state (Haider et al. 2006; Rudolph
567 et al. 2007).

568 Not only is the excitatory to inhibitory balance dynamically modulated by stimulus drive, the
569 history of this activity alters the circuit through plasticity. For example, the balance between excitation
570 and inhibition is dynamically shifted by differential sensitivity of excitation and inhibition to synaptic
571 depression, adaptation, and homeostatic plasticity (Heiss et al. 2008; Maffei et al. 2006; Varela et al.
572 1999). In addition, plasticity could alter the relative EI timing and correlation through activity
573 dependent changes in local circuitry. In somatosensory cortex, trains of stimuli induce adaption of
574 feedforward connections from the thalamus but do not alter intracortical synaptic responses (Chung et
575 al. 2002). In other experiments, it has been shown that while depression of EPSCs in feedforward and
576 feedback pathways within the cortex exhibit similar dependencies on the frequency of stimulation,
577 inhibitory synapses from feedback pathways are more depressed than those from feedforward pathways
578 when stimulated at high frequencies (Dong et al. 2004).

579 Our results indicate that an EI noise temporal delay modulates response gain for a single excitatory
580 pyramidal neuron. More complex models will need to be tested that take into account the spatial
581 arrangement of synaptic inputs as well as synaptic plasticity (Azouz 2005). It will be important to
582 examine whether the effects observed here are present in other types of cortical neurons, such as
583 various classes of inhibitory neurons, since different cell types likely have unique statistical patterns of
584 synaptic input for excitation and inhibition. In addition, a recent study demonstrated that subthreshold
585 membrane potential fluctuations from synaptic inputs reflect the sensory drive and degree of network
586 correlation (El Boustani et al. 2009). Further studies will be needed to measure the full range of
587 synaptic input statistics present *in vivo*. In particular, determining the impact of synaptic patterns that

arise from specific visual stimuli will be important for characterizing the relevance of neuronal sensitivity to EI temporal interactions to visual processing.

Understanding the modulatory effects of synaptic background noise on response properties of neocortical neurons is a necessary component to decoding cortical processing. It will be essential to consider these effects in order to form accurate models of cortical function. Not only is our understanding of the effects of EI interactions on cortical responses important for the understanding of normal cortical function, it is also expected to provide insight into the mechanisms of diseases linked to cortical dysfunction (Uhlhaas and Singer 2006).

FIGURE LEGENDS:

Figure 1:

Statistical interaction between excitation and inhibition. The synaptic current, I_{syn}, was calculated in real-time based on the instantaneous membrane potential recoding and the time sampled conductances for excitation and inhibition (*top box*). Simulated synaptic noise based on the O-U stochastic processes allowed for the independent control of the excitatory and inhibitory mean (μ_e and μ_i) and standard deviation (σ_e and σ_i). Excitation and inhibition were combined such that they were either uncorrelated (not shown), (A) correlated, (B) partially correlated with no EI delay, or (C) correlated with an EI delay. The degree of correlation between excitation and inhibition scales the peak of the cross-correlogram (A-B, *bottom*). Prior to temporally shifting the inhibitory synaptic array to generate an EI delay, the correlation between excitation and inhibition, or the pre-delay correlation (pdc), is 1.0. The EI delay (5 ms) causes the cross correlation peak to shift from zero (C, *bottom*). (D) Plot of correlation as a function of delay to determine the transformation from EI delay to correlation. Conductances defined by a temporal delay between excitation and inhibition display a corresponding correlation, which corresponds to the cross-correlation at time shift zero (*vertical dashed line* in C, see inset for expansion of the region around zero). Negative delay values indicate conditions where inhibition preceded excitation (enlarged in E) while positive delay values represent the condition where inhibition followed excitation (enlarged in F). The solid gray curve in (D) illustrates the correlation resulting from the simulation of excitatory and inhibitory conductances with corresponding delays for a single 2s long noise trace. The solid black curves in (D-F) are the average correlation over 20 repeats of the simulation, with unique random sequences for each repeat. *Vertical dashed line* indicates zero delay in (D). Exponential equations (*dashed curves* in E&F) were fitted separately to each tail of the

normalized correlation transformation function. The fitted parameters of the exponential were used to determine the correlation for a given excitatory to inhibitory relative delay. The thick gray lines indicate the delay value at a correlation of 0.5.

Figure 2:

Background synaptic noise statistics modulate response gain. Representative firing rate response (mean rate) curves as a function of EI synaptic noise statistics are shown for three representative neurons (1-3. Conductance injection was a step function of combined excitation and inhibition with either a given EI correlation (corr = 0.0-1.0, gray curves) or a given EI delay (delay = 0-50 ms, black curves). (A1-3) Firing rate responses (spikes/s) are shown as a function of the degree of EI correlation for correlations defined empirically by Cholesky factorization, as illustrated in Fig. 1A&B. (B1-3) Responses for the same neurons in (A) to varied EI temporal delays are shown in the center column. Inhibition followed excitation, as illustrated in Fig. 1C&F. (C1-3) Responses to both types of EI noise (i.e. with or without temporal delay) are shown as a function of their corresponding EI correlation. The EI correlation for synaptic noise steps with a temporal delay were estimated from the delay to correlation relationship in Figure 1D. The response gain was greater for synaptic noise signals that contain a temporal delay between excitation and inhibition (*black*) compared to those with equivalent predefined correlations between excitation and inhibition but no temporal delay (*gray*).

Figure 3:

Representative response vs. EI correlation tuning curves. (A1-3) Three representative neurons (same cells as in Figure 3) are shown with mean firing rate responses fitted to empirical functions. Response curves evoked with EI noise conductance steps with no EI temporal delay (*gray curve*) were well fitted

with a linear regression. EI delay noise steps were fitted with sigmoidal functions (*black curve*). (B1-3) Firing rate responses are shown as a function of the standard deviation of the dynamic-clamp command current, I_{syn}, for noise steps with a temporal delay (*black*) and without an EI temporal delay (*gray*) next to the corresponding response vs. correlation plots. *Gray line* is the linear regression of the response vs. I_{syn} standard deviation for the no EI delay condition.

Figure 4:

Population analysis of response vs. EI correlation tuning curves. (A) For EI noise with a temporal delay, the correlation that produced a half-maximal response, c_{50}, was extracted from the sigmoidal function fits and is shown across the population of cells (median = 0.79, n = 29). (B, C) The mean firing rate responses are shown for noise steps with a temporal delay vs. without an EI temporal delay, estimated from the sigmoid and linear regression fits, respectively, at a low EI correlation (corr = 0.1). The responses are highly correlated ($r^2 = 0.95$) and are not significantly different from one another (median *response* % difference (delay – no delay) = 2.9). Vertical arrow indicates the median in (C). (D, E) Fitted response estimates are shown for high EI correlation (corr = 0.75). The mean firing rates with and without delay are correlated ($r^2 = 0.97$), and responses are significantly greater (p = 2.8e-6, Wilcoxon rank sum test) for noise steps with an EI temporal delay (median *response* % difference (delay – no delay) = 17.5). For scatter plots in (B) and (D), firing rate responses are shown as spikes/s. (F, G) The response vs. EI noise correlation slopes are shown for noise input with an EI temporal delay vs. no EI delay. The response slopes were estimated from the sigmoid fits and linear regressions, respectively. On average, the response vs. EI correlation slopes were significantly less (p = 3e-6, Wilcoxon rank sum test) for noise steps lacking an EI delay (median *slope* % difference (delay – no delay) = -61.6) and were not significantly correlated ($r^2 = 0.53$).

Figure 5:

Population analysis of response vs. command current standard deviation. (A) Across the population of cells (n = 31) the response vs. command current standard deviation was fitted with a linear regression. The r-squared goodness of fit was estimated for each curve on a cell by cell basis. Responses resulting from noise steps with no EI delay were well fitted by a linear regression ($r^2 > 0.9$, *vertical line*), but the majority of responses from noise steps with an EI temporal delay were poorly fitted with a linear regression ($r^2 < 0.9$, *horizontal line*). (B) On average, the responses from noise steps with an EI delay produced lower r-squared values (median *r-squared* % difference (delay – no delay) = -13, *vertical arrow*). (C) The slopes of the linear regressions for firing rate vs. command current standard deviation are shown. The slopes for responses resulting from noise steps with an EI delay were not significantly correlated ($r^2 = 0.23$) with slopes for responses resulting from noise steps with no EI delay.

Figure 6:

Noise modulates the response gain as a function of the statistical balance between excitation and inhibition. (A-B) The firing rate (Hz) response as a function of injected conductance mean is shown for two representative neurons. *Black curves* indicate conductance steps with no noise. *Gray curves* indicate conductance steps with the same mean conductance as the corresponding black curve with the addition of a synaptic noise (σ_e = 15 nS, σ_i = 15 nS, μ_i = 15 nS, μ_e = conductance step) composed of excitatory and inhibitory conductances with correlation of 0.5 and no EI delay. *Dashed curves* indicate response functions with mean conductance equal to the corresponding black curve with the addition of a synaptic noise (σ_e = 15 nS, σ_i = 15 nS, μ_i = 15 nS and μ_e = conductance step) composed of excitatory and inhibitory synaptic conductances with a correlation of 0.5 (pdc = 1.0, delay = 5 ms, see Figure 1).

(C-F) Across the population (n = 11), synaptic noise increased the firing rate responsiveness. Individual function fitted parameters (see Methods), R_{max}, n and c_{50} and the calculated slope were compared for conductance injection steps with noise vs. no noise. *Open circles* represent parameter estimates from response curves with no noise compared to conductance steps with synaptic noise composed of EI conductances with an EI delay (5 ms) and a correlation of 0.5. *Solid points* represent estimates from response curves with no noise compared to conductance steps with synaptic noise composed of EI conductances with no EI delay and a correlation of 0.5.

Figure 7:

Population analysis of modulation of response gain by EI balance noise statistics. Correlated excitation and inhibition which contained a temporal delay (inhibition lagging excitation) had a greater effect of increasing response gain than noise with an equivalent correlation (corr = 0.5) which lacked a temporal delay. Individual sigmoid function fitted parameters (see Methods), R_{max}, n and c_{50} and the calculated slope were compared. Parameters for response rate vs. injected mean conductance curves for cases where the injected conductance contained synaptic noise defined by correlated excitatory and inhibitory synaptic conductances with a temporal delay (delay = 5 ms, corr = 0.5) to those with an equivalent correlation (corr = 0.5) and no temporal delay. *Vertical arrow* indicates parameter median. Response slope and maximal response, R_{max}, showed significantly greater values for conditions where there is a temporal delay compared to no delay ($p = 0.02$ and 0.014 respectively, Wilcoxon signed rank sum test).

Figure 8:

Effects of synaptic noise in a conductance-based model simulation. (A-C) Firing rate responses are

shown as a function of the EI correlation for noise conductance steps. Responses were averaged over 10 repeats.Firing rate is shown as a function of the EI correlation (A) and as a function of EI temporal delay (B). (C) The firing rate responses for EI noise with a temporal delay (*black points*) are elevated relative to responses with no EI temporal delay (*gray points*). The solid black and gray curves represent sigmoid and linear fits to the data respectively. (D) The firing rate response from (C) are shown plotted as a function of the standard deviation of the model current drive, I_{syn}. Unlike the neuron recordings, both the responses from the noise steps with a temporal delay (*black points*) and with no delay (*gray points*) are well fit by the same linear regression (ANACOVA).

Figure 9:

Correlation statistics and corresponding circuit models. The degree of correlation between excitation and inhibition depends in part on whether excitation and inhibition have a common input. Excitation with no common input, partial common input or complete common input would correspond to corr = 0.0, 0.5 and 1.0 respectively. Correlated excitation and inhibition with a temporal delay would result from disynaptic inhibition with a common input.

Supplementary Figure 1. Neurons are sensitive to the correlation and relative delay between E and I even when intracellular calcium is buffered with EGTA. Our internal solution for the experiments described in Figures 2-5 was free of calcium buffer, consistent with previous studies of synaptic noise (Chance et al. 2002) and E-I balance (Dani et al. 2005). We also performed the same experiments using

735 the internal electrode solution described for Figures 6 & 7, which contains 1mM EGTA. **A-B,**
736 Representative firing rate response (mean rate) curves as a function of EI synaptic noise statistics are
737 shown for 2 representative neurons. Conductance injection was a step function of combined excitation
738 and inhibition with either a given EI correlation (corr = 0.0-1.0, black curves, left column) or a given
739 EI delay (delay = 0-20 ms, gray curves, middle column). Responses to both types of EI noise (i.e. with
740 or without temporal delay) are shown as a function of their corresponding EI correlation (right
741 column). The EI correlation for synaptic noise steps with a temporal delay were estimated from the
742 delay to correlation relationship in Figure 1D. The response gain was greater and nonlinear for synaptic
743 noise signals that contain a temporal delay between excitation and inhibition (*gray*) compared to those
744 with equivalent predefined correlations between excitation and inhibition but no temporal delay
745 (*black*).
746
747
748
749 **Supplementary Figure 2:**
750 Isyn current ($g_e(V_m - E_e) - g_i(V_m - E_i)$) with a temporal delay show differences in the auto correlation
751 and power spectrum compared to no EI delay. (A) Autocorrelation function of synaptic noise
752 conductance with correlated excitation and inhibition with no EI temporal delay (*gray curve*) and with
753 an EI delay and equivalent correlation (5 ms, *black curve*). Combined EI noise conductance with an EI
754 delay shows sharpening of the autocorrelation function compared to no EI delay which also appears as
755 harmonic oscillation in the power spectrum (B). Power spectra were averaged over 20 repeats of
756 random samples of EI synaptic noise. The degree of sharpening of the autocorrelation function and the
757 frequency of the oscillation present in the EI synaptic noise depends on the EI delay value.

Acknowledgements:

We would like to thank the RTXI project (www.rtxi.org) for generous sharing of their software. We would also like to thank *Jonathan Bettencourt* for helpful assistance with programming RTXI models and setup.

765 References

766

767 **Anderson JS, Lampl I, Gillespie DC, and Ferster D**. Membrane potential and conductance changes
768 underlying length tuning of cells in cat primary visual cortex. *J Neurosci* 21: 2104-2112, 2001.
769 **Azouz R**. Dynamic spatiotemporal synaptic integration in cortical neurons: neuronal gain, revisited. *J*
770 *Neurophysiol* 94: 2785-2796, 2005.
771 **Azouz R, and Gray CM**. Stimulus-selective spiking is driven by the relative timing of synchronous
772 excitation and disinhibition in cat striate neurons in vivo. *Eur J Neurosci* 28: 1286-1300, 2008.
773 **Borg-Graham LJ, Monier C, and Fregnac Y**. Visual input evokes transient and strong shunting
774 inhibition in visual cortical neurons. *Nature* 393: 369-373, 1998.
775 **Chance FS, Abbott LF, and Reyes AD**. Gain modulation from background synaptic input. *Neuron* 35:
776 773-782, 2002.
777 **Chung S, Li X, and Nelson SB**. Short-term depression at thalamocortical synapses contributes to rapid
778 adaptation of cortical sensory responses in vivo. *Neuron* 34: 437-446, 2002.
779 **Connors BW, Malenka RC, and Silva LR**. Two inhibitory postsynaptic potentials, and GABAA and
780 GABAB receptor-mediated responses in neocortex of rat and cat. *J Physiol* 406: 443-468, 1988.
781 **Dani VS, Chang Q, Maffei A, Turrigiano GG, Jaenisch R, and Nelson SB**. Reduced cortical activity
782 due to a shift in the balance between excitation and inhibition in a mouse model of Rett syndrome.
783 *Proc Natl Acad Sci U S A* 102: 12560-12565, 2005.
784 **Dayan P, and Abbott L**. *Theoretical Neuroscience: Computational and Mathematical Modeling of*
785 *Neural Systems*. MIT Press, 2005.
786 **de la Rocha J, Doiron B, Shea-Brown E, Josic K, and Reyes A**. Correlation between neural spike
787 trains increases with firing rate. *Nature* 448: 802-806, 2007.

Destexhe A, Rudolph M, Fellous JM, and Sejnowski TJ. Fluctuating synaptic conductances recreate in vivo-like activity in neocortical neurons. *Neuroscience* 107: 13-24, 2001.

Destexhe A, Rudolph M, and Pare D. The high-conductance state of neocortical neurons in vivo. *Nat Rev Neurosci* 4: 739-751, 2003.

Dong H, Shao Z, Nerbonne JM, and Burkhalter A. Differential depression of inhibitory synaptic responses in feedforward and feedback circuits between different areas of mouse visual cortex. *J Comp Neurol* 475: 361-373, 2004.

Dorval AD, Christini DJ, and White JA. Real-Time linux dynamic clamp: a fast and flexible way to construct virtual ion channels in living cells. *Ann Biomed Eng* 29: 897-907, 2001.

Douglas RJ, and Martin KA. A functional microcircuit for cat visual cortex. *J Physiol* 440: 735-769, 1991.

Douglas RJ, and Martin KA. Neuronal circuits of the neocortex. *Annu Rev Neurosci* 27: 419-451, 2004.

Douglas RJ, Martin KA, and Whitteridge D. An intracellular analysis of the visual responses of neurones in cat visual cortex. *J Physiol* 440: 659-696, 1991.

El Boustani S, Marre O, Behuret S, Baudot P, Yger P, Bal T, Destexhe A, and Fregnac Y. Network-state modulation of power-law frequency-scaling in visual cortical neurons. *PLoS Comput Biol* 5: e1000519, 2009.

Fellous JM, Rudolph M, Destexhe A, and Sejnowski TJ. Synaptic background noise controls the input/output characteristics of single cells in an in vitro model of in vivo activity. *Neuroscience* 122: 811-829, 2003.

Ferster D, and Jagadeesh B. EPSP-IPSP interactions in cat visual cortex studied with in vivo whole-cell patch recording. *J Neurosci* 12: 1262-1274, 1992.

Ferster D, and Miller KD. Neural mechanisms of orientation selectivity in the visual cortex. *Annu Rev Neurosci* 23: 441-471, 2000.

Fries P, Nikolic D, and Singer W. The gamma cycle. *Trends Neurosci* 30: 309-316, 2007.

Gillespie DT. Exact numerical simulation of the Ornstein-Uhlenbeck process and its integral. *Phys Rev E Stat Phys Plasmas Fluids Relat Interdiscip Topics* 54: 2084-2091, 1996.

Graham LJ, and Schramm A. In Vivo Dynamic-Clamp Manipulation of Extrinsic and Intrinsic Conductances: Functional Roles of Shunting Inhibition and IBK in Rat and Cat Cortex. In: *Dynamic-Clamp: From Principles to Applications*, edited by Destexhe A, and Bal TSpringer Press, 2009, p. 141-163.

Haider B, Duque A, Hasenstaub AR, and McCormick DA. Neocortical network activity in vivo is generated through a dynamic balance of excitation and inhibition. *J Neurosci* 26: 4535-4545, 2006.

Heiss JE, Katz Y, Ganmor E, and Lampl I. Shift in the balance between excitation and inhibition during sensory adaptation of S1 neurons. *J Neurosci* 28: 13320-13330, 2008.

Higgs MH, Slee SJ, and Spain WJ. Diversity of gain modulation by noise in neocortical neurons: regulation by the slow afterhyperpolarization conductance. *J Neurosci* 26: 8787-8799, 2006.

Hirsch JA, and Martinez LM. Circuits that build visual cortical receptive fields. *Trends Neurosci* 29: 30-39, 2006.

Huguenard JR, and McCormick DA. Simulation of the currents involved in rhythmic oscillations in thalamic relay neurons. *J Neurophysiol* 68: 1373-1383, 1992.

Kondgen H, Geisler C, Fusi S, Wang XJ, Luscher HR, and Giugliano M. The dynamical response properties of neocortical neurons to temporally modulated noisy inputs in vitro. *Cereb Cortex* 18: 2086-2097, 2008.

Leger JF, Stern EA, Aertsen A, and Heck D. Synaptic integration in rat frontal cortex shaped by

network activity. *J Neurophysiol* 93: 281-293, 2005.

Maffei A, Nataraj K, Nelson SB, and Turrigiano GG. Potentiation of cortical inhibition by visual deprivation. *Nature* 443: 81-84, 2006.

Maffei A, Nelson SB, and Turrigiano GG. Selective reconfiguration of layer 4 visual cortical circuitry by visual deprivation. *Nat Neurosci* 7: 1353-1359, 2004.

Mitchell SJ, and Silver RA. Shunting inhibition modulates neuronal gain during synaptic excitation. *Neuron* 38: 433-445, 2003.

Monier C, Fournier J, and Fregnac Y. In vitro and in vivo measures of evoked excitatory and inhibitory conductance dynamics in sensory cortices. *J Neurosci Methods* 169: 323-365, 2008.

Murphy BK, and Miller KD. Multiplicative gain changes are induced by excitation or inhibition alone. *J Neurosci* 23: 10040-10051, 2003.

Nirenberg S, and Latham PE. Decoding neuronal spike trains: how important are correlations? *Proc Natl Acad Sci U S A* 100: 7348-7353, 2003.

Okun M, and Lampl I. Instantaneous correlation of excitation and inhibition during ongoing and sensory-evoked activities. *Nat Neurosci* 11: 535-537, 2008.

Ozeki H, Finn IM, Schaffer ES, Miller KD, and Ferster D. Inhibitory stabilization of the cortical network underlies visual surround suppression. *Neuron* 62: 578-592, 2009.

Pillow JW, Shlens J, Paninski L, Sher A, Litke AM, Chichilnisky EJ, and Simoncelli EP. Spatio-temporal correlations and visual signalling in a complete neuronal population. *Nature* 454: 995-999, 2008.

Prescott SA, and De Koninck Y. Gain control of firing rate by shunting inhibition: roles of synaptic noise and dendritic saturation. *Proc Natl Acad Sci U S A* 100: 2076-2081, 2003.

Rauch A, La Camera G, Luscher HR, Senn W, and Fusi S. Neocortical pyramidal cells respond as

857 integrate-and-fire neurons to in vivo-like input currents. *J Neurophysiol* 90: 1598-1612, 2003.

858 **Rudolph M, Pospischil M, Timofeev I, and Destexhe A**. Inhibition determines membrane potential

859 dynamics and controls action potential generation in awake and sleeping cat cortex. *J Neurosci* 27:

860 5280-5290, 2007.

861 **Sceniak MP, and Maciver MB**. Cellular actions of urethane on rat visual cortical neurons in vitro. *J*

862 *Neurophysiol* 95: 3865-3874, 2006.

863 **Sceniak MP, and Maciver MB**. Slow GABA(A) mediated synaptic transmission in rat visual cortex.

864 *BMC Neurosci* 9: 8, 2008.

865 **Sceniak MP, Ringach DL, Hawken MJ, and Shapley R**. Contrast's effect on spatial summation by

866 macaque V1 neurons. *Nat Neurosci* 2: 733-739, 1999.

867 **Series P, Lorenceau J, and Fregnac Y**. The "silent" surround of V1 receptive fields: theory and

868 experiments. *J Physiol Paris* 97: 453-474, 2003.

869 **Shu Y, Hasenstaub A, Badoual M, Bal T, and McCormick DA**. Barrages of synaptic activity control

870 the gain and sensitivity of cortical neurons. *J Neurosci* 23: 10388-10401, 2003.

871 **Stepanyants A, Martinez LM, Ferecsko AS, and Kisvarday ZF**. The fractions of short- and long-

872 range connections in the visual cortex. *Proc Natl Acad Sci U S A* 106: 3555-3560, 2009.

873 **Thomson AM, Bannister AP, Mercer A, and Morris OT**. Target and temporal pattern selection at

874 neocortical synapses. *Philos Trans R Soc Lond B Biol Sci* 357: 1781-1791, 2002a.

875 **Thomson AM, West DC, Wang Y, and Bannister AP**. Synaptic connections and small circuits

876 involving excitatory and inhibitory neurons in layers 2-5 of adult rat and cat neocortex: triple

877 intracellular recordings and biocytin labelling in vitro. *Cereb Cortex* 12: 936-953, 2002b.

878 **Trevelyan AJ, and Watkinson O**. Does inhibition balance excitation in neocortex? *Prog Biophys Mol*

879 *Biol* 87: 109-143, 2005.

Uhlhaas PJ, and Singer W. Neural synchrony in brain disorders: relevance for cognitive dysfunctions and pathophysiology. *Neuron* 52: 155-168, 2006.

Varela JA, Song S, Turrigiano GG, and Nelson SB. Differential depression at excitatory and inhibitory synapses in visual cortex. *J Neurosci* 19: 4293-4304, 1999.

Wehr M, and Zador AM. Balanced inhibition underlies tuning and sharpens spike timing in auditory cortex. *Nature* 426: 442-446, 2003.

Winograd M, Destexhe A, and Sanchez-Vives MV. Hyperpolarization-activated graded persistent activity in the prefrontal cortex. *Proc Natl Acad Sci U S A* 105: 7298-7303, 2008.

Wu N, Enomoto A, Tanaka S, Hsiao CF, Nykamp DQ, Izhikevich E, and Chandler SH. Persistent sodium currents in mesencephalic v neurons participate in burst generation and control of membrane excitability. *J Neurophysiol* 93: 2710-2722, 2005.

Xing J, and Gerstein GL. Networks with lateral connectivity. I. dynamic properties mediated by the balance of intrinsic excitation and inhibition. *J Neurophysiol* 75: 184-199, 1996.

Zsiros V, and Hestrin S. Background synaptic conductance and precision of EPSP-spike coupling at pyramidal cells. *J Neurophysiol* 93: 3248-3256, 2005.

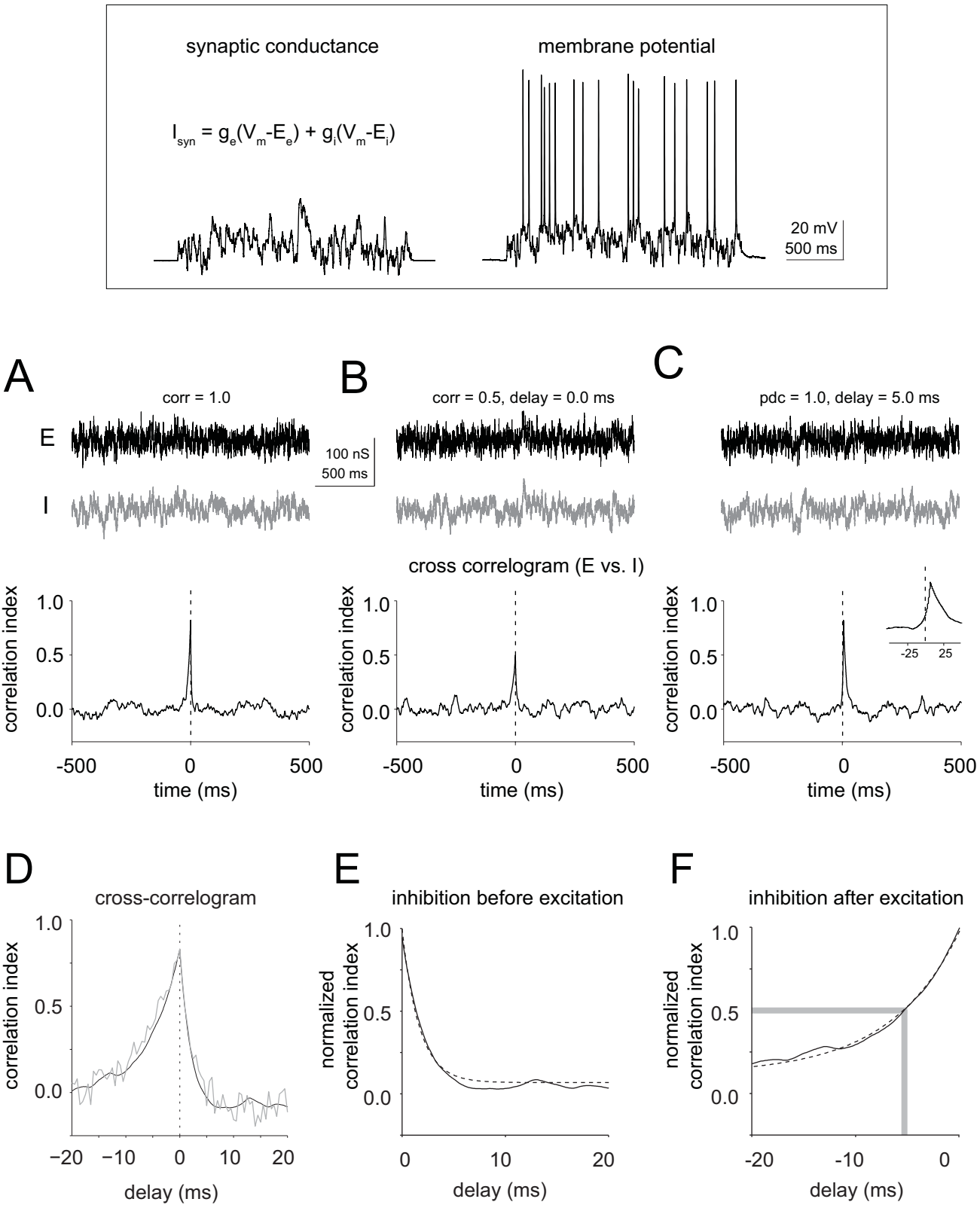
synaptic conductance
membrane potential
$I_{syn} = g_e(V_m-E_e) + g_i(V_m-E_i)$
20 mV
500 ms
A
corr = 1.0
E
I
100 nS
500 ms
B
corr = 0.5, delay = 0.0 ms
C
pdc = 1.0, delay = 5.0 ms
cross correlogram (E vs. I)
correlation index
1.0
0.5
0.0
-500
0
500
time (ms)
-25
25
D
cross-correlogram
−20
−10
0
10
20
delay (ms)
E
inhibition before excitation
normalized correlation index
F
inhibition after excitation

Figure 1

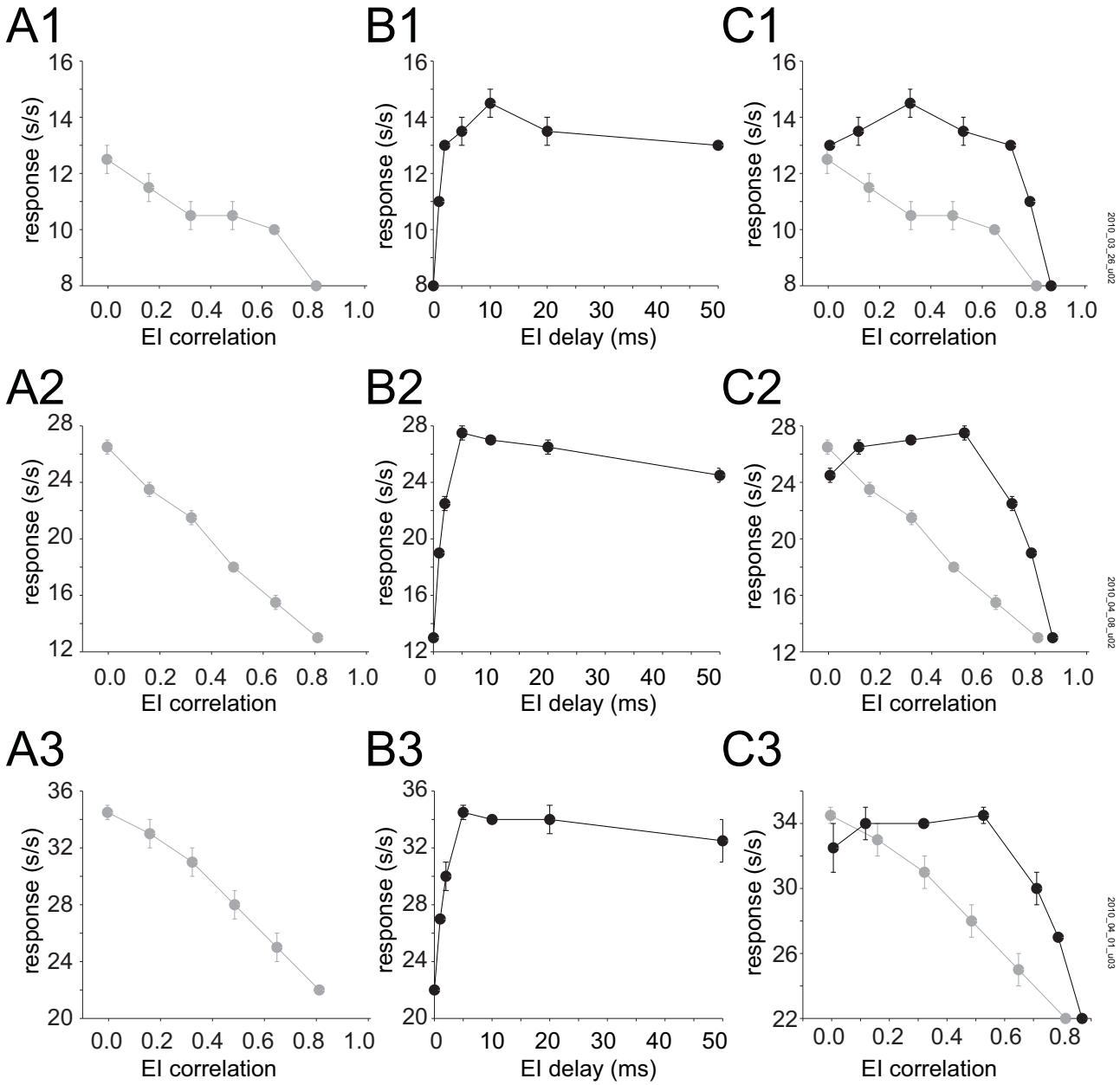
A1
B1
C1
A2
B2
C2
A3
B3
C3
response (s/s)
EI correlation
EI delay (ms)
2010_03_26_u02
2010_04_09_u02
2010_04_01_u03

Figure 2

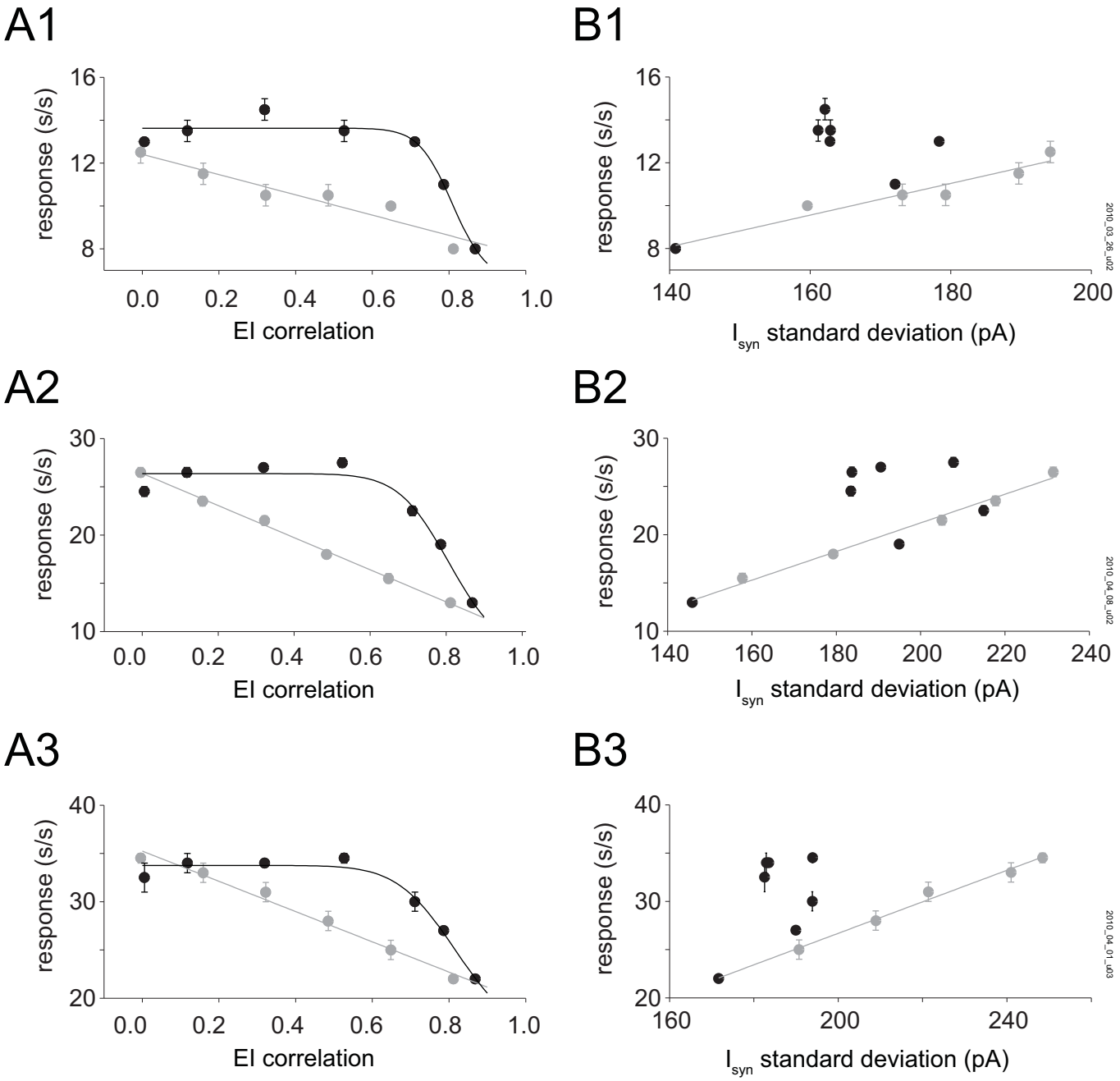
A1
B1
A2
B2
A3
B3
response (s/s)
EI correlation
I_{syn} standard deviation (pA)
2010_03_26_u02
2010_04_08_u02
2010_04_01_u03

Figure 3

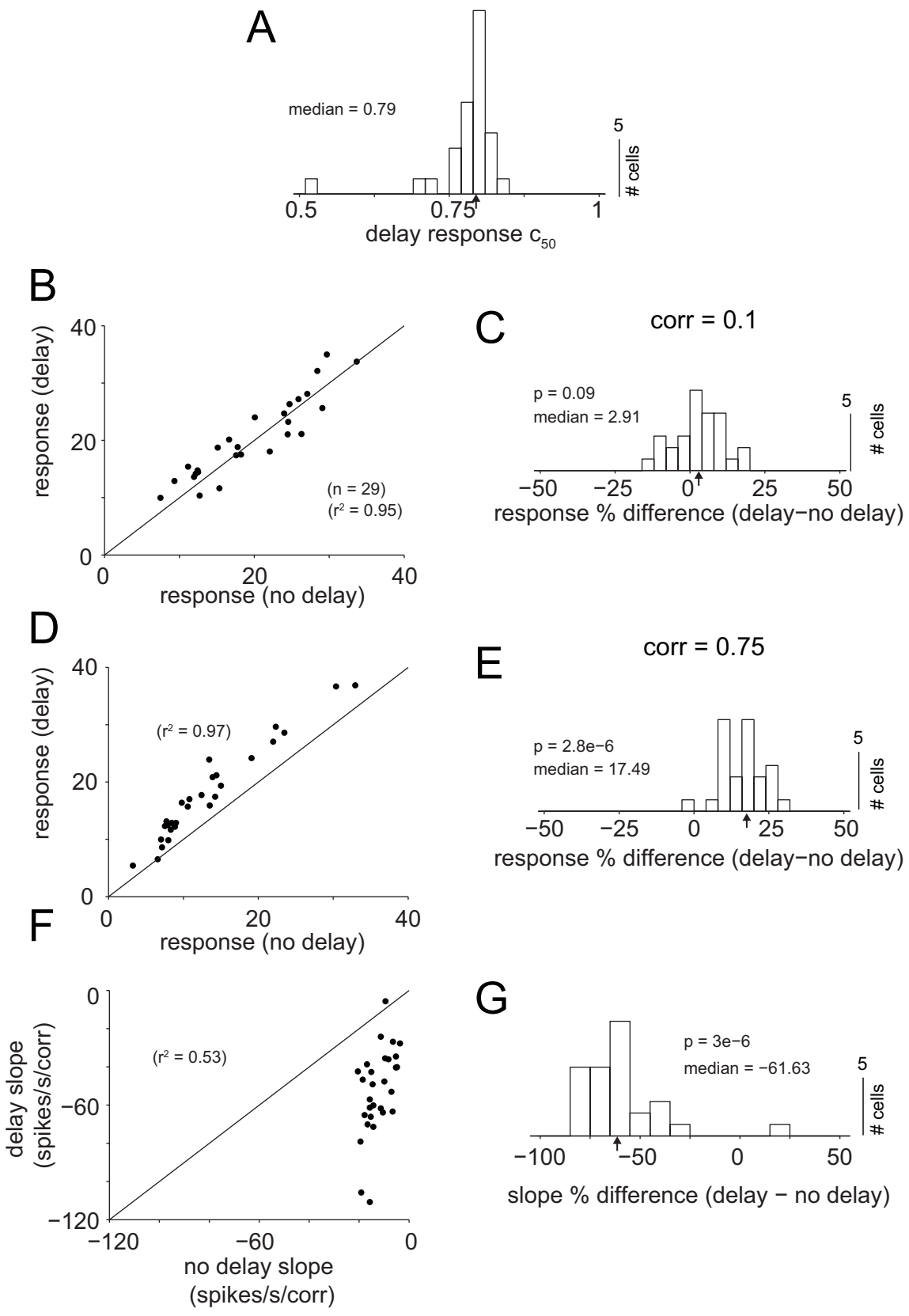
A
median = 0.79
5
cells
0.5
0.75
1
delay response c50
B
response (delay)
40
20
0
0
20
40
response (no delay)
(n = 29)
(r2 = 0.95)
C
corr = 0.1
p = 0.09
median = 2.91
5
cells
−50
−25
0
25
50
response % difference (delay−no delay)
D
response (delay)
40
20
0
0
20
40
response (no delay)
(r2 = 0.97)
E
corr = 0.75
p = 2.8e−6
median = 17.49
5
cells
−50
−25
0
25
50
response % difference (delay−no delay)
F
delay slope
(spikes/s/corr)
0
−60
−120
−120
−60
0
no delay slope
(spikes/s/corr)
(r2 = 0.53)
G
p = 3e−6
median = −61.63
5
cells
−100
−50
0
50
slope % difference (delay − no delay)

Figure 4

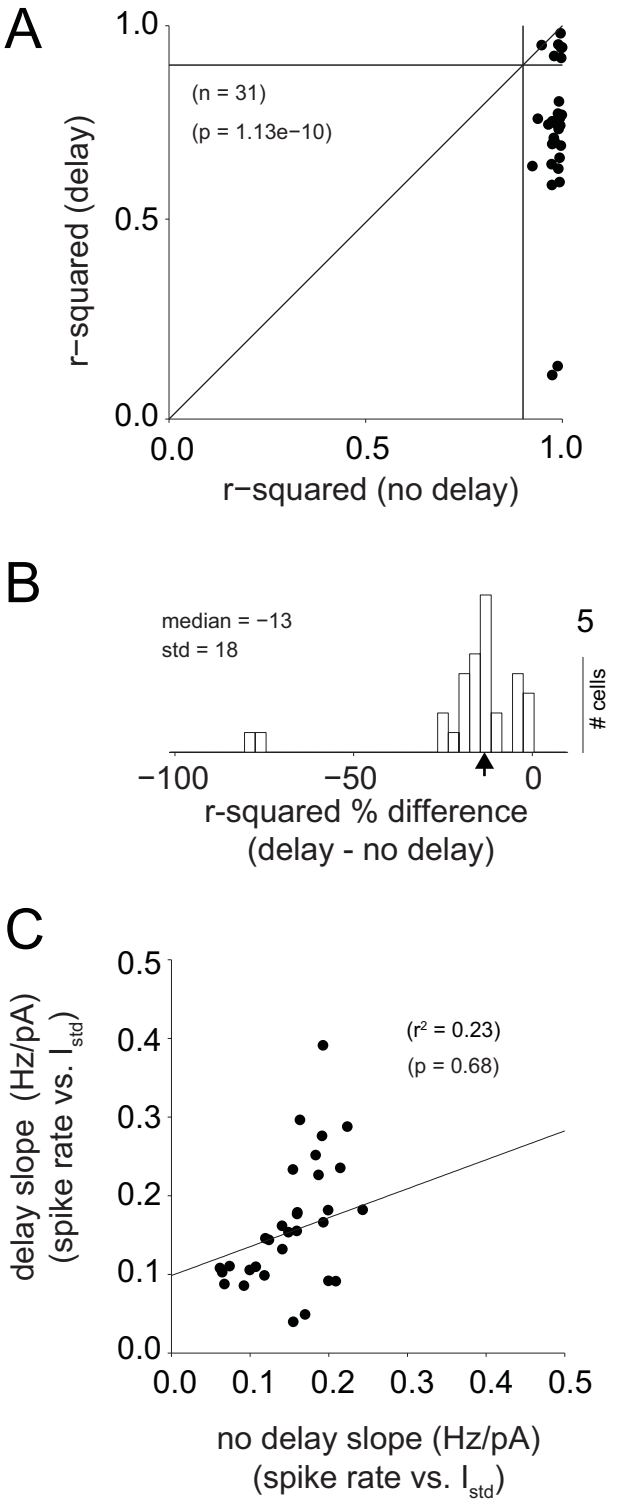
A
1.0
0.5
0.0
0.0
0.5
1.0
(n = 31)
(p = 1.13e−10)
r−squared (delay)
r−squared (no delay)
B
median = −13
std = 18
5
cells
−100
−50
0
r-squared % difference
(delay - no delay)
C
0.5
0.4
0.3
0.2
0.1
0.0
0.0
0.1
0.2
0.3
0.4
0.5
(r² = 0.23)
(p = 0.68)
delay slope (Hz/pA)
(spike rate vs. I_std)
no delay slope (Hz/pA)
(spike rate vs. I_std)

Figure 5

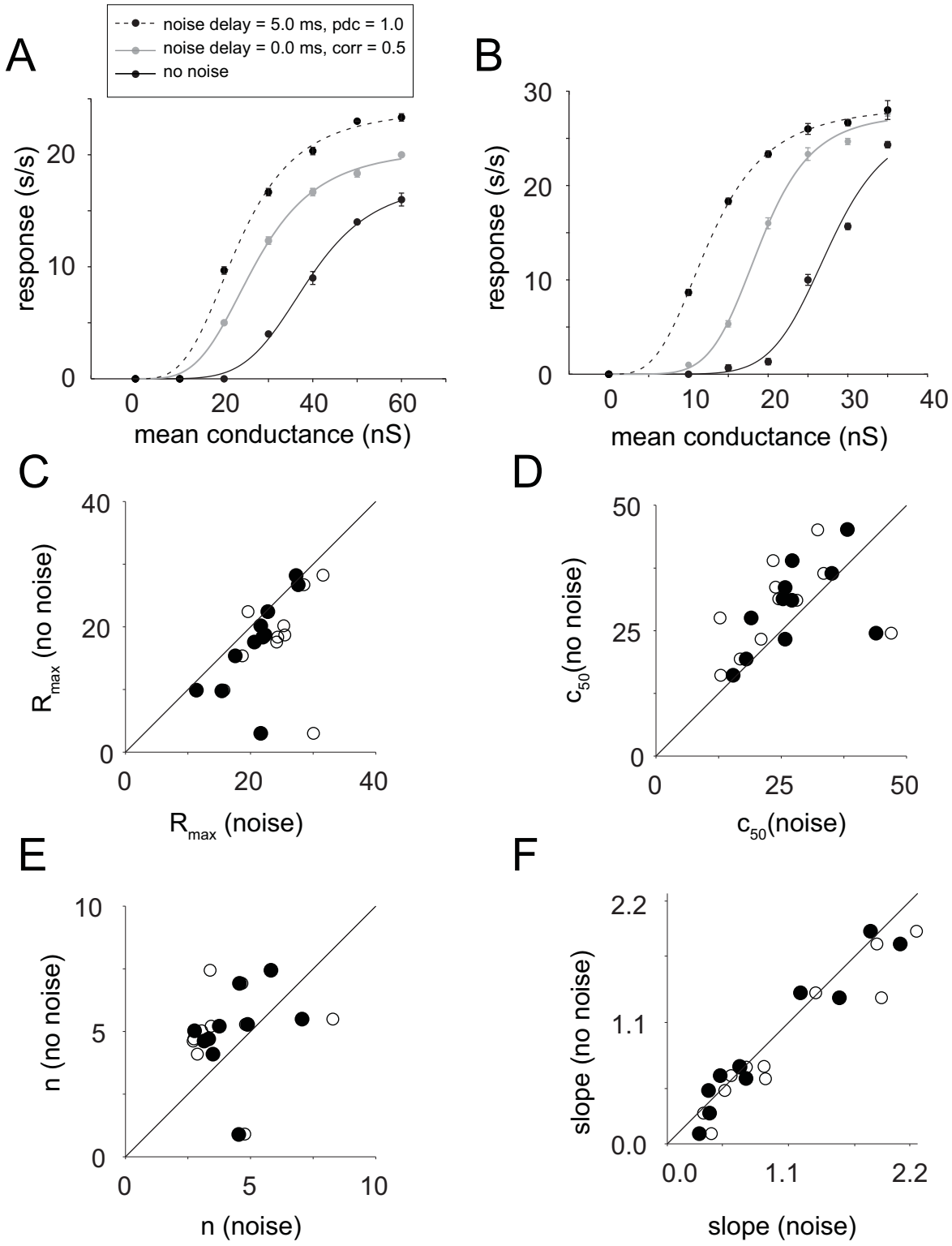
A
noise delay = 5.0 ms, pdc = 1.0
noise delay = 0.0 ms, corr = 0.5
no noise
response (s/s)
mean conductance (nS)
B
response (s/s)
mean conductance (nS)
C
R_max (no noise)
R_max (noise)
D
c50(no noise)
c50(noise)
E
n (no noise)
n (noise)
F
slope (no noise)
slope (noise)

Figure 6

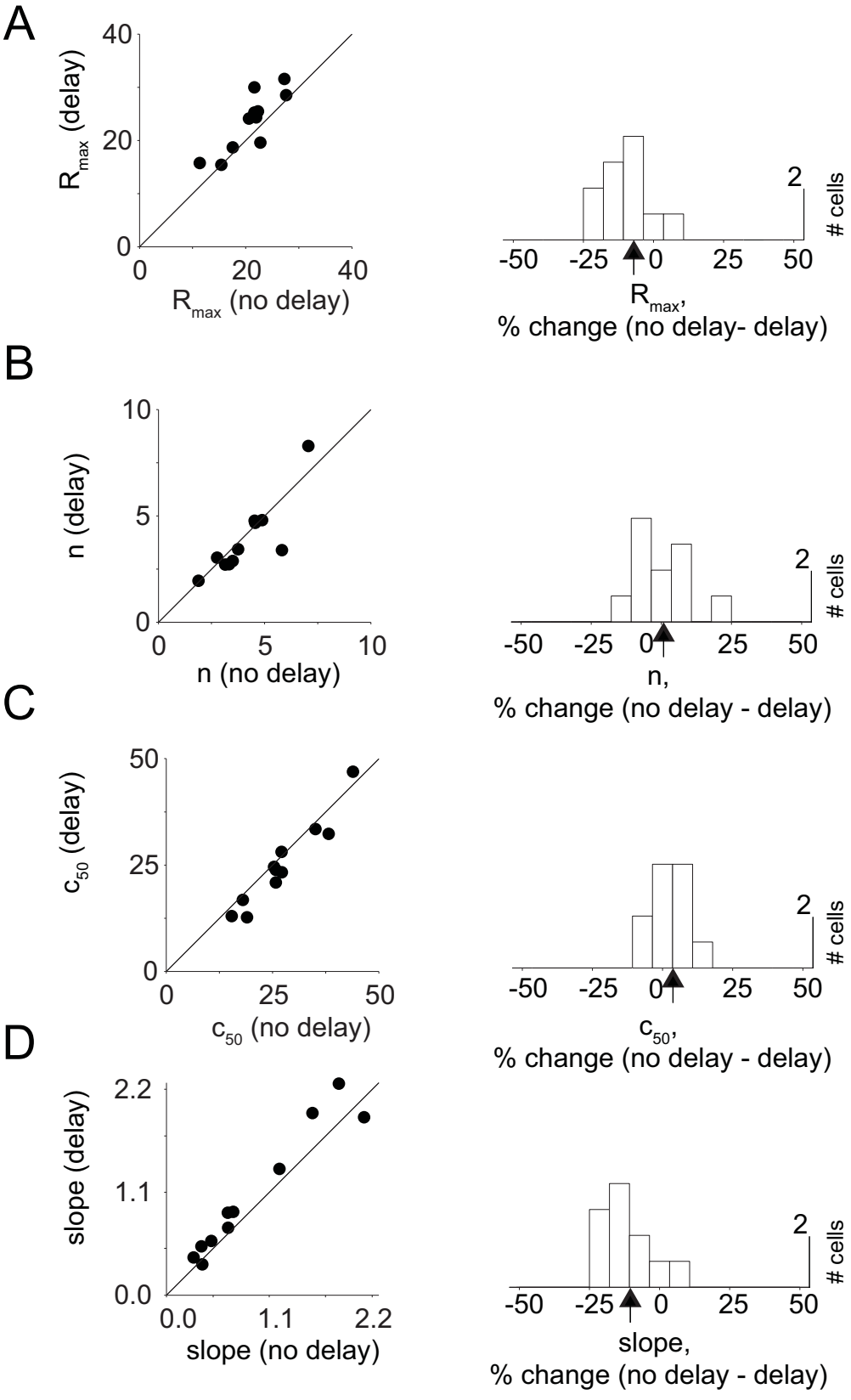
A
40
20
0
0
20
40
R_{max} (delay)
R_{max} (no delay)
2
cells
-50
-25
0
25
50
R_{max},
% change (no delay- delay)
B
10
5
0
0
5
10
n (delay)
n (no delay)
2
cells
-50
-25
0
25
50
n,
% change (no delay - delay)
C
50
25
0
0
25
50
c_{50} (delay)
c_{50} (no delay)
2
cells
-50
-25
0
25
50
c_{50},
% change (no delay - delay)
D
2.2
1.1
0.0
0.0
1.1
2.2
slope (delay)
slope (no delay)
2
cells
-50
-25
0
25
50
slope,
% change (no delay - delay)

Figure 7

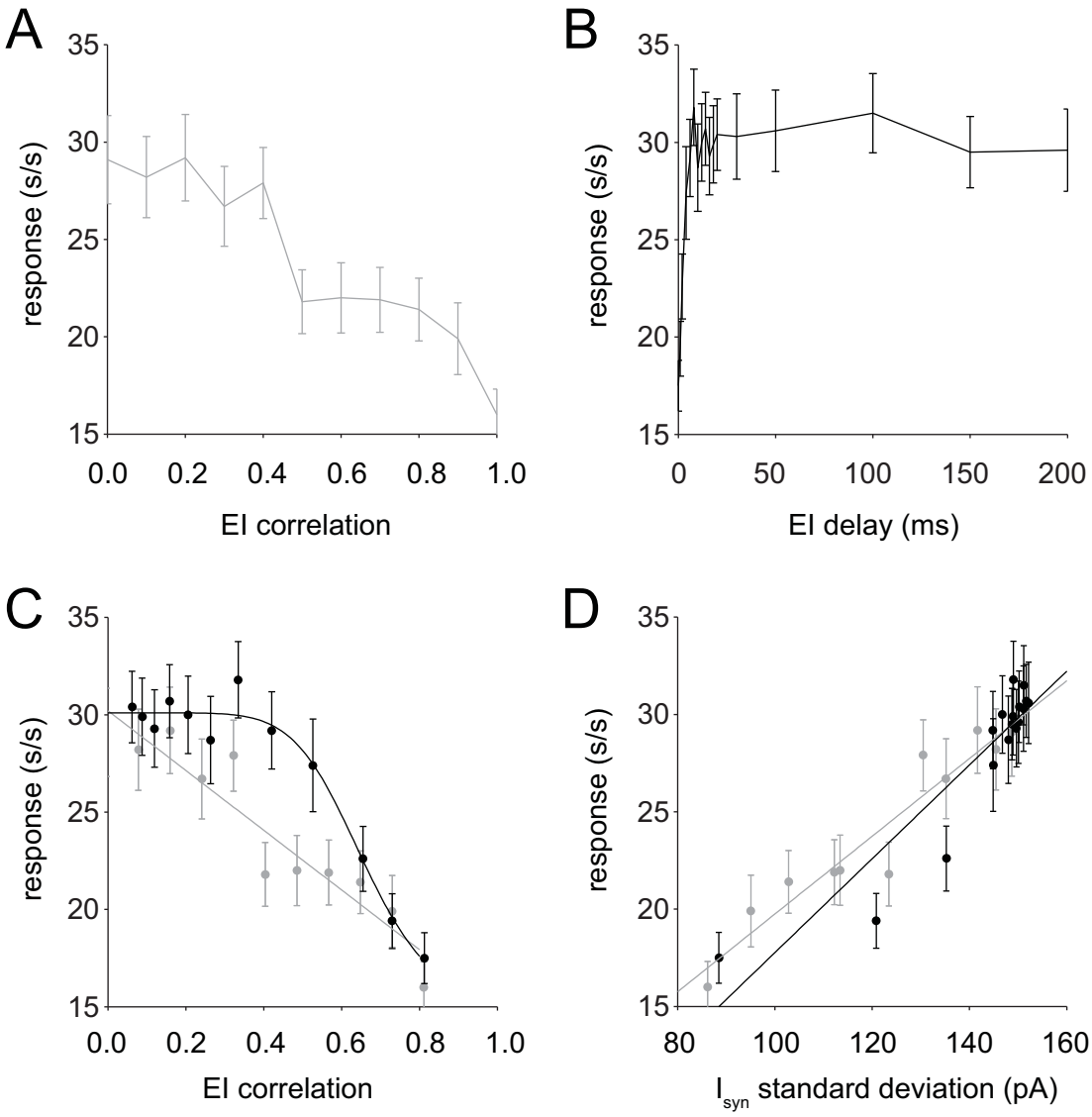
A
response (s/s)
35
30
25
20
15
0.0
0.2
0.4
0.6
0.8
1.0
EI correlation
B
response (s/s)
35
30
25
20
15
0
50
100
150
200
EI delay (ms)
C
response (s/s)
35
30
25
20
15
0.0
0.2
0.4
0.6
0.8
1.0
EI correlation
D
response (s/s)
35
30
25
20
15
80
100
120
140
160
I_{syn} standard deviation (pA)

Figure 8

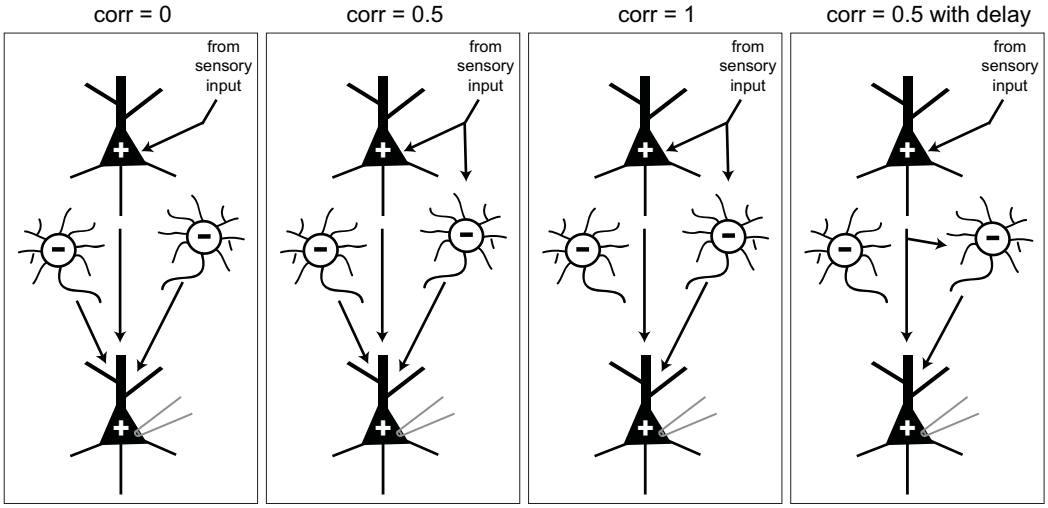
corr = 0
corr = 0.5
corr = 1
corr = 0.5 with delay
from sensory input
from sensory input
from sensory input
from sensory input

Figure 9